Feature Detection in Mammographic Image Analysis

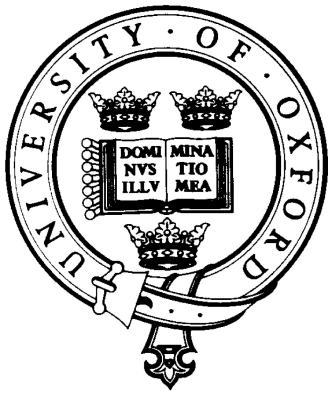

Marius George Linguraru

A thesis submitted to the Department of Engineering Science, the University of Oxford, in partial fulfilment of the requirements for the degree of Doctor of Philosophy.

The University of Oxford
Department of Engineering Science
Medical Vision Laboratory

Michaelmas Term
2002

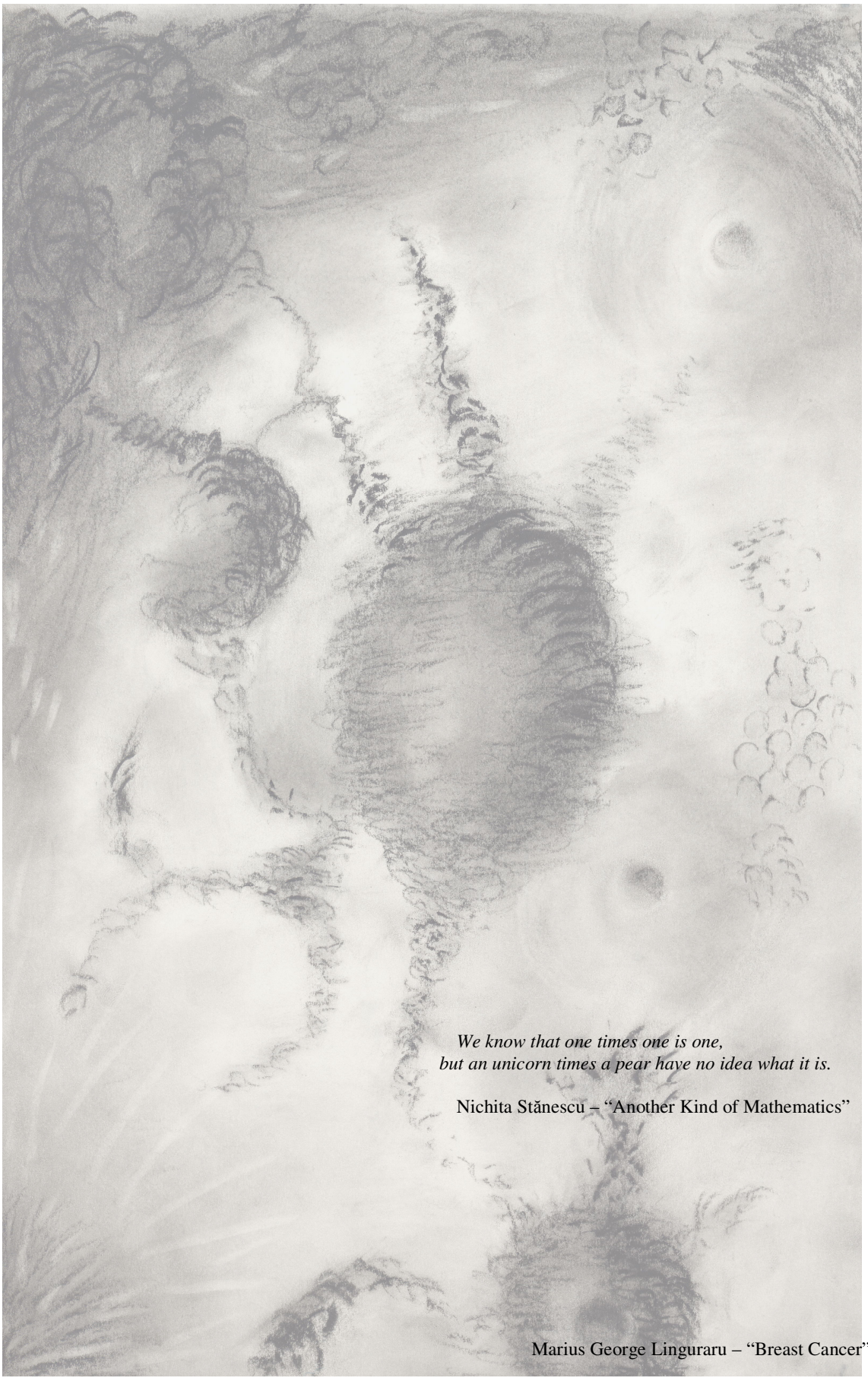

We know that one times one is one,
but an unicorn times a pear have no idea what it is.

Nichita Stănescu – "Another Kind of Mathematics"

Marius George Linguraru – "Breast Cancer"

Feature Detection in Mammographic Image Analysis

Marius George Linguraru

A thesis submitted for the degree of Doctor of Philosophy
at the University of Oxford

Medical Vision Laboratory
Department of Engineering Science

Keble College
Michaelmas Term, 2002

Abstract

In modern society, cancer has become one of the most terrifying diseases because of its high and increasing death rate. The disease's deep impact demands extensive research to detect and eradicate it in all its forms. Breast cancer is one of the most common forms of cancer, and approximately one in nine women in the Western world will develop it over the course of their lives. Screening programmes have been shown to reduce the mortality rate, but they introduce an enormous amount of information that must be processed by radiologists on a daily basis.

Computer Aided Diagnosis (CAD) systems aim to assist clinicians in their decision-making process, by acting as a second opinion and helping improve the detection and classification ratios by spotting very difficult and subtle cases. Although the field of cancer detection is rapidly developing and crosses over imaging modalities, X-ray mammography remains the principal tool to detect the first signs of breast cancer in population screening. The advantages and disadvantages of other imaging modalities for breast cancer detection are discussed along with the improvements and difficulties encountered in screening programmes. Remarkable achievements to date in breast CAD are equally presented.

This thesis introduces original results for the detection of features from mammographic image analysis to improve the effectiveness of early cancer screening programmes. The detection of early signs of breast cancer is vital in managing such a fast developing disease with poor survival rates. Some of the earliest signs of cancer in the breast are clusters of microcalcifications. The proposed method is based on image filtering comprising partial differential equations (PDE) for image enhancement. Subsequently, microcalcifications are segmented using characteristics of the human visual system, based on the superior qualities of the human eye to depict localised changes of intensity and appearance in an image. Parameters are set according to the image characteristics, which makes the method fully automated.

The detection of breast masses in temporal mammographic pairs is also investigated as part of the development of a complete breast cancer detection tool. The design of this latter algorithm is based on the detection sequence used by radiologists in clinical routine. To support the classification of masses into benign or malignant, novel tumour features are introduced. Image normalisation is another key concept discussed in this thesis along with its benefits for cancer detection.

Acknowledgments

This thesis resulted from three wonderful years that I spent at the University of Oxford, three memorable years in a town filled but not hampered by tradition, a place of intellectual challenges and stimulation, where inspiration can be found amidst great halls and weighty libraries, evergreen parks and narrow alleys, famous collections and historic houses—and particularly among its people. I would need many more pages to eulogise Oxford, but it is with its people that I fell in love.

There is a long list of those who contributed to my work and well-being during the years I spent in Oxford and I will undoubtedly miss a few names. I start by thanking my supervisor, Professor Sir Mike Brady, a man of amazingly broad knowledge and fantastic support, the scholar I would like to become one day. The Medical Vision Laboratory was an exquisite combination of scientific merit and friendliness. And I have kept great friends and colleagues among its members, some of them who participated actively in this work. I am especially grateful to: Kostas Marias, Maud Poissonnier, Djamal Boukerroui, Robert McLaughlin, Chris Behrenbruch, Styliani Petroudi, Margaret Yam, Timor Kadir, Alexis Roche, Carolyn Evans, Veit Schenk, Byong-Woo Wang and Alison Noble. I would also like to acknowledge the teams from Mirada Solutions and Churchill Hospital Breast Cancer Unit. I am equally indebted to Professor Averil Cameron, the Warden of Keble College. And I owe particular gratitude to those closest to my heart, my mother Elena, my father Gheorghe and my sister Georgiana.

Funding for this work was generously provided by the University of Oxford's Scatcherd European Scholarship and the Overseas Research Scholarship from the Committee of Vice-Chancellors and Principals of the Universities of United Kingdom. Additional funds were granted by the Graduate Academic Fund Award from Keble College, University of Oxford and the Rațiu Family Foundation.

Table of Contents

CHAPTER 1

1 Introduction

It is the mark of an educated mind to be able to entertain a thought without accepting it.

Aristotle

1.1 The Prevalence of Breast Cancer

The incidence of cancer in the Western world is enormous and its threatening presence is an unfortunate reality of our environment. The impact this fierce affliction has for a large percentage of the population has become a galvanising cultural phenomenon. We grow and live with *the fear of cancer* invading our privacy and shadowing the existence of people dear to us. We read about the spread of cancer, and not only in specialised literature. On television, we see how tumours are formed, we hear stories about the lives of people just like people we know. Everywhere we sense the pain and suffering of this disease. The hospital lost its "copyright" on the term "cancer" and now shares it with general sciences and, through its massive impact on everyday lives, the entire society. While society reacts to the burden of cancer, science attempts to get a reaction from the disease and discover the elusive solution for improving its worrying statistics.

When considering figures and statistics of breast cancer, we refer to studies conducted in developed countries of the Western world. This is mainly due to the lack of information on this subject from under-developed and developing countries. Although the number of studies carried out in such regions of the world has increased, the lack of appropriate technical equipment to

detect cancer, associated with the high costs of the procedure, makes the records of such studies quite imprecise. We should normally expect much higher rates of incidence than reported in the poorer areas of the world, due to the present lack of radiologists and detection equipment in those regions. That will likely become more of an issue once people in undeveloped countries live long enough to die from cancer.

The disease has a far higher incidence in Europe (especially Western Europe) and North America. In the Far East and parts of Africa, the mortality rate due to breast cancer is much lower, with an incidence about 5 times smaller than in the West, although there has been a substantial increase in the number of new cases. During the last few years, Japan has witnessed a growth of 10 times in the number of breast cancers. In the Western world, recent figures show that breast cancer accounts for a high percentage of the overall cancer incidence in women, approximately 24% of all cancer cases. Around the world, there are approximately 945,000 new cases of breast cancer every year, of which the Western world accounts for half of the number of cases and the European Union accounts for over a quarter of diagnoses (figures published in 2001 [40]). The USA reported over 188,000 cases of breast cancer in 2005 and over 41,000 related deaths (www.cdc.gov). These figures show a rapid increase in the number of breast cancer cases compared to, for example, 1993 when there were only 570,000 cases world wide [34].

Breast cancer is second only to lung cancer (28% of cancer cases), the most feared form of cancer related death in women of all ages [186, 187]. Once cancer has been diagnosed, the chances of survival are reduced to just over 60% [34]. The astounding rise in the impact that of cancer on Western Europe and the Americas has increased the population's awareness of the disease and the number of studies related to it. It is estimated that approximately 1 in 10 women [15, 189] (1 in 9 in Britain and 1 in 8 in the USA [132]) will be victims of breast cancer (only 0.1% of the total incidence of breast cancer is attributed to men), with an approximate increase of 0.55% per year in the number of women developing the disease. If the rate of change remains constant, the number of cases of breast cancer will double by 2020 along with the percentage of the female population that will be exposed to the disease at some stage in their lives.

Why is the incidence of cancer growing so rapidly in modern society? Could the causes be environmental? Researchers have tried to trace both genetic and environmental causes, but there is so far insufficient evidence to support many of the theories that attribute the expansion of the disease to unhealthy food, hormonal treatments or pollution. Many attribute this to a change in the lifestyle of women, particularly those seeking a career other than homemaker, and in diet that includes fatty foods. It is estimated that 70% of cancers have their origins in the foods we eat. Reports [68] emphasise the carcinogenic factors found in diet, smoking, alcohol consumption, sunbathing and sedentary lifestyles. However, our diet is full of surprises; while fruits, vegetables, fish and milk are some the most effective sources of protection against cancer, commonly available foods are stripped of their nutrients by modern farming and therefore become less efficient as cancer deterrents. Fruits and vegetables may contain a high level of pesticides and farmed fish are a source of toxins. Among the dangerous foods, red meat, salt, soy, and baked, fried, grilled and barbequed food (containing acrylamide), sweeteners and thickeners found in processed food are the best-known triggers. Other well-established factors refer to family history, ethnic background, early menarche or late menopause, the absence of childbirth and obesity. And there are increasingly worrying signs related to the use of hormone replacement therapy (HRT) [7, 110].

1.1.1 A Brief Anatomy of the Female Breast

To better understand the development of breast cancer, an overview of female breast anatomy is necessary. Throughout a woman's life, the breast goes through a set of continuous changes. The first major development occurs in the teen-age years, when the lactation system evolves. A second

important stage is at menopause, when the milk-producing tissue changes into fat.

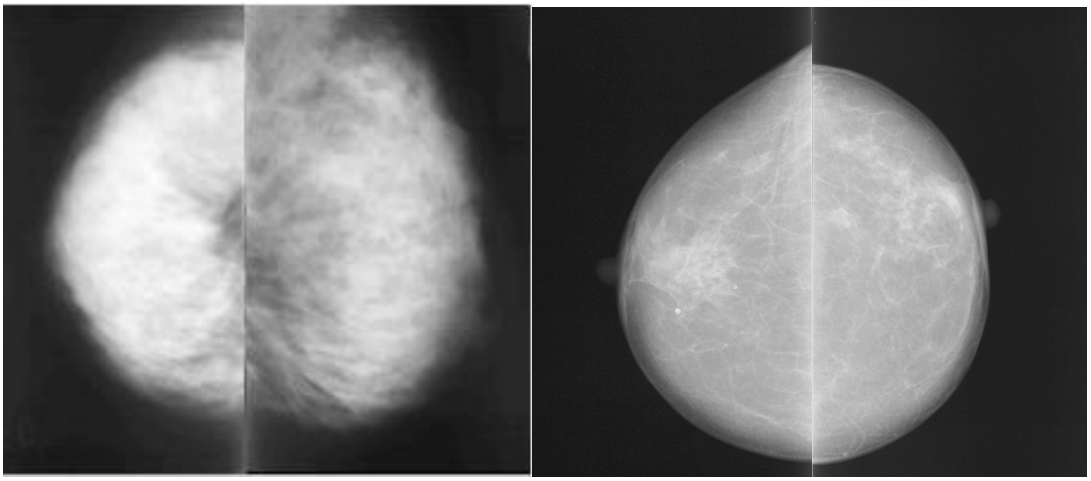

Figure 1 uses mammography to compare the appearance of a young woman's breast with those of a post-menopausal woman.

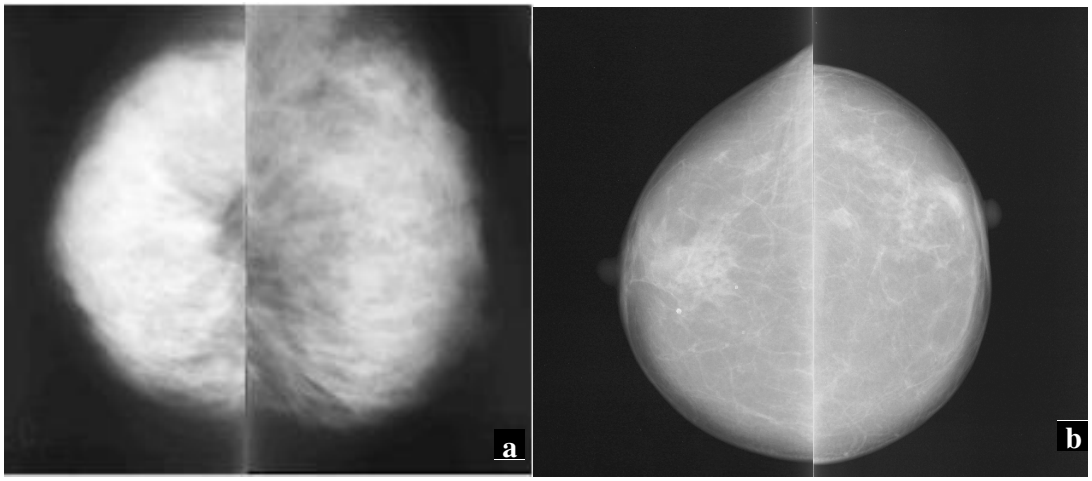

Figure 1 The appearance of young versus menopausal breasts in mammography: (a) A pair of left and right cranio-caudal mammograms of a pre-menopausal woman with very dense appearance due to the presence of milk-producing tissue; (b) a pair of left and right cranio-caudal mammograms of a post-menopausal woman with larger amounts of fat-tissue.

The simplest portrayal of the mature female breast would have to enumerate the following types of incorporated tissues: epithelial or glandular tissue (the milk-producing tissue), which appears very dense in mammograms due to the high percent of calcium it contains; adipose tissue (fatty tissue, which is mainly transparent in X-ray), fascia (the connective tissue), muscles, ligaments and lymphatic and blood vessels [30, 53, 65]. Figure 2 presents the main anatomical

features of the breast. The arborescent structure of the breast is nourished by acini (milk producing sacs inside a lobule) connected through terminal ducts. Lobules are fruits on the branches represented by subsegmental ducts that grow from the mammary ducts converging in the nipple.

1.1.3 The Pathology of the Breast

Breast cancer is an abnormally fast reproductive process of the epithelial cells in the lobular unit. It is also referred as carcinoma (the other type of cancer is sarcoma, which is much rarer and arises from a bone, muscle or other soft tissue [188]). The preferred spreading routes of cancer are the blood and lymph vessels (which makes the axillary nodes an important feature in signalling metastatic diseases), but the direct invasion of the surrounding tissue may have the same effect. Therefore, one would naturally speak about forms of cancer that are spreading (invasive or infiltrating) and non-spreading (*in situ* – which stay within the lobular or ductal unit and have not gone though the basal membrane). *In situ* cancers are sometimes referred as pre-invasive since further developments of the tumour may occur and invade the neighbouring tissue. Both invasive and *in situ* breast carcinomas are commonly divided into lobular or ductal. Besides the ductal and lobular forms of cancer, other types of carcinoma may be medullar, tubular, papillary, cribriform and mucinous [53, 189].

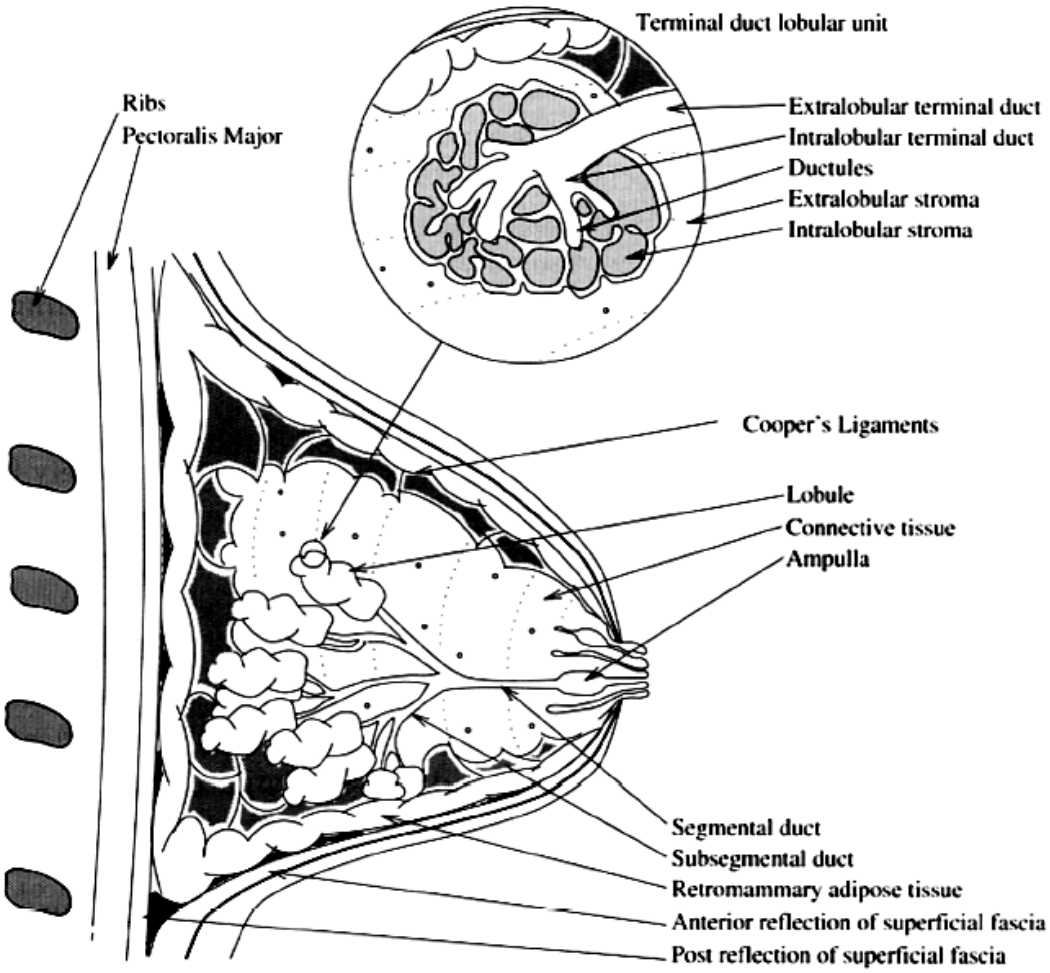

Figure 2 A brief anatomy of the breast showing the branching internal structure of ducts and lobules [65].

Most ductal and lobular cancers lead to secretions that form calcifications. The smallest of these (under 1 mm in diameter) are called microcalcifications and represent some of the earliest signs of breast cancer. Microcalcification clusters may be the only indication of *in situ* tumours. Architectural distortions are another distinctive sign of breast cancer, when the tumour has no central mass [65]. Approximately 80% of microcalcification clusters are benign [65, 81, 166], and their shape and topology distinguish them from the malignant type.

Ductal Carcinoma in Situ (DCIS) is one of the most common types of *in situ* cancer and can involve a large number of ductal structures. It is mainly associated with microcalcification clusters

and corresponds to one of the earliest signs of malignancy. It appears in 40% of the screening detected cancers [95]. Its treatment may involve a partial mastectomy.

Infiltrating Ductal Carcinoma (DC) is the most usual invasive cancer (over 70% of tumours), a form of disease with very poor prognosis and which may require a total mastectomy, including the removal of the axillary lymph nodes and post-operatory radiotherapy. It may be associated with microcalcifications.

Among the special types of cancer is the Phyllodes Tumour's [189] whose clinical behaviour is still not fully understood. Most of these tumours are benign, but there are also malignant forms. They can be cystic and sarcomatous and usually recur after initial excision. Their treatment is particularly difficult through the atypical behaviour of the tumour.

The treatment given to a women diagnosed with breast cancer depends on the specific characteristics of that tumour. Moreover, the management of the disease varies considerably with the different stages of the same type of cancer. So does the prognosis, as a statistical measure of the chances of having a positive outcome of the treatment the patient is undergoing. The most relevant factors for a doctor considering the prognosis are the size and type of the tumour, the presence of metastasis, the stage of the disease, the status of the axillary lymph nodes, and the patient's age and medical condition. The prognosis is especially positive for tumours smaller than 2 cm with no lymph node involvement or other remote metastatic areas. A combination of surgery, radiotherapy and chemotherapy are typically necessary to eradicate advanced malignancy; still, the prognosis remains rather poor.

Benign diseases may develop within or outside the ductal and lobular system and most of them are associated with microcalcification clusters. Adenosis, necrosis, hyperplastia, fibroadenomas and arterial calcifications represent an important source of false positives (FP) in the classification of breast tumour.

Section 2.2 illustrates some typical cases of breast pathology in both the form of masses and microcalcifications.

1.2 Are Screening Programmes the Solution?

The signs of breast cancer that appear in X-ray mammograms present a significant challenge to radiologists and they are generally difficult to distinguish in the highly textured breast anatomy. Breast screening programmes attempt to detect and eradicate cancer at the earliest possible stage to reduce mortality rates. From the first trials in USA and Canada in the sixties and the very first implementation in the seventies in Sweden, screening programmes were found to reduce mortality caused by breast cancer in women by nearly 30% [4, 29, 163].

Some results of the mass screening in UK showed a very high rate of false negatives (FN), when *in situ* cancers are left to metastise or invasive cancers are not detected, as well as a high rate of FP, where women are operated on without finding breast cancer. Hence, it is essential in the early detection of breast carcinomas to further improve the subsequent classification of mammographic findings as either benign or malignant.

Breast cancer's incidence is low in women under 30 years old (although extremely aggressive when present) and thereafter increases with age. Between the ages of 40 and 50, women face a doubling of the rate of incidence which continues to increase over the age of 50, but more slowly. Younger women are encouraged to check the status of their breasts by simple palpation. Unfortunately, most women cannot reliably palpate a tumour smaller than 1 cm; therefore more thorough examinations are required. In the UK, the screening programme was arguably implemented for women between 50 and 70, since this is the group of age most vulnerable to breast cancer, and mammography has not to date been demonstrated to be clinically effective before menopause. Other countries, such as USA, begin screening at the age of 40 and do not have an upper age limit.

There are several criteria that need to be fulfilled before starting a screening programme. These include:

- the disease to be screened must be very common and a treatment must be available for it, since there are very high costs involved and there would be little point screening for a non-treatable affliction;
- the detection method must be robust and reliable and lead to good results for the overall screening process;
- it must have high specificity;
- patients must accept it, since the method would not be cost-effective without a large number of patients to be examined.

The key method used in breast cancer screening programmes is X-ray mammography, as the most reliable process fulfilling the above criteria. If a mammogram presents any features that seem suspicious to the radiologist, the patient will be asked to attend an assessment clinic where more investigations will be performed by means of medical imaging and consulting. Magnetic Resonance Imaging (MRI) and ultrasound (US) are secondary imaging techniques used in the triple assessment (palpation, imaging, and core biopsy). Chapter 2 expands on the advantages and disadvantages of these imaging methods.

According to some optimistic predictions, the screening programme should, almost double the chances of survival in women who develop breast cancer. Studies have shown that 8% of women are recalled for further investigation [65], most of them not presenting any malignancy. There is intensive debate as to whether the breast screening clinical assessments should be performed more often than a three-year period, as it has been noticed that the assessed women sometimes develop cancer over a period shorter than three years ("interval cancer"). While the UK has a screening interval of 3 years, other European countries have already decreased the period to 2 years [29], while in USA screenings are recommended yearly after the age of 40 and every 2-3 years for women between 20 and 40 year old. It is estimated that nearly 20% of cancers were visible in the mammograms previous to the current screening [150] and that interval cancers generally develop in the upper outer quadrant of the breast [17].

Segmentation methods may be more sensitive in detecting abnormalities at an earlier stage, but it is the radiologist who will need to make the final decision. Even though screening programmes improve the results of detection, there is sufficient room for progress in the clinical performance to warrant further research.

1.3 The Need for Image Segmentation

Medical image processing is a fascinating but challenging task. Working with mammograms is especially difficult due to the complex appearance of the structures of interest in this particular type of image representation. Although a mammogram is a good "picture" of the breast, this is hardly sufficient when searching for small, subtle and complex anatomical features, such as microcalcifications, masses or curvilinear structures (CLS) in the process of early detection of breast cancer. Both human errors and the quality of image acquisition contribute to the difficulty of diagnosing the breast.

1.3.1 Reading Errors in Mammography

Statistics show that approximately 25% of cancers are missed by radiologists and about 80% of biopsies are performed on benign cases [11, 169]. Furthermore, it is estimated that about 22% of films are usually lost between visits and 5% of mammograms have to be retaken. Such numbers draw attention to the additional requirements of the diagnosis process. Besides saving lives, doctors are also expected to find the least stressful and painful way to check the status of the disease: malignant versus benign. Given the unpleasantness of both mammograms and core biopsy acquisition, reducing the number of FP becomes as important as reducing the number of FN.

The complex anatomy of the breast is the inevitable source of the highly textured structure of the mammograms. Its input is very difficult to analyse, and radiologists are expected to distinguish very subtle abnormalities out of this mass of structural ambiguity. The variability between any two cases adds to the difficult task that the human decision maker faces. The inter- and intra-radiologist

variability of 30% emphasises the need for reliable image processing tools to assist the process of diagnosis. According to Krupinski and Nodine [92], radiologists only investigate 87% of the mammogram area; in contrast, an automatic detection algorithm will not leave any area of the image unexamined.

With up to 3 million new mammograms to be analysed each year in the UK, the amount of information becomes overwhelming for radiologists, especially since a second opinion is requested before a decision is made in diagnosing a patient. These figures are doubled as the previous mammograms of the patient are compared to the current ones at each screening session. Computer-aided diagnosis (CAD) can assist the radiologist at this point, by helping to balance the measure of confidence of the specialist and eliminate the second analysis. However, as highlighted in insert name of source [76], CAD systems can only be evaluated from a radiologist's point of view:

- on annotated databases, in which case the effect of the CAD in practice cannot be predicted;
- on databases of known human readers, to compare their evolution with that of the clinician by receiver operating characteristic (ROC) curve analysis and predict the effect of the CAD in practice;
- by comparing the work of the radiologists with and without CAD;
- by doing prospective evaluations.

1.3.2 Image Quality

The quality of the medical image is crucial to diagnosis and depends on several physical factors. The most important are the time of exposure and the breast thickness along with various other imaging factors. Since the X-ray dosage must be minimised for patient safety, there is a compromise between dosage and the signal-to-noise ratio (SNR) of the mammogram. Decreasing of X-ray exposure degrades the quality of the image, which already reduces the complex three-dimensional (3D), superimposed structures of the breast to a simplified two-dimensional (2D)

projection. Noise further obscures these features. This presentation of the mammogram could be easily reduced to that of a large-textured noisy image, which still represents the best tool for early cancer detection to be used around the world. Different deformations of the breast during the shooting of the X-ray cause more difficulties in the detection process.

1.3.3 Future Trends

Computer aided image segmentation plays an important role in overcoming the present limitations of medical image analysis There are several implemented techniques that bring improvements in the field of medical imaging. Many of them have proved to be unsatisfactory for the purpose that they are used, such as automatic detection and managing mammograms. Moreover, although the resulting images may look quite impressive, they have not always improved the work of radiologists. Therefore, there is sufficient room for improvements and further development in image processing. Some trends in the field include:

- the development of soft-copy reading workstations [12, 37, 142, 177], as the tool for the future use of digital mammograms;
- friendlier user-interfaces (touch-screen, automatic report generation, robust display) which require minimal intervention from the radiologist;
- the development of training-systems with immediate feedback and the use of larger databases;
- the development of real-time applications for making the best use of the image processing methods in clinical applications;
- the introduction of more reliable, more robust and faster image processing algorithms;
- software integration of robust algorithms to build strong performing medical systems.

1.4 Making a Difference

The earliest possible detection breast cancer is fundamental to saving the lives of many patients facing the disease. The challenges enumerated in the previous section combine to create a complex problem that has to be solved using basic science.

1.4.1 The Incentive of Work

The research described in this thesis is motivated by the intrinsic facts of managing breast cancer through early detection. The first question is: Why detect microcalcifications and not just masses? The answer is quite straightforward: The presence of microcalcifications is one of the earliest indications of malignancy. Whether or not they appear in independent clusters or associated with masses, the existence of microcalcifications in a mammogram is often a clear warning of abnormality. They can be visible long before any palpable lesion has developed and their early detection can indeed "make a difference" in the prognosis. Moreover, the detection of masses is also investigated to a smaller extent in this thesis.

A second question arises at this stage: What type of medical imaging procedure should be used in the detection process? Although nuclear images of the breast are currently available, clinical practice reveals only three techniques are commonly used in a breast assessment. These are: X-ray mammography, MRI and ultrasound (the main characteristics of each technique will be highlighted in Chapter 2). Unlike mammography, the latter two (and especially ultrasound) are only used to complete and reinforce the conclusion of the triple assessment (palpation, imaging, and biopsy). Hence, the fundamental and primary procedure in the diagnosis remains X-ray mammography. As part of screening programmes, X-ray mammography provides the data that the radiologist will subsequently use to conclude whether an abnormality is benign or malignant. Only mammograms can provide the necessary spatial-resolution and signal-to-noise ratio to distinguish microcalcifications from the background breast tissue. Both MRI and ultrasound remain inadequate for this general purpose.

1.4.2 Remarkable Achievements to Date

The task of CAD systems is to draw the radiologist's attention to suspicious regions in an image. All methods begin with image acquisition and visualisation and extend to quantitative and functional analysis. Directly digital mammography (cf. Chapter 2) simplifies the acquisition and eliminates the digitisation stage. The results of analysis will tell the radiologist the size of the highlighted abnormality, its shape, texture and behaviour. Studies proved that the performance of radiologists increases when a good segmentation or classification system is used [42, 48, 135, 152].

Techniques for enhancing the appearance of the mammogram range from improving the contrast and reducing the noise [65, 80] to compensating for breast margin and segmenting the pectoral muscle [20, 79]. For diagnosis, two main branches in mammographic image segmentation have been developed: the detection and classification of microcalcification clusters, and of breast masses. Chapter 2 outlines a number of notable methods.

The ultimate goal of any method is to be robust and reliable enough for routine clinical use in the hospital environment. A short review of the latest CAD systems is provided by Marchese in [108]. A remarkable technique worth mentioning in this introduction was launched by R2 Technology with their ImageChecker®. This is a complex system that outputs both clusters of microcalcifications and dense regions and areas with radiating lines. The results are very promising, as it has been reported that when using the R2 ImageChecker® microcalcifications are detected with 98.3% TP rate with 0.5 FP/image [141]. Other reports mention 100% TP rate on microcalcification detection with 2.2 FP/image, while 81.6% of masses are found. [41]. However, while the diagnostic sensitivity of clinicians rose when using the system, the positive predictive value of their interpretations worsened due to the high number of FP [42]. Furthermore, approximately half of the increase in the recall rate in screening programmes is due to the high number of FP in microcalcification detection [41].

The Standard Mammogram Form (SMF) is an image normalisation technique that eliminates the current limitations of the imaging process and relies only on anatomical breast structures. Chapter 2 will briefly overview the h_{int} model [65]. The SMF™ Workstation developed by Mirada Solutions (now part of Siemens Medical Imaging) represents the 3D quantification of the amount of non-fat and fat tissue for each pixel, temporal registration of the breast, reconstruction of the uncompressed breast, and localising microcalcification clusters [180]. This system obtained a microcalcification cluster detection rate of 95% TP with 0.38 FP per image.

1.4.3 Objectives

The systems enumerated previously, part of a large research effort in the field, show impressive advances in detecting and diagnosing breast cancer. Although we have almost reached a perfect detection rate, the large number of women undergoing screening (about 3 million mammograms annually in UK only) means that every percent that remains undetected represents a large number of patients who will likely confront cancer at an incurable stage. In the European Union alone, 1% of the missed cancers would force approximately 3000 women each year (ec.europa.eu) to undergo long and painful treatments, both physically and psychologically, with small chances of survival.

This thesis is motivated by the imperative to develop detection techniques suitable for clinical application. Such systems must be sufficiently robust and trustworthy to be used in hospitals and in real-time. When dealing with particularly delicate problems, such as human lives, we must assure that results are optimal and accept full liability.

Many methods described in the literature attempt to improve the results of detection of breast abnormalities by fine tuning the variety of parameters used in the implementation of the algorithm to suit each individual case. Although the outcome is impressive, the consistency and reproducibility of results is highly dependant on the operator's ability to find the best parametrical configuration for the detection. The approach used in this thesis proposes a fully automated non-

parametric method to detect microcalcifications using the SMF normalised representation of the breast. The aim is to overcome some of the current limitations of methods used to tackle this problem. The algorithm presented here can be similarly used for un-normalized (intensity) images, since its implementation would follow the same logic on grey-level mammograms.

The first objective is the removal of noise as a major source of FP. The algorithm presented here considers several types of noise from quantum mottle to shot-noise and uses subsequent filters to eliminate it. Curvilinear structures (CLS) – ducts, blood vessels, ligaments or tumour spiculations - proved to be equally important for the specificity of the method and a major challenge. A CLS removal step is embedded in the method, prior to the final segmentation. Built on a combination of partial differential equations (PDE), wavelets and statistics, the technique presents the user with a map of detected microcalcifications. The detection of these early signs of malignancy in the breast is meant to assist the radiologists in diagnosing breast cancer. The free-response receiver operating characteristic (FROC) curve of the microcalcification detection method is shown in Figure 3, along with some examples of detection that illustrate the sensitivity and specificity of the approach in Figures 4-7. The detection of masses in temporally registered enhanced mammograms is also investigated. Finally, a number of features of breast masses are extracted from their physical properties and discussed in the thesis.

1.5 Overview

The thesis aims to detect features that indicate the early development of breast cancer in mammographic images. Some basic facts about breast cancer and its impact were reviewed in the Introduction. A brief anatomy of the breast was also presented along with some of the most common mammographic anomalies. The incentive of the work is closely related to screening programmes; therefore, the screening programme was analysed along with future trends in mammography.

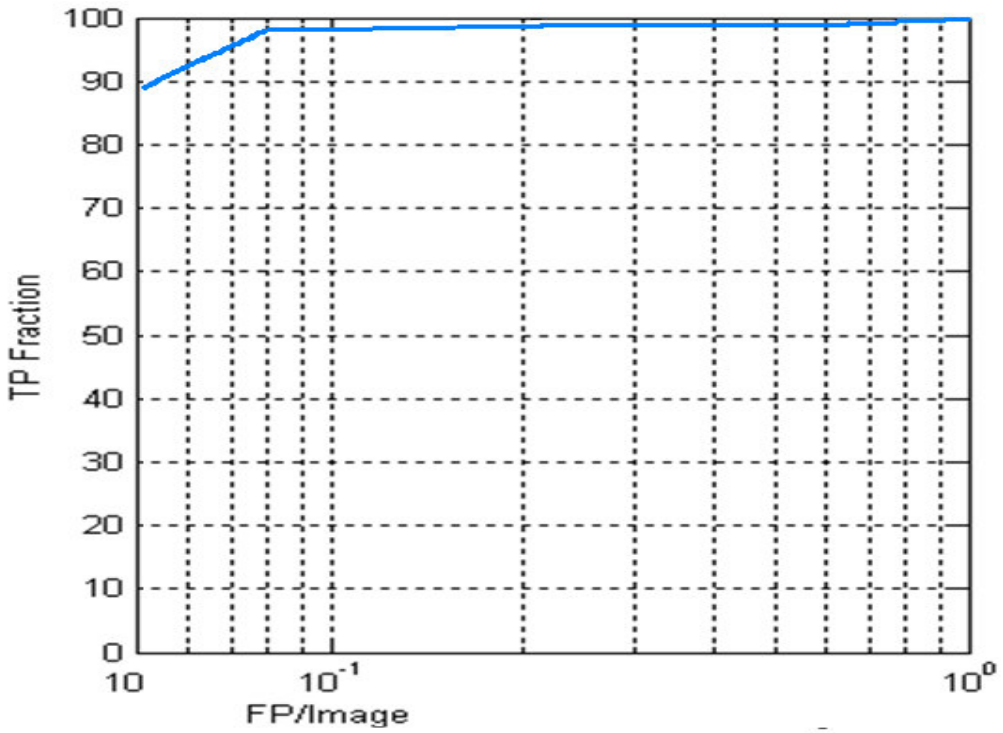

Figure 3: The FROC curve of the microcalcification-detection method**.**

Chapter 2 begins with a comparative overview of current imaging modalities to detect breast cancer. Mammography (X-ray and digital), Magnetic Resonance Imaging (MRI), Ultrasound (US) and Nuclear Imaging (PET, SPECT) are described and their strengths and weaknesses analysed. A discussion of the detection of anomalies in mammograms follows and the detection and classification of both masses and microcalcifications using state-of-the-art algorithms are reviewed. The chapter ends with a description of the Standard Mammogram Form (SMF), the image normalisation technique at the heart of robust detection of breast cancer.

Chapter 3 presents the first set of results for the detection of microcalcifications. The beginning of the chapter introduces analytically the concept of diffusion and particularly anisotropic diffusion, a cornerstone idea in the development of the enhancing filter used throughout the thesis. This work represents the first attempt to use anisotropic diffusion to filter mammographic images and analyse them**.** This is a priori a reasonable thing to attempt, as anisotropic diffusion smoothes the image, reduces noise (hence increases signal to noise, which is generally poor for mammographic images), and yet does a reasonable job at preserving image

structure. The filter and its parameters are described and the chapter concludes with the presentation of the first results.

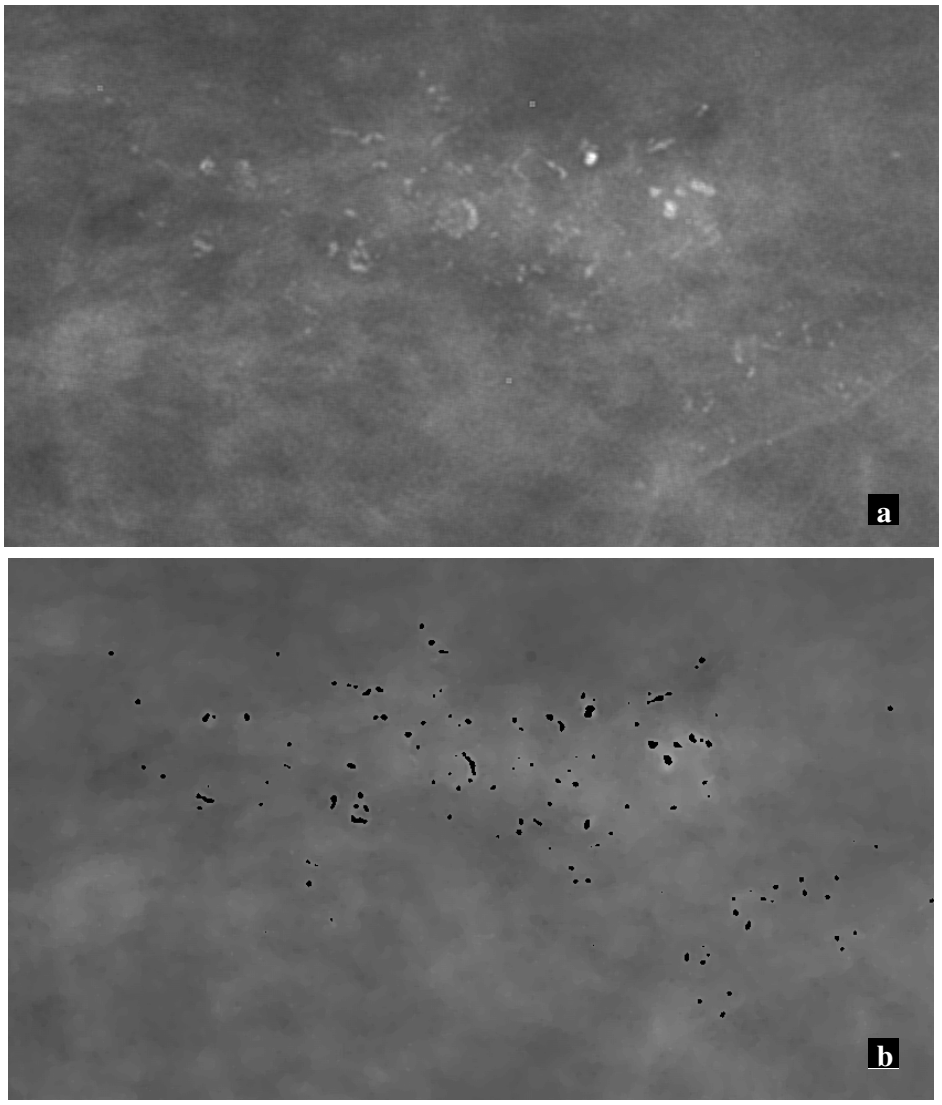

Figure 4: Detection example 1; (a) the original contrast-enhanced SMF sample with a very large microcalcification cluster in a dense area of the breast; (b) the detection map of the detection method presented in this thesis depicting correctly the cluster.

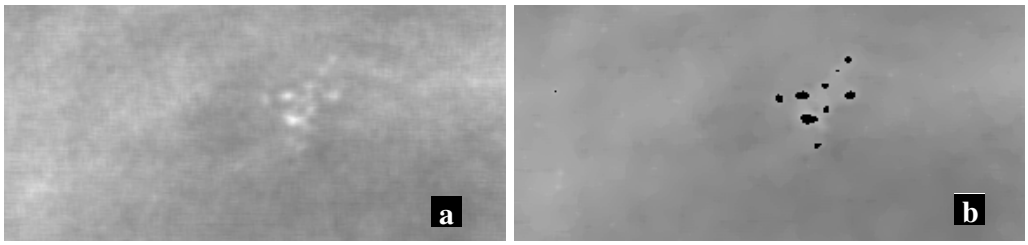

Figure 5: Detection example 2; (a) the original contrast-enhanced SMF sample with a subtle microcalcification clusters in a dense breast area; (b) the detection map.

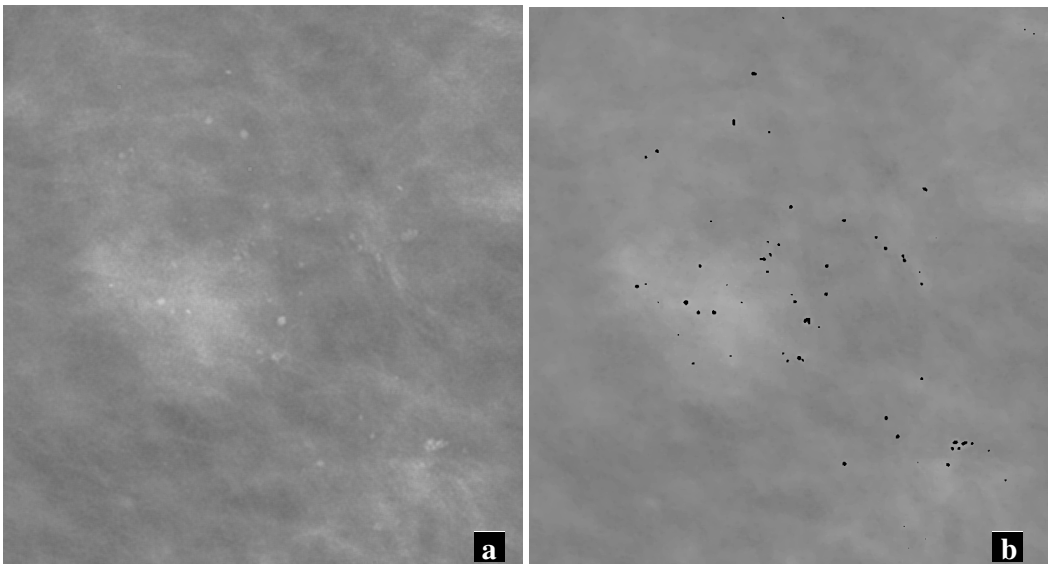

Figure 6: Detection example 3; (a) The original contrast-enhanced SMF sample with a widespread microcalcification cluster; (b) the detection map

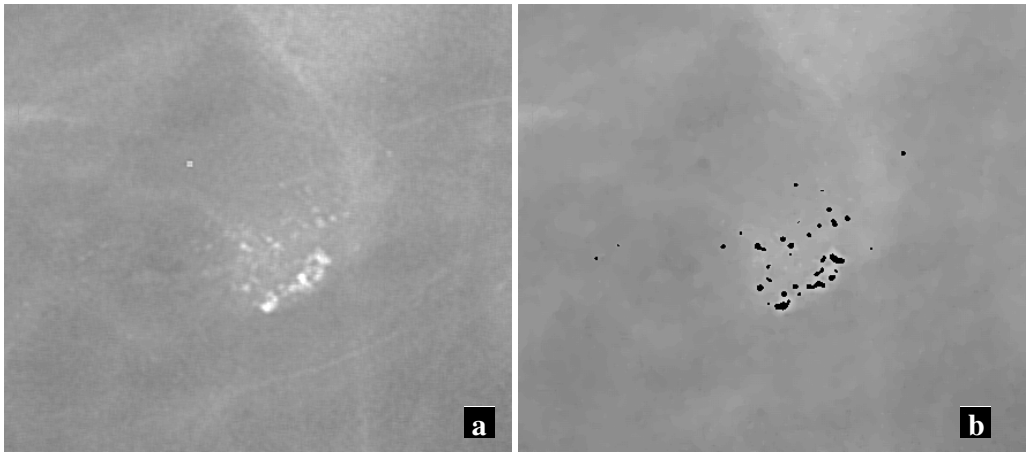

Figure 7 Detection example 4. (a) The original contrast-enhanced SMF sample with a cluster of very small microcalcifications in an area with several curvilinear structures; (b) the detection map.

Chapter 4 introduces the essential and original contributions of the thesis. The removal of shot-noise and curvilinear structures (CLS) is introduced in image pre-processing. It is accompanied by a statistical approach to the automated derivation of the enhancing anisotropic diffusion filter's

parameters. The second original step is the development of a method for adaptively thresholding the filtered images to facilitate the segmentation of microcalcifications. The approach is based on a model originally proposed to account for certain findings about the human visual system. This is based on the human eye's ability to sort through complex backgrounds and detect subtle image characteristics. Part of the novelty of the method is its alternation of normalisation filtering and segmentation. Several FROC curves for validating the detection algorithm were built and detection methods on SMF images compared. The outcome of the microcalcification detection algorithm was analysed on both SMF and intensity images.

Chapter 5 expands the use of the enhancing filter to the detection of masses. An original method to prompt mammographic masses is investigated; it uses image registration and enhancement as a pre-processing step, followed by segmentation based on texture analysis and visual comparison between temporal mammographic pairs. The chapter concludes with a discussion of features for mass classification.

The final chapter of the thesis, Chapter 6, lays down a general summary of the work presented in the thesis accompanied by discussion, conclusions and future work ideas based on the characteristics of false positives.

Three Appendices accompany the thesis and offer theoretical and practical details the concepts of phase congruency and monogenic signal, image registration in mammographic image analysis, and the interpretation of receiver operating characteristic (ROC) curves.

CHAPTER 2

2 Diagnosing the Breast

Real knowledge is to know the extent of one's ignorance.

Confucius

The diagnosis of breast diseases is based on a routine process called triple assessment that involves breast surgeons, histopathologists, radiologists and oncologists. Medical imaging procedures form a key part of the evaluation. Generally, when speaking of medical images, a variety of imaging techniques should be mentioned. Whether referring to X-ray and computed tomography (CT), magnetic resonance imaging (MRI), ultrasound (US), positron-emission tomography (PET) and scintimammography, tissue impedance imaging, infrared or optical imaging [170], there are three major problems to be dealt with:

- images tend to have poor signal-to-noise ratio (SNR);
- most images are highly textured and vary from one subject to another;
- clinically significant details are often subtle.

Each imaging technique has its advantages and disadvantages and the clinicians often use a combination of them for best results.

Breast imaging suffers from the same difficulties. While X-ray mammography is the primary imaging method used in screening programmes around the world, MRI and US have become auxiliary tools in the triple assessment process. Nuclear imaging has also shown rapid advances in

breast cancer detection, but the cost of installing and maintaining PET systems has until recently slowed its adoption. This is likely to change rapidly in the near future. The next sections will expand on each of the techniques used in breast imaging, followed by a summary of their strengths and weaknesses.

2.1 Imaging Modalities

2.1.1 X-ray Mammography

X-ray mammography has been widely used to detect the earliest signs of breast cancer since the beginning of last century, due in part to the cost-effectiveness of the procedure relative to other imaging modalities [5]. Screening programmes throughout the world have proved its effectiveness to image non-palpable abnormalities in the breast with very high resolution (the equivalent of a 25μm pixel resolution [75]). The earlier the detection, the better the chance to cure the cancer and to date, mammography is considered to be the best modality to depict microcalcifications and even small tumours. Mammography has the best combination of sensitivity, specificity, low cost and short acquisition, as underlined in Section 2.1.6.

A mammogram is a two-dimensional X-ray image of the mammary gland produced by a radiation beam passing through the compressed breast. Photons are attenuated according to their initial intensity, the thickness of the tissue they pass through and the attenuation coefficient of the respective tissue. The breast must be initially compressed between two plates to even its thickness and spread out the breast tissue for the radiologist to detect density variations easier in a mammogram. This improves the appearance of the mammogram and the image quality is even across the breast, while exposing the patient to a lower radiation dose. Figure 8 shows the clinical imaging machine. From the X-ray source, the photons traverse the breast compressed between the superior and the inferior plates and their intensity will change. The beam eventually reaches the film cassette, which, in the case of a film-screen device, contains the anti-scatter grid, the film and

CHAPTER 3

3 Filtering h_{int} Images

'Contrariwise', …, 'if it was so, it might be, and if it were so, it would be; but as it isn't, it ain't. That's logic!'

Lewis Carroll - "Alice in Wonderland"

The field of medical imaging is constantly looking for new and better techniques to represent and analyse the human body in a way that is useful for clinicians. Unfortunately, as previously discussed, medical images have quite poor signal-to-noise ratios, and thus need to be enhanced in order to become useable. It is important to realise that the SNR of medical images tends to be an order of magnitude poorer than for regular visible images, for which most image enhancement schemes have (naturally) been developed. Few image enhancement schemes have been developed specifically for medical images, nor have they been adequately tested on such images. It has repeatedly been demonstrated that filtering methods can substantially improve the quality of the image by eliminating artefacts and reducing unwanted information in the original image. They can also simplify the appearance of otherwise complicated anatomical structures.

Image filtering has already been discussed in the previous Chapter as an image pre-processing step used with several calcifications and mass detection algorithms. Conventional filtering methods include a background smoothing stage (e.g. convolution with a low pass filter) followed by enhancement of the structures of interest (e.g. high pass filtering) and the subtraction of the two newly obtained images. A single such method is not capable of dealing with the large variability of

the anatomical features that must be considered. There are numerous algorithms based on evolving partial differential equations (PDE) for noise removal and image enhancement, but, as noted above, few of them have been tested thoroughly on medical imaging. Ultrasound images are particularly noted for their very noisy appearance and there have been many attempts to develop noise removal filters in medical ultrasound imaging [117]. Several other algorithms deal with the application of diffusion tensors in MRI [140, 149, 173]. Since the detection of microcalcifications is hampered significantly by the presence of noise of similar shape and magnitude, a PDE filter for noise removal in X-ray mammography is developed in this thesis. The next section introduces the basic theory behind anisotropic diffusion, a particularly important example of such a PDE filter.

3.1 Anisotropic Diffusion

Anisotropic diffusion has its origins in the classical nonlinear diffusion filter developed by Perona and Malik in 1987 [133], which is based on a PDE in divergence form. It is the cornerstone for new developments in multi-scale image analysis aiming to simplify the image appearance while enhancing structures of interest, such as edges or coherent structures. Its name is derived from the classical diffusion (or heat) equation.

Anisotropic diffusion is the solution we adopt for its inherent properties of smoothing and edge enhancement, but other methods are reported in literature with good results in image regularisation. Amongst them, we mention morphological methods [125], which have a geometrical interpretation of images and are based on finding specific spatial characteristics in an image. Grey-scale morphology decomposes the image into its level sets [172]. The SUSAN noise removal and feature detector [155] is a nonlinear approach to feature detection that uses a circular mask for local measurements (excluding the central pixel). Those parts of the local image that are similar to each central pixel are used to compute the pixel's value. Wavelet packages [107] are also used to filter out high frequency noise through subspace decomposition of a characteristic

CHAPTER 4

4 Adapting Characteristics of the Human Visual System to Digital Mammography

Unlike the wine, science shouldn't be let to age

Grigore Moisil

In this Chapter, we present the results of a newly developed method to identify microcalcifications in mammograms using a model based on human vision. It is critical that any programme designed to assist radiologists detect microcalcification clusters misses few, if any, clinically important clusters. It is equally important that it does not yield too many false positives (FP). However, no method is perfect and though some have reportedly reduced the numbers of missed calcification clusters by as much as 20%, they continue to return too many FP. Previous methods can be classified as primarily statistical [80, 81] or structural [179].

Our method relies upon using a quantitative representation of breast tissue such as the Standard Mammogram Form (SMF) developed by Highnam and Brady [65]. Although the results presented below have been obtained using the SMF quantitative representation of breast tissue, this method *does not* depend upon the specific characteristics of the h_{int} and SMF representations. Our method will work interchangeably on any such representation, though, as we will demonstrate, there are significant advantages to applying it to the SMF representation.

The novelty of the technique derives from (a) the way in which the method analyses the statistical characteristics of the mammogram and (b) the particular combination of filters that are applied in sequence (statistical analysis, image enhancement, adaptive segmentation). In particular,

the algorithm adapts to digital mammography a model of how the human visual system functions for conventional visual images. The eye of a trained radiologist is more effective at detecting microcalcifications from a cluttered image than existing algorithms. For this reason, we use a novel measure for adaptively estimating image contrast, as explained further in this Chapter. The new measure adapts to local brightness and adjusts a threshold. Critically, this automated approach is adaptive and does not depend on the selection of multiple parameters. This is important for large-scale employment in mammography, where it is simply unfeasible to re-set parameters for each mammogram. We do this by a new method of adapting the filters to the characteristics of the particular image under consideration.

An overview of the algorithm is presented in Figure 40 with a clear separation of the stages we use to detect microcalcifications. While the top row in the diagram relates to the SMF generation (see Section 2.3) and Wiener filter (discussed in detail in Chapter 2), the bottom row underlines the steps that will be described in the following sections of this Chapter. Therefore, our input image is in SMF format and addressed as SMF-blurred-noGlare. In the pre-processing stage we remove shot noise and curvilinear structures (CLS) according to Section 4.1 and obtain SMF-noCLS. Then we compute the parameters of the anisotropic diffusion filter (addressed as statistical analysis and described in Section 4.2) and enhance the mammogram while removing the remaining noise; the result is SMF-AD. The map of microcalcifications is the output of the foveal segmentation explained in Section 4.3. Results and a comprehensive discussion of the parameters setting are included at the end of the chapter.

4.1 Pre-Processing

We have previously presented in Section 2.3 the new approach by Highnam and Brady for mammographic image normalisation offering a quantitative representation of the breast tissue, the h_{int} [65]. There is a drawback however, the extremely noisy appearance of these images that makes

their analysis more difficult. Although the signal-to-noise ratio (SNR) of the mammogram is improved slightly by the process that generates the h_{int} representation prior to glare removal, the subsequent glare removal step, which has the advantage of reducing the number of FP, has the disadvantage of drastically decreasing the SNR due to the amplification of high frequency noise.

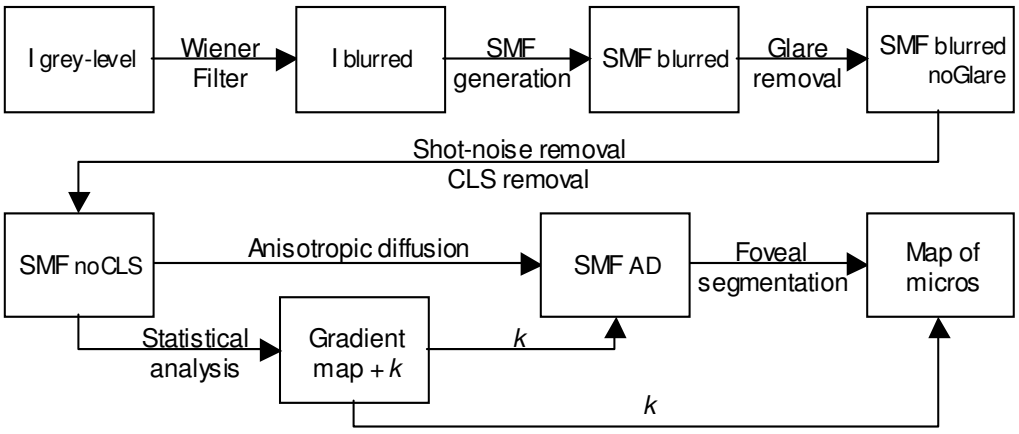

Figure 40: The diagram of the foveal algorithm to detect microcalcifications in Standard Mammogram Form images. The top row underlines the typical generation of an SMF image, including glare removal. The bottom row highlights the method described above: pre-processing, statistical analysis, image enhancement and adaptive segmentation.

Yam *et al*. [178] introduce a de-noising algorithm, which attempts to remove radiographic mottle [65], a major source of FP in microcalcification detection. This is achieved by applying a Wiener filter, adapted to the characteristics of radiographic noise, to the original image *prior to* the generation of the h_{int} image. As a result, the SNR is increased and the overall appearance of the h_{int} image improved. Since microcalcifications are also subject to noise, the amplified high frequency noise in the original h_{int} tends to disrupt small structures, such as microcalcifications. The new smoother version would reduce the number of false negatives (FN) in our detection algorithm.

To detect microcalcifications, we aim to filter the image in a way that blurs the background, but enhances calcium. Prior to the image enhancement and detection of microcalcifications, the normalised mammogram is pre-processed for shot-noise and curvilinear structures (CLS) removal. This step, described in the following section, eliminates some major sources of FP, as will be seen in the detection results.

The above flow diagram outlines the steps of the detection method including the foveal segmentation (c.f. Section 4.3). In the diagram, SMF is taken to mean any suitable quantitative representation of breast tissue, such as Standard Mammogram Form, I is the original grey-level image; *k* is the contrast parameter used in the anisotropic filter and the foveal segmentation:

4.1.1 Shot Noise Removal

The main causes of FP that we aim to eliminate are shot-noise and curvilinear structures [65]. The SMF generation process can easily detect film-screen artefacts [3, 66], at the glare removal stage. Therefore, glare removal may reduce the SNR, but would also minimise the number of FP in the detection of microcalcifications. Shot-noise generally refers to a noise process in a sensor in the scanner. Dust, hair or scratches on the intensifying screen or on the surface of the film (when it is subsequently digitised) are light attenuating. They have sharp boundaries in mammograms and can be treated as shot-noise. It has visual properties that are similar to those of microcalcifications. Highnam and Brady [65] note the absence of blur in such structures of noise in mammograms. The 3D shape of noise is sharp, as seen in Chapter 3, Figure 31. Using the point spread function of the intensifying screen; the points are identified and marked on a map (the energy imparted becomes negative after glare compensation where shot-noise is present, since it has been introduced to the image after the main blurring stage [66]). Using the binary information from the shot noise map, the artefacts can be removed from the SMF image by interpolating between their surrounding backgrounds. Figure 41 shows an example of shot noise removal.

4.1.2 Curvilinear Structures Removal

Curvilinear structures (CLS) in the mammogram arise due to anatomical features, such as milk ducts, ligaments, blood vessels and tumour spiculations. They appear relatively bright, thought not necessarily with high contrast, in mammograms and are typically long thin lines crossing parts of

the breast. They are locally linear, but may also curve on larger scales. Their detection is difficult due to the large variety of widths and lengths. Noise can easily disrupt the appearance of CLS in mammograms leaving isolated bright spots behind, which can easily be confused with microcalcifications. Also, at an intersection of two CLS in the image, corresponding to overlap of the CLS in the 3D compressed breast, the attenuations of the individual CLS add, producing a localised region of higher attenuation. Such points also appear similar to calcifications rather than noise.

The method we propose for CLS removal is based on the local energy model for feature detection of Kovesi [90] and is presented in [35, 36, 181]. For a more detailed review of local energy and phase congruency please refer to Appendix A. A recent development of CLS detection and removal is presented in [154] and we show results on initial experiments after removing CLS from mammograms using Schenk's multiresolution algorithm later in this Chapter.

The principles behind local energy and phase congruency methods are discussed next. From local energy we can search for features at points of maximum phase congruency, which are the points where the local Fourier components are maximally in phase [90]. Phase congruency highlights those points with maximum local energy. It is invariant to changes in image brightness and contrast, but scale affects the detection of relevant features. Local energy (*LE*) and phase congruency (*PC*) are expressed by Evans *et al.* as in Equations (57) and (58) [36]. (We used their formulae for computation; but for Kovesi's approach refer to Appendix A.) For the spatial frequency *j*, the local Fourier coefficients of a one-dimensional signal are:

$$\sum_{j=1}^{N}\left(A_j + iB_j\right) \qquad (56)$$

$$LE = \left(\sum_{j=1}^{N} A_j\right)^2 + \left(\sum_{j=1}^{N} B_j\right)^2 \qquad (57)$$

$$PC = \sqrt{\frac{LE}{\sum_{j=1}^{N}\left(A_j^2 + B_j^2\right)}} \quad (58)$$

When the Fourier components of the signal are in phase, *PC* becomes 1.

Things become slightly more complicated in the case of two-dimensional images (intensity mammograms, SMF images). *PC* becomes a function of position in the image and filter orientation. Kovesi proposes the convolution of the logGabor function with the image using the Fast Fourier Transform over 6 orientations and 4 scales. The logGabor filter appears as a hill of approximative Gaussian shape on the positive side of frequency (see Figure 105). This is in the frequency domain a good approximation of the sum between an even symmetric and an odd symmetric filter (multiplied by *i*) and the convolution with a logGabor can be seen as the sum of convolutions with both these symmetric filters. Performing the inverse FFT, we obtain the real part as the result of convolving with the even symmetric filter, while the imaginary part is the result of the convolution with the odd symmetric filter. For every scale and orientation, the magnitude and the phase of the convolution are computed. The size of the bandwidth is set as seen in Appendix A. The logGabor with a transfer function as in Equation (59) is used to obtain oriented wavelet filter (61), where ω_o is the centre spatial frequency of the filter (oriented wavelet filter), θ_o is the orientation of the wavelet, σ_o is the angular spread of the wavelet, $\log(k/\omega_o)$ is the wavelet's frequency spread and $S(\theta)$ is the cross-section of the transfer function in the angular direction (60). Through the computation of $LG(\omega)$, *PC* becomes $PC_\theta(x)$.

$$LG(\omega) = \exp\left(\frac{(\log(\omega/\omega_0))^2}{2(\log(k/\omega_0))^2}\right) \quad (59)$$

$$S(\theta) = \exp\left(-\frac{(\theta-\theta_0)^2}{2\sigma_\theta^2}\right) \quad (60)$$

$$G(\theta,\omega) = S(\theta)\times LG(\omega) \quad (61)$$

Evans, Yates and Brady [36, 181] make the following two assumptions in detecting CLS from *PC*:

- the intensity profile of a CLS perpendicular to its local orientation is a one-dimensional peak (e.g. cos(φ)), with a phase within $-\pi/2 \le \varphi \le \pi/2$;
- $PC_{\theta+\pi/2} > PC_{\theta}$ at a CLS of orientation θ, since CLS are long and thin.

The weighted mean local phase in the direction θ, φ_{θ}, is calculated using scaled wavelet filters and unless $-\pi/2 \le \varphi_{\theta} \le \pi/2$ for a given pixel, then the pixel does not belong to a peak and is discarded. Alternatively, PC_{θ} is calculated. The step is repeated at regularly spaced intervals of θ and a pixel is labelled as CLS if $| PC_{\theta+\pi/2} - PC_{\theta}| > 0$ for all orientations θ. The CLS labelled pixels are now output in a binary map of CLS. The choice of scale and parameters is critical for a good CLS detection, as Evans and Yates remark [35, 181].

The CLS removal algorithm, in its original implementation [35, 36], gets the best estimation of CLS as in Figure 102. One major reason behind this over-estimation is the development of the method for mammograms of smaller resolutions than the one we use to find microcalcifications. Also, calcifications were not relevant for the validation of the original CLS removal method and therefore their removal along the CLS not considered important. The implementation we propose uses a smaller wavelength, which makes it more sensitive to smaller scales. Furthermore, we reduced the number of scales over which features are detected by phase congruency to avoid marking as CLS the calcifications, as small structures that still have local orientation. The downfall is that there are discontinuities that appear in the true CLS and their removal leaves bright areas on the mammogram that do not correspond to real structure with that particular form and characteristics (similar to microcalcifications). To avoid having such discontinuities and major errors in image manipulations, we followed the original algorithm proposed by Evans *et al.* and dilated the features appearing in the binary CLS map. After dilation, a smooth interpolation is required.

To perform the smooth interpolation, we adopted the solution proposed by Evans, which uses the Matlab Image Toolbox function *roifill*. This function takes as input (in this particular

application) the mammogram and the corresponding binary CLS map. The interpolation is done from the boundary of the non-zero contours in the CLS map inwards, using the pixel values from the mammogram. Each non-zero region is treated separately during the interpolation. The criterion used is to solve Laplace's equation with specified boundaries. This may be interpreted as finding the smoothest interpolation on the interior of the boundary by solving a heat equation. The Matlab implementation of Laplace's equation solves a sparse linear system using finite differences.

Figure 41 shows an example of CLS removal and a binary CLS map. The amount of estimated CLS is large and shows responses of the algorithm to very weak edges, which induces a smoothing effect in those areas when the removal/interpolation is performed. This is an undesired side effect of the algorithm. These are the results obtained using Evans et al.'s method, when a good compromise is achieved in removing CLS without removing microcalcifications. A more accurate CLS removal technique is proposed in Section 4.4.2 and will be employed in future work.

4.2 Statistical Analysis and Image Enhancement

There are various methods, which may be used to do image enhancement, for example anisotropic diffusion-based filtering (cf. Chapter 3) which aims to blur the input mammographic image while preserving certain intensity changes, such as small regions of interest. The process relies on the use of a set of numerical parameters, often referred to in the image processing literature as time, contrast, and size. It has been found in practice that it is essential to determine the right choice of parameters to obtain good reproducible results. Our method automates the parameter setting for each individual image, and in this way it eliminates the need to set parameters.

The method exploits Weickert's solution [172] for the diffusion tensor. It uses a similar simplified and stronger tensor having eigenvalues (62), where I is the initial image, I_σ the Gaussian smoothed image (σ is the standard deviation or scale), k a contrast measure and n a suitably high power, such as 8 or 12.

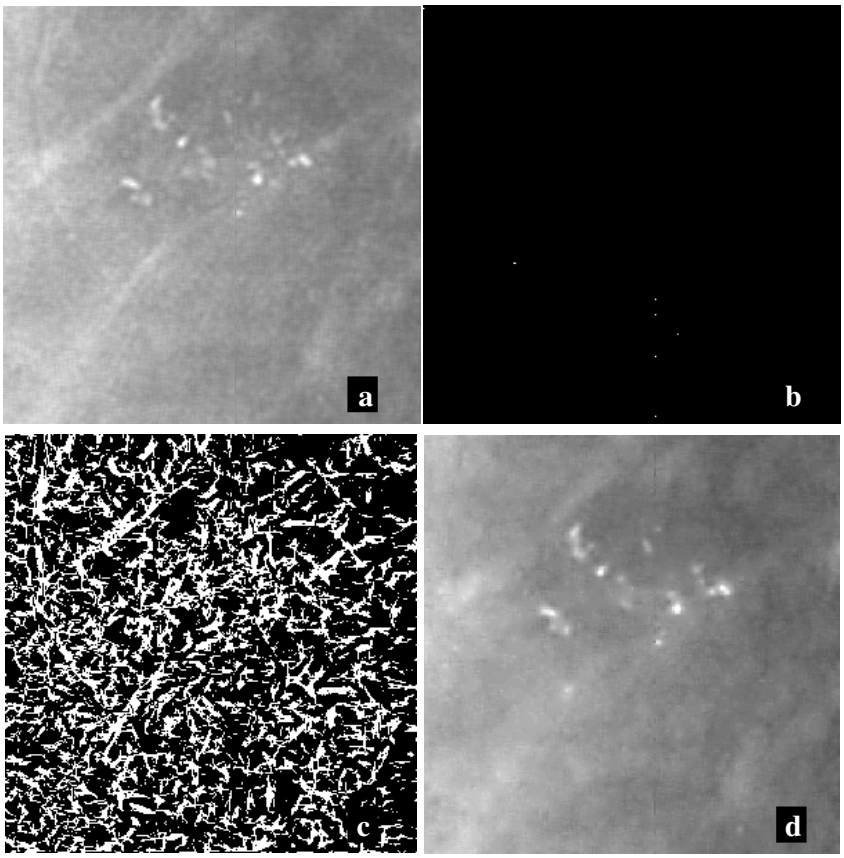

Figure 41: Removing artefacts; (a) the original image; (b) the binary shot-noise map (white dots are noise); (c) the binary CLS map; (d) the 'clean' image after shot-noise and CLS removal.

$$\lambda_1 = \begin{cases} 1 & |\nabla I_\sigma| = 0, \\ 1 - \exp\left(\dfrac{-1}{(|\nabla I_\sigma|/k)^n}\right) & |\nabla I_\sigma| > 0 \end{cases} \qquad (62)$$

$$\lambda_2 = 1$$

As we have noted in the previous Chapter, the parametric format of anisotropic diffusion makes this process highly dependent on the fine-tuning of its input parameters. In practice, the more complex and variable the images in a dataset, the more problematical it is to choose a single set of values for these parameters that works well for the entire dataset. Critically, by any measure, mammograms are very complex images, whose appearance varies widely across a population (at a centre, hospital, region, country, or continent), yet any microcalcification detection algorithm must

generate very few FP and have even fewer false negatives (FN). One possible approach is to provide for interactive setting of parameter values; but this is unacceptable in clinical practice.

Microcalcifications are typically extremely small, therefore a small scale σ is desirable. Since *t* is not an image characteristic, we choose to vary only *k,* which is image dependent. Now we can iterate the blurring filter for a constant number of iterations over the image, but this raises the problem of how to choose the contrast parameter to determine the values of the eigenvalues (**62)**.

Our method uses an adaptive Gaussian derivative filter (**63)**- (**66)**. The application of this filter to a de-noised, glare-removed h_{int} image results in a gradient-map that highlights suspicious regions as regards microcalcification detection. Furthermore, the same filter outputs the value of *k* for the subsequent diffusion. Figure 43.c.,d. shows two examples of such gradient maps. Having the gradient map and the resulting value of *k,* we apply the anisotropic diffusion filter to the h_{int} image with the corresponding value of *k* for a fixed number of iterations and set scale. The new images will generally be blurred, except possibly for some suspicious regions that will have their edges preserved, as in Figure 43.e.,f. Note the emphasised outline of the microcalcifications, while most of the background is blurred. By using the adaptive filter to compute the value of *k,* the anisotropic diffusion filter becomes robust, easy to use and automatically adapted to the image characteristics. The value of *k* represents the threshold selecting only the top 4.4% outstanding features in an image, a statistical value related to the sum between the *mean* and two *standard deviations*. Since the mean of our matrix is null (see Figure 42), equation (66) takes a simpler form.

$$K_\sigma(I) = \frac{1}{2\pi\sigma^2} * \exp\left(-\frac{|I|^2}{2\sigma^2}\right) \quad (63)$$

$$M = |K_\sigma'(I)|; \quad (64)$$

$$g_i = M_i - \frac{1}{N}\sum_{j\in\delta_i} M_j \quad (65)$$

$$k = 2*\mathrm{std}(g) \quad , \quad (66)$$

where $K_\sigma(I)$ is the Gaussian of image I, M the Gaussian derivative, g_i a classical measure of local contrast in a neighbourhood of N pixels, while k is the computed contrast value to be subsequently used to filter the image.

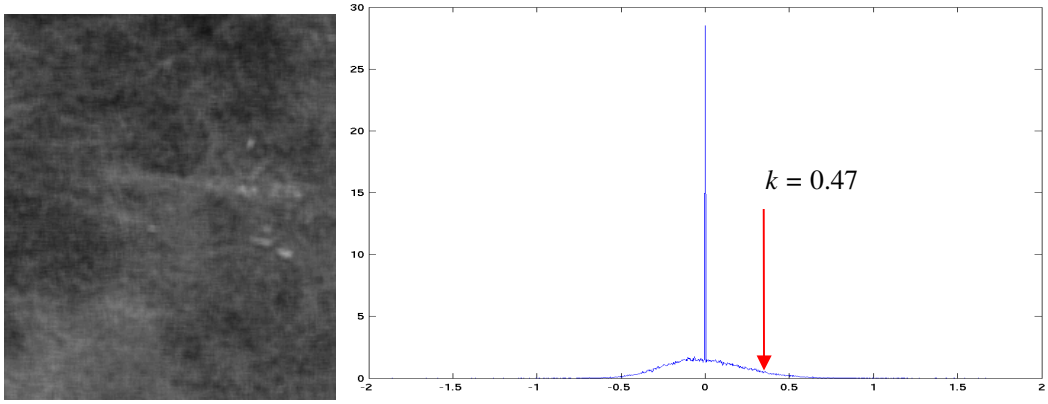

Figure 42: An example of estimating k. The image shown on the left (after expanded display contrast) has the associated histogram of function g in the right. We note the zero mean value of g, as well as where the value of 0.47 of k falls.

4.3 Foveal Segmentation

An important goal in present image processing and computer vision methods is to integrate spatial models that reveal the sensitivity of the human visual system (HVS) at various intensity transitions and texture variations in an image. There is over one century of research behind trying to fully understand the way the HVS functions. A major contribution to this on-going research was brought by Holladay in 1926 [69] and later by Moon and Spencer in 1943 [118]. They introduced the fundamentals of the way the human processes visual scenes. Nevertheless, the process is very complex and still not entirely understood [6], which make it difficult to design comprehensive models of HVS.

The final step in our method to detect microcalcifications is an adaptive segmentation method. It is well known that the Human Visual System (HVS) is highly sensitive and can detect fine details in noisy or textured images. Image processing aims to reproduce the quality of these results.

Recently, Heucke *et al.* [62] introduced a computational model for the HVS. In their method, foveal contrast depiction is adapted to the object surrounding and background.

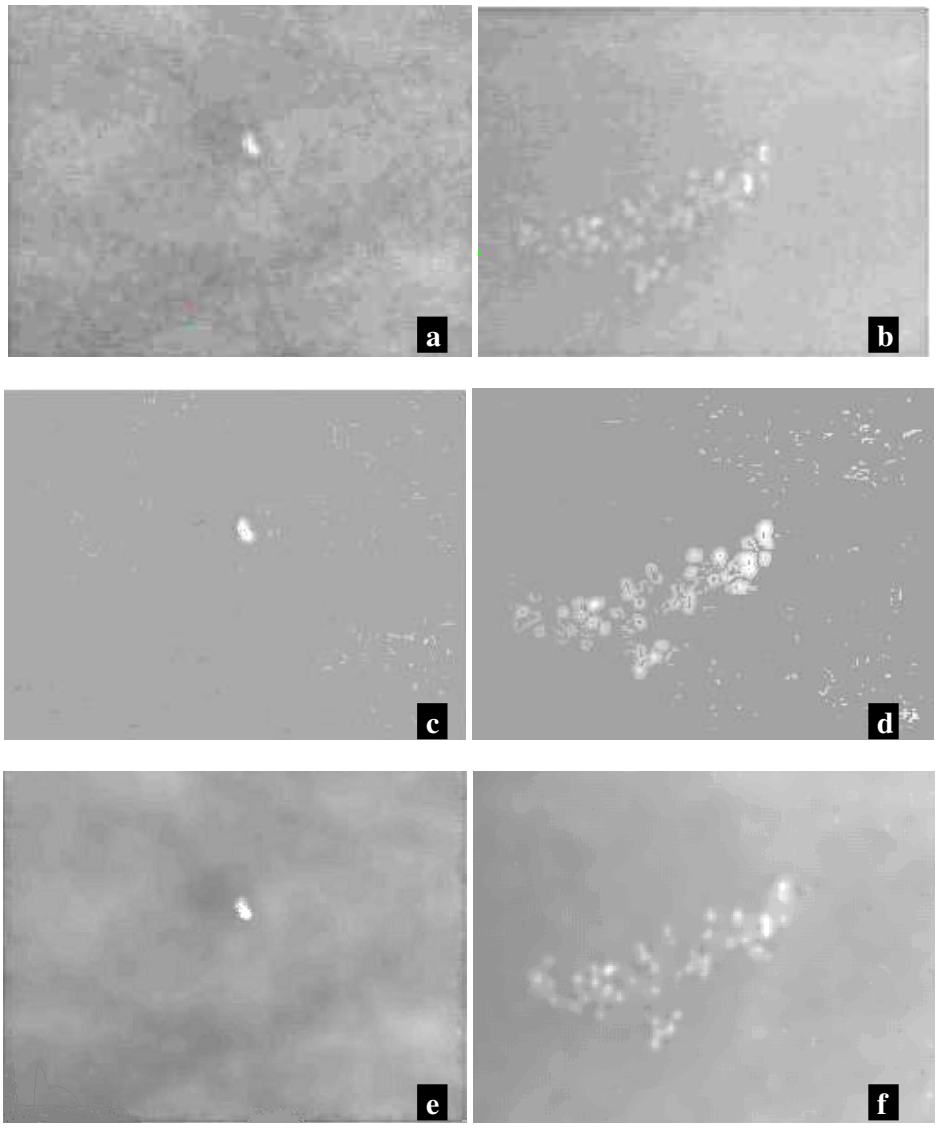

Figure 43: Automated image enhancement; (a) an image with an isolated calcification; (b) an image with a microcalcification cluster; (c) the corresponding gradient map for image (a) depicting the microcalcification and some extra undesired regions; (d) the corresponding gradient map for image (b) with a good representation of the cluster, but some falsely suspicious areas as well; (e) the automatically diffused image (a); (f) the diffused image (b);

The adaptation of the eye to light changes is a continuous process in HVS. We perceive objects differently if they are against a bright surface (for instance a window in a sunny day) or dark area

(a dark wooden panel). The adaptation luminance proposed in [118] is the response of the eye in adding an average luminance within the central visual field or fovea (L_{fov}) and an equivalent veiling luminance caused by the luminance of surfaces surrounding the peripheral field of view (L_{seq}) as in (67). However, the foveal adaptation owes mainly to the luminance within the foveal field and only approximately ten percent to the luminance of the field of view outside of that of the fovea [118]. The literature proposes 7.7% of the adaptive luminance to be due to the background luminance [62], which gives a value of 0.923 to our weight w (see below). In practice, we studied the effect of varying w with 10% more or less than the proposed value and a comparative FROC curve is shown in Figure 61.

$$L_a = L_{fov} + L_{seq} \qquad (67)$$

Furthermore, the visual perception of the eye is dependent on the spatial perception of the object we perceive. This effect is called lightness assimilation. The same object may appear lighter on a dark background and darker over a light surface (see Figure 44). The eye is still perfectly capable of distinguishing the three central areas, but this is not obvious for a computer programme.

Figure 44: An illustration of the lightness assimilation. We show three synthetic images with dark (left), medium (middle) and bright (right) backgrounds. All have central objects of the same size and intensity, but are perceived differently by our eyes, due to the variance in background lightness.

In the mammographic environment, the main advantage of the human eye over CAD methods is the depiction of microcalcifications in dense areas of the breast. At the same time, the radiologist must not pick FP in the dark areas. This is the result of the adaptation to background, which is

equivalent to lowering thresholds in bright areas and increasing them in dark areas, basically an inverse proportionality to the background. While in our synthetic images the background is constant, in a mammogram we must consider the neighbouring area of the foveal kernel, as shown in equation (**70)**. The adaptive threshold model that we propose for the detection of microcalcification applies the above-mentioned concepts in the mammographic setting for the improvement of abnormality detection in the breast.

Previous contrast measures used in mammography seek to establish a minimal constant contrast difference all over the mammogram [80]. The contrast ($C_{classic}$) is calculated at every pixel as the difference between that pixel value (p_0) and a weighted sum of the pixel values in an immediate neighbourhood (N) (68), where n is the number of pixels in N. $C_{classic}$ is then compared with a fixed threshold, C_{thresh}, over the whole image and microcalcifications are marked. The variation in height in an SMF image or intensity in a typical mammogram makes it far easier to detect microcalcifications against a fatty background but more difficult to detect correctly against a denser background [9]. In like manner, computer vision algorithms often find it more difficult to detect faint contrast changes against a bright background than against a dark background. The HVS, however, adapts to the local image contrast, and detects faint contrast changes in a manner essentially independent of the background. We have adopted a similar model of contrast detection in the HVS for mammography with the aim of improving the accuracy of the detection.

We initially remove the glare, shot-noise and CLS from the SMF image. Having the SMF_{noCLS} image, we compute a set of mean values using masks for the inner area (within the boundary of calcification), its neighbourhood (the local area around the calcification) and background (the rest of the breast tissue). The histogram of the inner surface will provide the mean of the object (μ_O), as the histogram of the whole image will give us the mean of the background (μ_B). The mean of the neighbourhood (μ_N) is defined as the weighted sum of intensities depending on the scale of the mask. A synthetic image designed to illustrate the kernels used for object (O with the mean μ_O), neighbourhood (N with the mean μ_N) and background (B with the mean μ_B) is shown in Figure 45. The perceivable contrast C is calculated according to equation (69):

$$C_{classic} = p_0 - \frac{1}{n}\sum_{i \in N} p_i \quad (68)$$

$$C = \begin{cases} \dfrac{\mu_o - \mu_N}{\mu_N}, & if \mu_o > \mu_N \\ 0, & otherwise \end{cases} \quad (69)$$

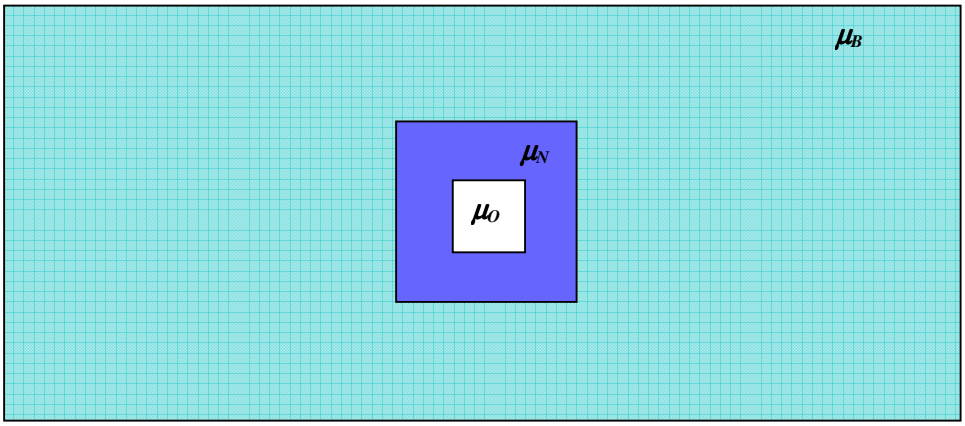

Figure 45: The foveal masks used for the computation of μ_O, μ_N and μ_B. The object *O* is the area of the *fovea centralis*, *N* its neighbourhood (twice the size of *O* in our applications) and *B* the background.

We then compute C_{min} (70), where $\mu_A = w\,\mu_N + (1\text{-}w)\,\mu_B$ and w is a suitable weight between 0 and 1 affecting the amount of background implied in the computation of contrast. We have found that w=0.877 to 0.923 gives good results. We will use the value of 0.923 for the default value in comparative studies, as proposed in literature [62]. The segmentation parameters are set-up automatically based on the image-adapted value of *k*, as computed from the statistical analysis, (discussed in Section 4.2). We found that $c_w = \sqrt{k}/200$ is appropriate for a conservative detection. Areas in the SMF image having $C > C_{min}$ are marked as microcalcifications. In practice we have found that the value b=0.0808 has given good values.

$$C_{\min} = \begin{cases} \frac{c_w}{\mu_N}\left(b + \sqrt{\mu_A}\right)^2, & \mu_A \geq \mu_N \\ \frac{c_w}{\mu_N}\left(b + \sqrt{\frac{\mu_N^{\,2}}{\mu_A}}\right)^2, & \mu_N > \mu_A \end{cases} \quad (70)$$

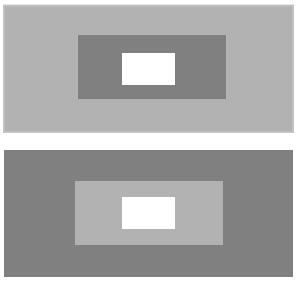

Using C_{min} instead of C_{thresh}, the contrast is adapted locally, not only globally, in a manner similar to that of the HVS. Figure 46 shows how the variation of perceivable contrast varies with the background in the HVS adaptation method versus classical methods. While C_{min} varies with the local image characteristics, C_{thresh} is constant over the whole image. Microcalcifications can be correctly depicted in a fat background for both contrast measures, but in a dense background the detection is facilitated by the adaptability of C_{min}.

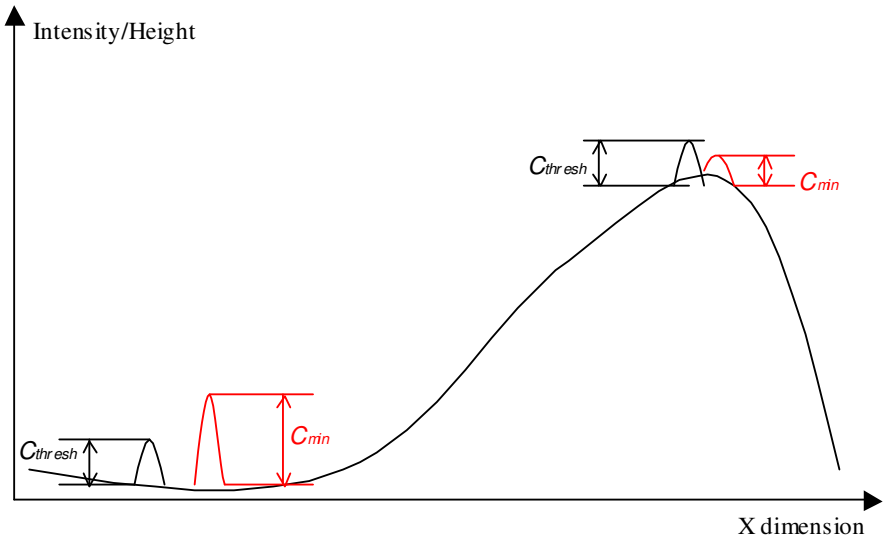

Figure 46: The simulation of a plot of a mammogram section containing microcalcifications over height/intensity variation. The variation of the perceivable contrast in the detection of microcalcifications is suited to the local characteristics for the adaptation of HVS using C_{min}. The classical minimal perceivable measure, (here called C_{thresh}) is a global characteristic of the mammogram and less flexible in the elimination of FP in the detection of microcalcifications.

The function C_{min} (70) is a measure of contrast sensitivity. It sets the threshold from which objects in the image are visible for the observer, a measure of the eye's ability to perceive luminance gradients. Through the use of the minimal perceivable contrast (c_w), it includes a measure of the image brightness. (Imagine varying the amount of objects we can distinguish with the naked eye by using a pair of sunglasses.) The variation of C_{min} over a set of synthetic images presenting variations between background (see Figure 47), neighbourhood and object is shown in Figure 48. Using the adaptive thresholding qualities of HVS we can depict all the high peaks in these images, which would be impossible with a simple threshold. For the parameter b in the C_{min} equation, we used the value 0.0808, as proposed in [118] with good segmentation results.

Figure 49 shows the Free-response Receiver Operating Characteristic (FROC) curve of the tested microcalcification detection method based on the adaptation of HVS. We used a database of 102 samples of digital SMF images. 78 of them contain between 1 and 3 clusters per image, while 24 are normal mammogram samples. There are a total of 98 clusters of microcalcification annotated in the database. All images were digitised at a resolution of 50μm and have sizes under 1500x1500. We further show some examples of microcalcification clusters detection in Figure 50 - Figure 54. A cluster is detected if it contains at least three microcalcifications, where a distance of maximum 0.5 cm (approximate value) connects each calcification to the rest of cluster. Recursively, we noted that the distribution of detected FP/image is equal in samples with microcalcifications and in normal samples. Along with the original SMF sample and the microcalcification detection map, the figures show intermediate results from the following stages; we also show the gradient map resulting from the statistical analysis, the CLS map and the enhanced SMF sample after applying the automated anisotropic diffusion filter described previously. The detection process is non-parametric and fully automated, being adapted to the local and global image characteristics.

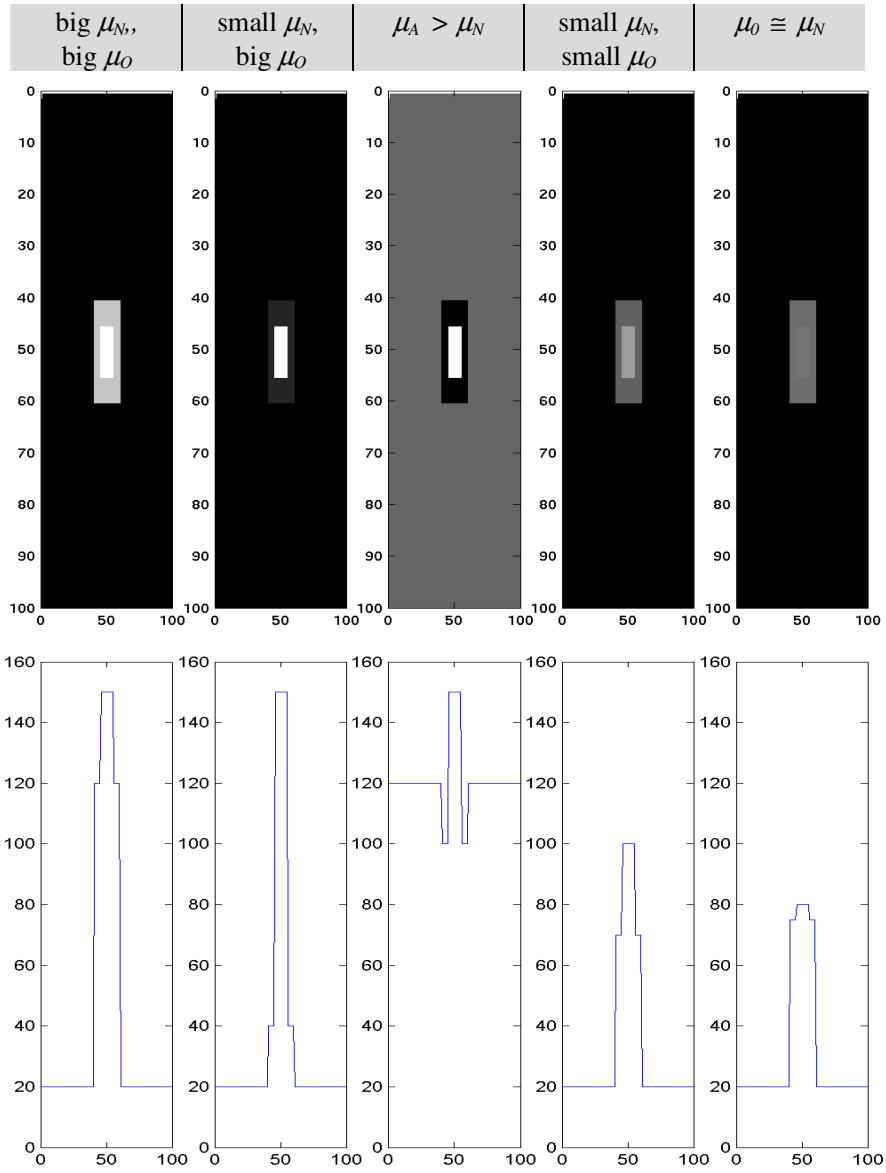

150	150	150	100	80	μ_O
120	40	100	70	75	μ_N
20	20	120	20	20	μ_B
0.25	2.75	0.5	0.4286	0.0667	C

Figure 47: A set of five synthetic images with variations between object, neighbourhood and background and their associated cross-sections. These examples cover a wide aspect of contrasts in image processing: bright on dark, bright on bright, dark on dark. The corresponding values of μ_O, μ_N, μ_B and C are shown in the table below the figure. The variation of the adaptive threshold is shown in Figure 48.

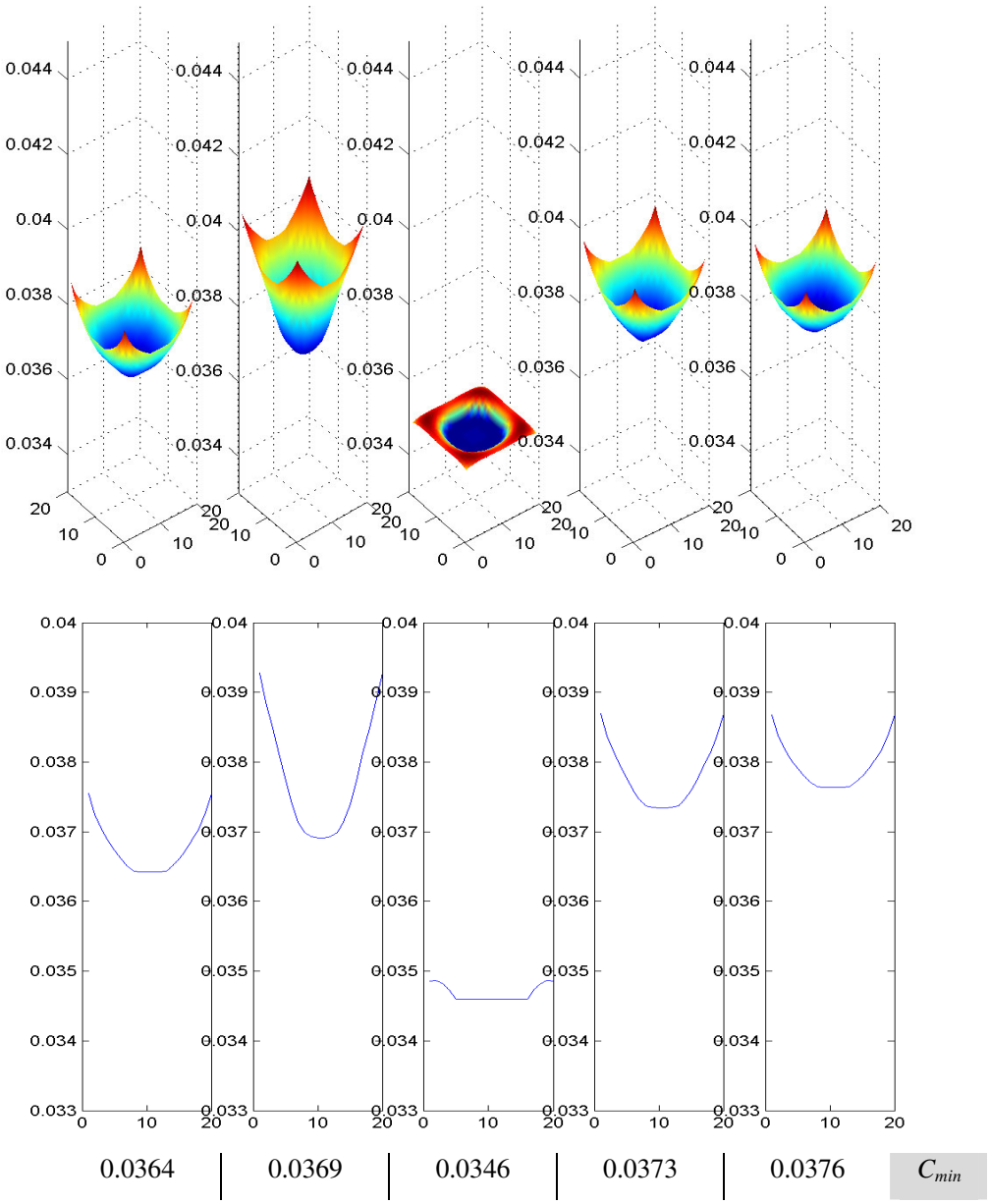

Figure 48: The variation of the adaptive threshold C_{min} for the synthetic images in Figure 47 in the central area of images, which corresponds to the object and neighbourhood surface. For this example, we used c_w=0.03. The value of C_{min} in the centre of fovea is shown in the table below the figure. We note that for the most delicate case (extreme right), C_{min} and C are in the same range of values. In such difficult cases, which approximate better the mammographic environment where transits between different intensities are much smoother, the adaptation of C_{min} become crucial. Moreover, $C > C_{min}$ in all five cases and all peaks are detected.

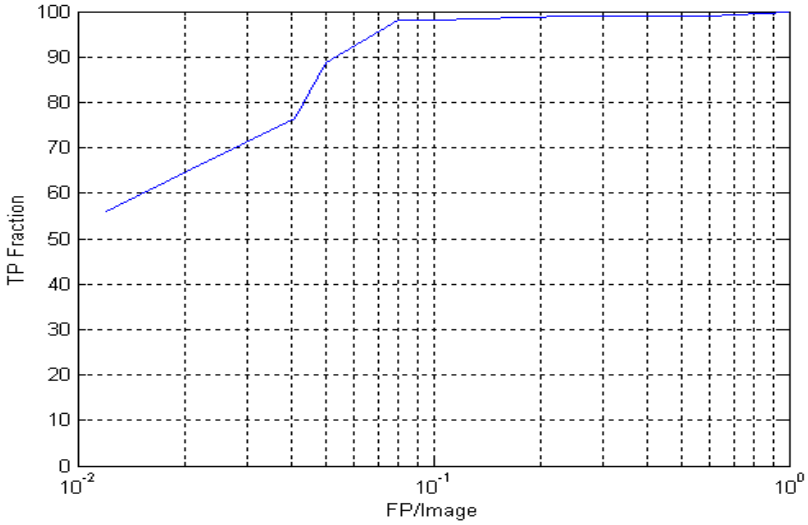

Figure 49: The FROC curve of the microcalcification-detection method based on the adaptation of HVS in digital mammography.

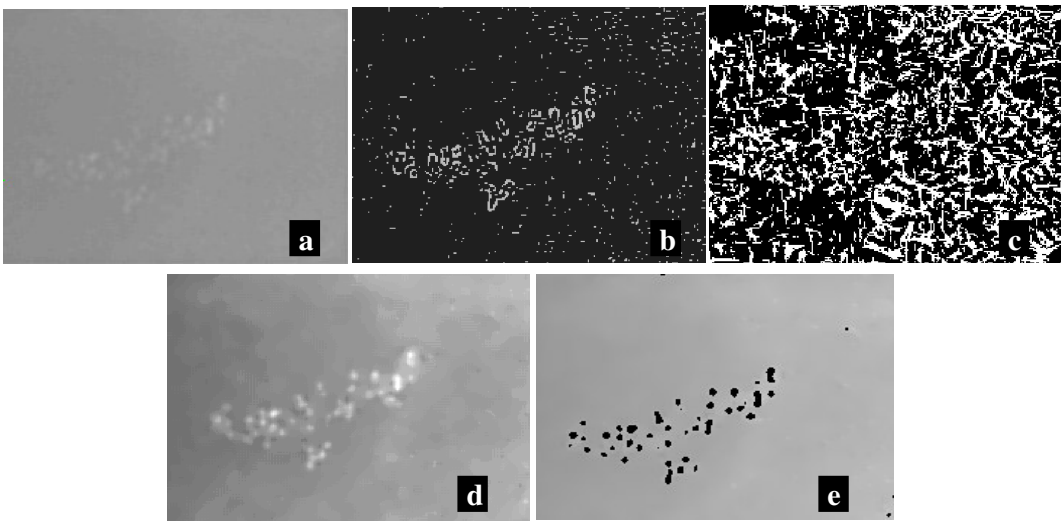

Figure 50: Detection example 1: (a) the original SMF images with a microcalcification cluster; (b) the gradient map from the statistical analysis depicting suspicious pixels; (c) the CLS map; (d) the enhanced image after diffusion; (e) the microcalcification detection map.

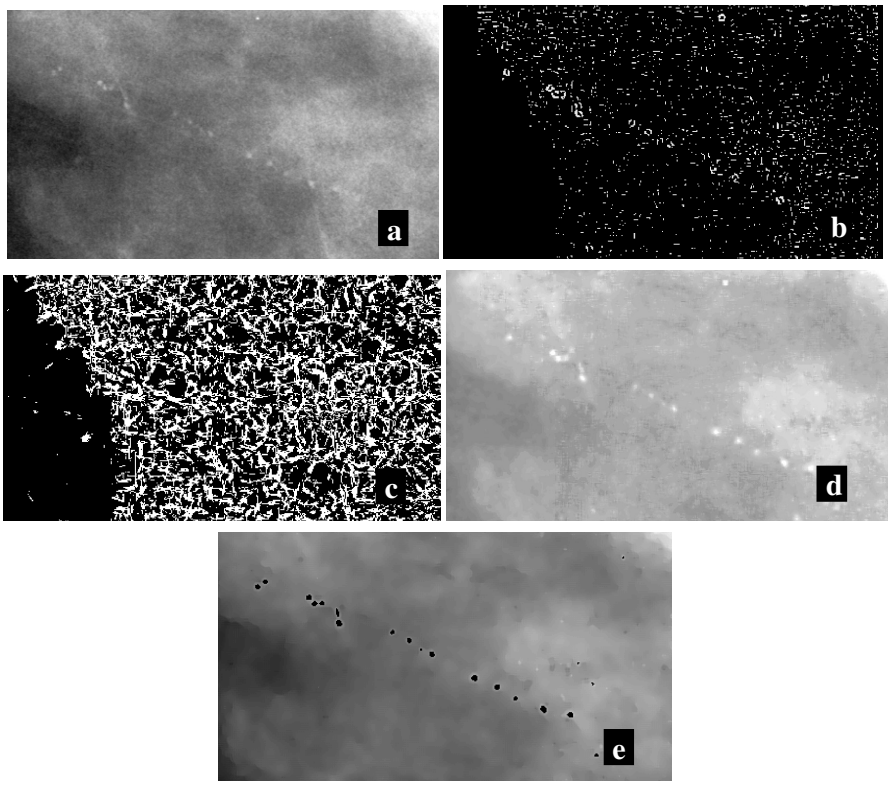

Figure 51: Detection example 2: (a) the original SMF images with a microcalcification cluster; (b) the gradient map; (c) the CLS map; (d) the enhanced image; (e) the microcalcification detection map.

4.4 Discussion

We have presented a fully automated non-parametrical method to detect microcalcifications in digital mammography. The result of applying it to a mammogram (typically an SMF image) is a map of detection, which highlights the microcalcifications present in the image. As the FROC curve in Figure 49 shows, the detection rate on a 102 set of mammogram samples reaches 98% TP fraction at 0.1 FP/image. All the microcalcification clusters in the tested images are correctly detected at 1.1 FP/image. The most difficult case was a cluster in the breast margin (see Figure 55). Since the margin of the breast in mammogram has not been compensated, the characteristics of microcalcifications in that area are atypical and their detection becomes difficult.

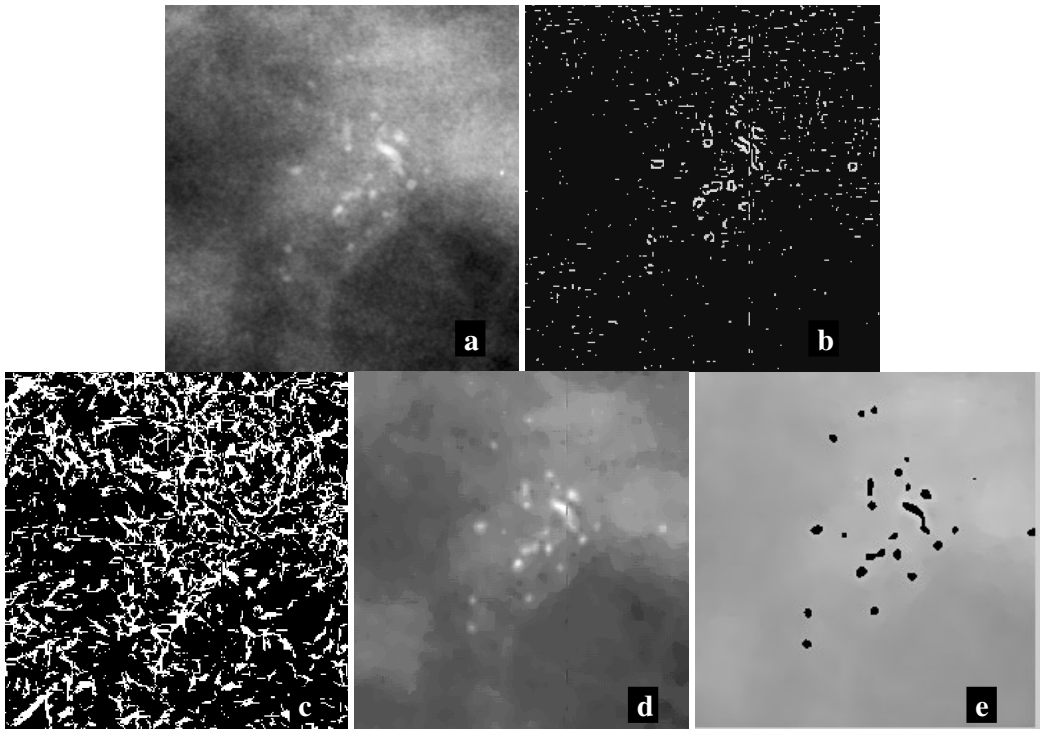

Figure 52: Detection example 3: (a) the original SMF images with a microcalcification cluster; (b) the gradient map; (c) the CLS map; (d) the enhanced image; (e) the microcalcification detection map.

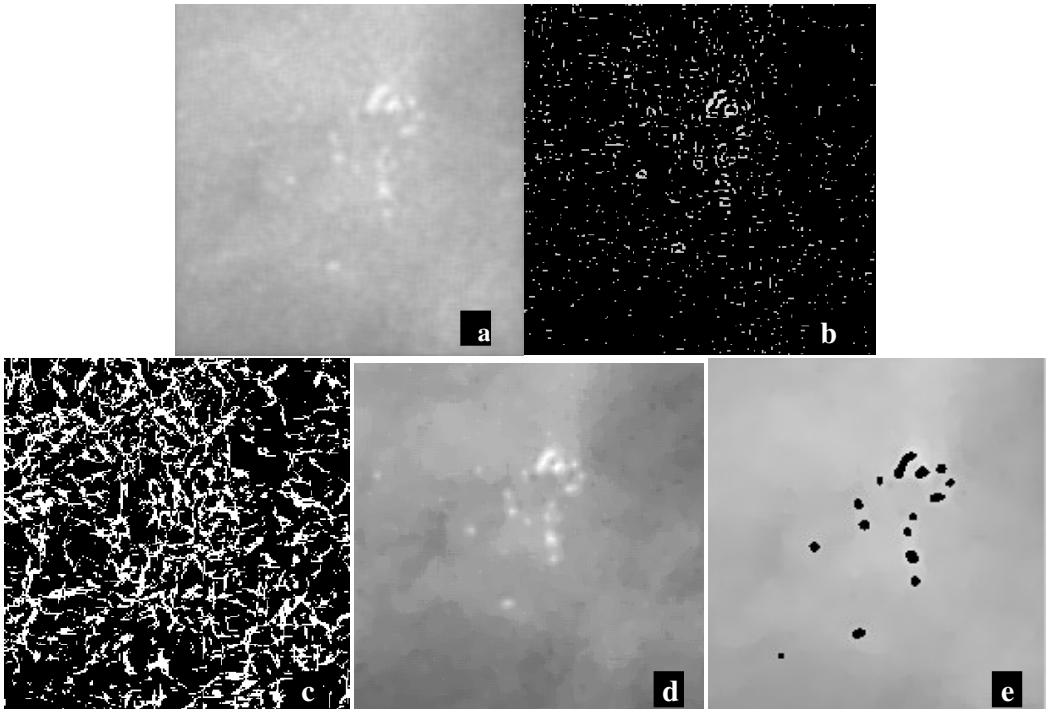

Figure 53: Detection example 4: (a) the original SMF images with a microcalcification cluster; (b) the gradient map; (c) the CLS map; (d) the enhanced image; (e) the microcalcification detection map.

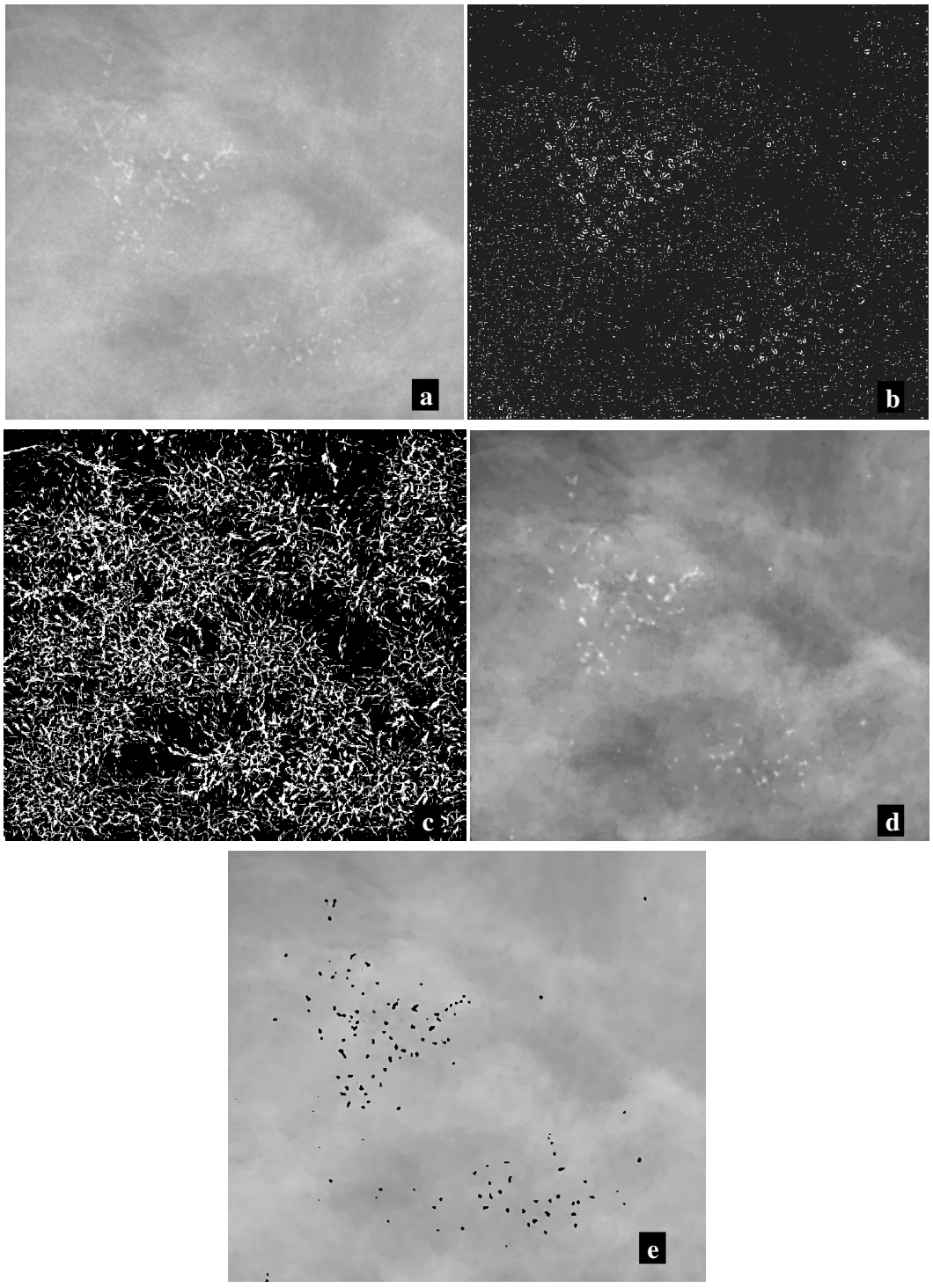

Figure 54: Detection example 5: (a) the original SMF images with a very large microcalcification cluster; (b) the gradient map; (c) the CLS map; (d) the enhanced image; (e) the microcalcification detection map.

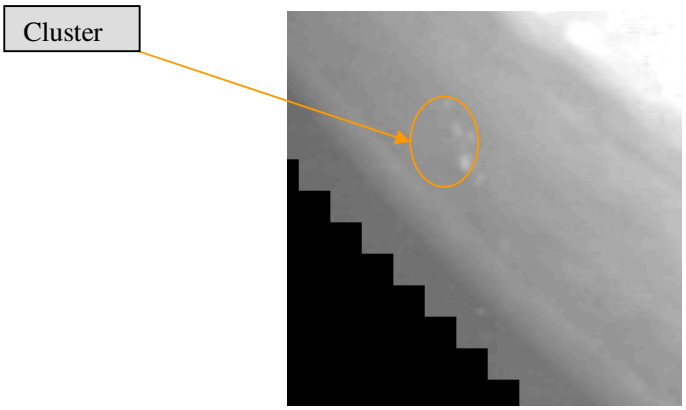

Figure 55: A case of difficult detection with a faint microcalcification cluster in the breast margin. The contrast in the image has been enhanced for the reader to help in the visualisation of the cluster.

Adding adaptive contrast segmentation based on human foveal processing significantly enhances the detection of microcalcifications (see Figure 76). However, the variability of microcalcification appearance is very large and the algorithm may struggle with some difficult cases. The robustness of the method comes from the sequence of filters applied to the mammogram; the complex processing of images makes the algorithm slow when working with entire mammograms (generally images of 4500x4500 pixels). Therefore, a faster implementation of it may be required.

4.4.1 Comparative ROC Analysis

In this section we present comparative FROC curves to test the response of our method with variations in algorithm and input images. We will see the impact of CLS removal, the changes with the variation of the minimal perceivable contrast, the results on intensity images and on whole mammograms.

4.4.1.1 CLS Removal

We will first test the influence of the CLS removal step in the detection of microcalcifications. Although the number of FP is lowered (see Figure 57 and Figure 56), the method is not perfect. To make sure that no microcalcifications are eliminated during this step, we preferred a conservative approach. This may leave some CLS residuals in the image, which may lead to FP in the detection. Also, we may still lose some small microcalcifications during the CLS removal, which does not seriously affect the detection of the cluster, as seen in the examples below.

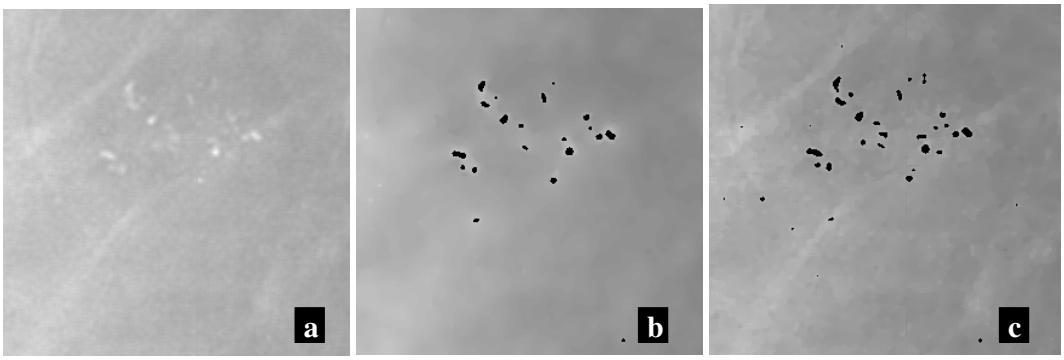

Figure 56; Another example of CLS removal in detection: (a) the original mammogram; (b) the detection map using the CLS removal; (c) the detection map without CLS removal with a few extra FP detected.

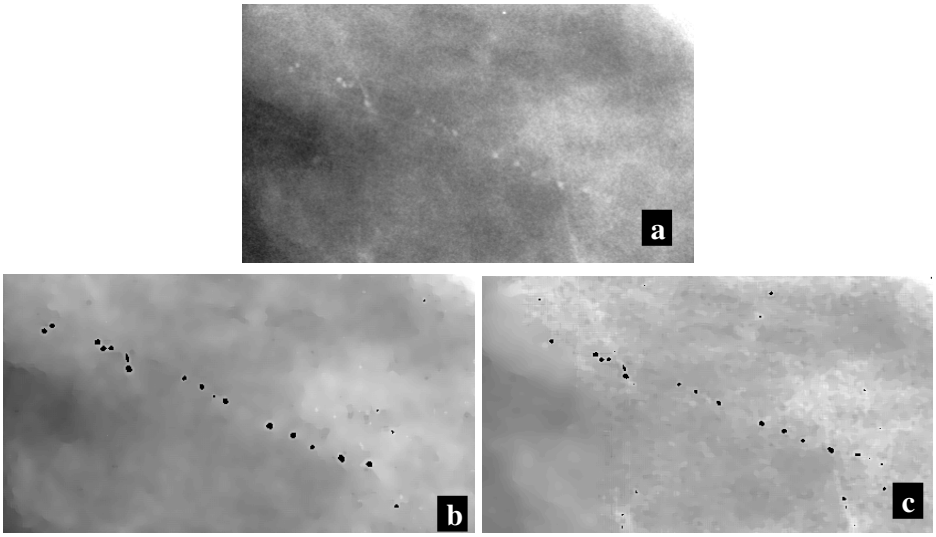

Figure 57: CLS removal in detection: (a) the original mammogram; (b) the detection map using the CLS removal; (c) the detection map without CLS removal with a few extra FP detected.

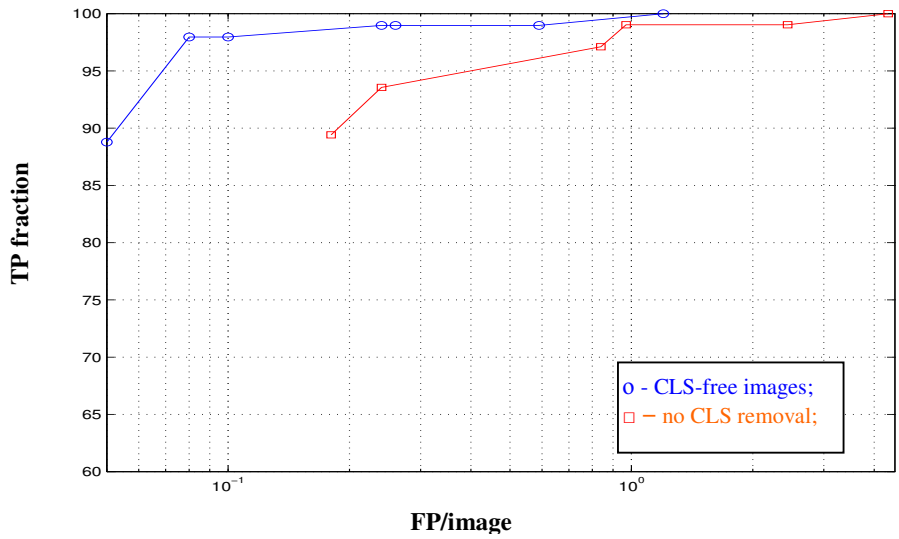

Figure 58: The comparative FROC curve when CLS are removed or not prior to the microcalcification detection

In Figure 58 we show the comparative FROC curve of our method applied on original images, which are not pre-processed with the CLS removal algorithm versus CLS-free images. The response of the algorithm is vastly superior when CLS are eliminated prior to microcalcification detection. The large number of FP caused by the presence of CLS delays the FROC response when CLS are not removed.

4.4.1.2 Image Diffusion

The pre-processing of our database includes, as highlighted along the manuscript, the smoothing of images by anisotropic diffusion. The reason for employing smoothing along the algorithm has already been mentioned in previous sections. What is still left to be done is comparing the performance of the method with and without smoothing to get a clear understanding of the effect of diffusion on the detection results. The whole algorithm is replicated without the smoothing step and the comparative FROC curve is shown in **Figure 59.** An example is also shown in Figure 60, where we can compare the detection results with and without smoothing on a mammogram sample. Although the smoothing is expected to remove some of the very small or faint microcalcifications, the clusters are well preserved using the nonlinear qualities of anisotropic

diffusion. Notably, the higher number of FP detected when no smoothing is present reduces considerably the performance of the algorithm.

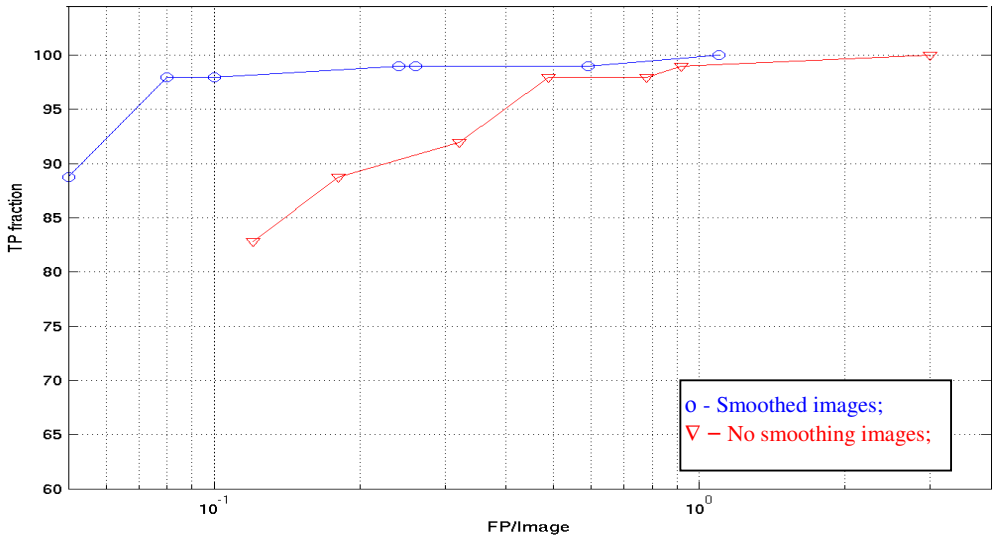

Figure 59: The comparative FROC curve when smoothing by anisotropic diffusion is performed or not prior to the segmentation of microcalcifications.

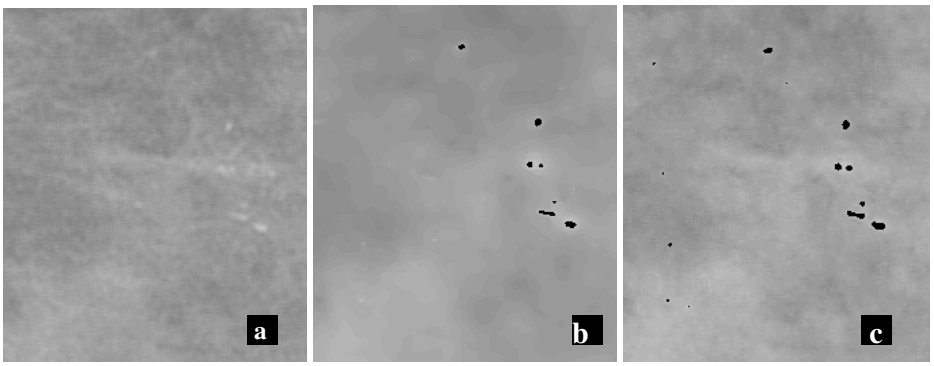

Figure 60: Image smoothing in detection; (a) the original mammogram sample; (b) the detection map using anisotropic diffusion; (c) the detection map without using smoothing with FP marked.

4.4.1.3 Perceptibility

In Section 4.3 we mentioned the significance of *w* in setting the minimal perceivable contrast for obtaining the best detection results when our algorithm is applied. We ran parallel tests to test the consistency of our conclusion to use the value 0.923 for *w*. Therefore, we varied the value of *w*

over 5-10% and found that the detection peak is achieved when *w* is set between 0.877 and 0.923. However, a 5% difference in the value of *w* does not change significantly the detection results, although the efficiency of the algorithm is slightly lowered. Figure 61 shows the comparative detection results with the variation of *w*.

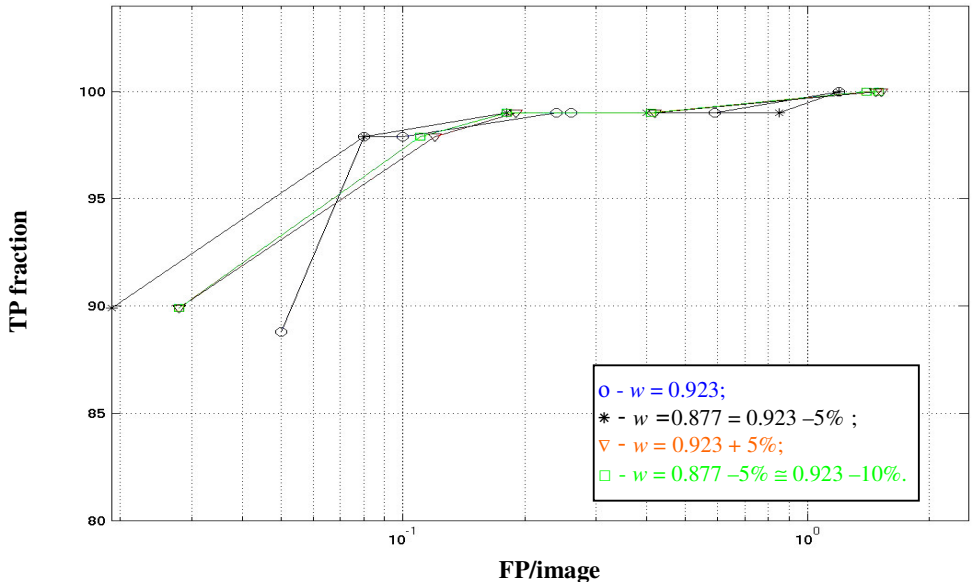

Figure 61: The comparative FROC curve when *w* is varied over a range of 5 to 10% of its default value of 0.923. The difference in detection results is quite small and all four algorithms converge smoothly to 100% TP ratio.

4.4.1.4 Intensity Images

The obvious question we have to ask ourselves at this point is how well would the algorithm perform on intensity images and if the results are similar to those obtained on SMF images. We used the same 102 images, this time intensity images corresponding to the previously used SMF images, and tested our method over the same range of parameters as in the case of the SMF images that generated the above FROC curve. The results are shown in Figure 62. The detection algorithm performs similarly on intensity image, with a slower convergence, for the same set of parameters as for SMF images. The shape of the FROC curves makes a great difference to the number of microcalcification clusters detected at a particular number of FP/images, especially on the left side of the curves. This is the area of the FROC curve that corresponds to clinical results.

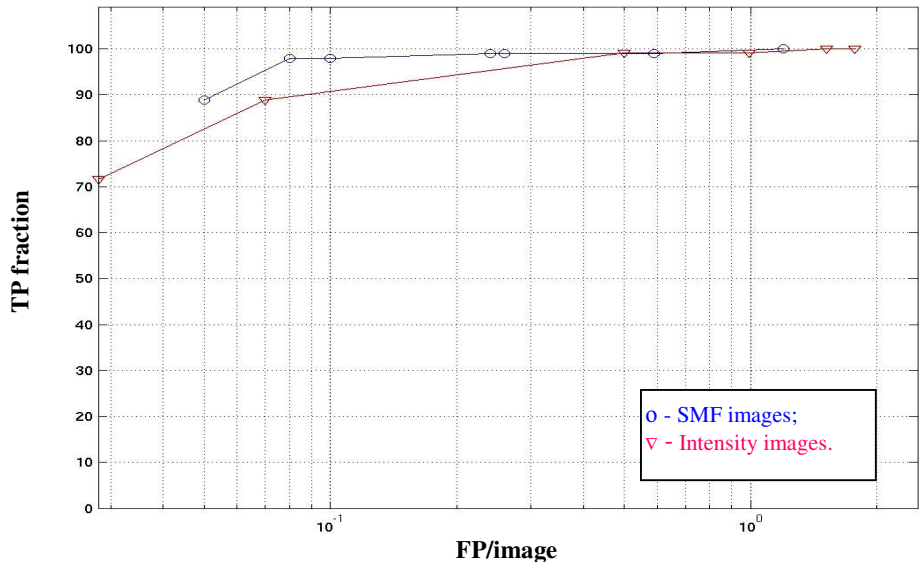

Figure 62: Intensity versus SMF comparative FROC curve. The detection algorithm converges slightly slower for intensity images, but reaches the same performance as for SMF images. One reason for the delay could be the use of same parameters when building the FROC curve, although the image characteristics (intensity versus SMF) are different.

4.4.1.5 University of South Florida Database

The ultimate goal of any CAD algorithm is to perform correctly on any given similar database, no matter where it comes from. As is acknowledged by many authors (not least those who constructed the University of South Florida database), without image normalisation this is hard to conceive of. The SMF generation algorithm is designed to help in this difficult situation, but excepting the Oxford database, no other image collections have mammograms in SMF format. Our detection algorithm, through its parametrical relation to the image attributes, facilitates the generalisation of detection standards, but without the use of a normalisation algorithm (a corner stone in our reasoning), the results are not ideal.

We used for comparison a collection of images from the University of South Florida Digital Database for Screening Mammography (DDSM). More precisely, we applied our algorithm to mammogram samples digitised at 43μm/pixel with annotated microcalcification clusters. They have similar sizes to the image samples from the Oxford Screening database (c.f. Section 4.3).

The major difference between these images and the ones from Oxford is the image resolution. To compensate for this difference, we conversed the values of σ in the anisotropic diffusion step (see Section 4.5.2) to build a Gaussian kernel of approximately same size. In the Oxford database (at 50μm/pixel), σ was 0.6, which has the same physical size as a σ of 0.7 at the new resolution. Also, the kernel of fovea in the foveal segmentation (see Section 4.5.2) becomes 11 instead of 9 to be in accordance with the parameter setting reasoning. These conversions are done automatically at the launching of the application in agreement with the user specified resolution.

The new database consists of 82 image samples, of which 58 show abnormalities in the form of microcalcification clusters and 24 are normal. The abnormal images contain between 1 and 4 clusters/image and the total number of clusters is 82. All images are intensity images, as termed before, therefore the FROC curve shown in Figure 63 compares the performance of the microcalcification detection algorithm between the Oxford Screening Database in intensity form and the DDSM collection.

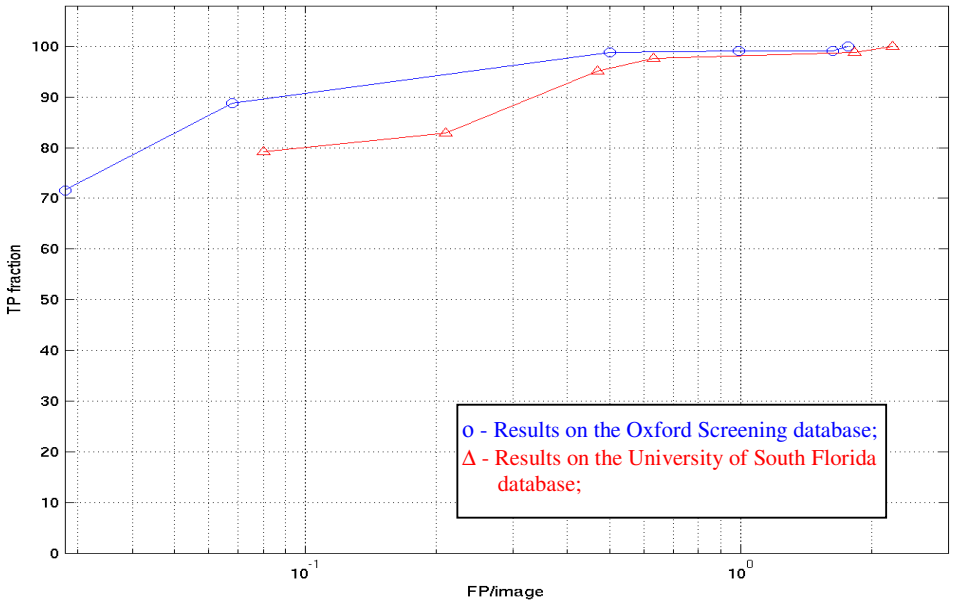

Figure 63: The comparative FROC curve between the detection results on intensity images from the Oxford Screening Database and the University of South Florida Digital Database for Screening Mammography .

As expected, the algorithm performs better on the Oxford Screening database, on which the parameters were originally trained. Nevertheless, the detection results on the two databases converge at about 0.5 FP/image and they both achieve 100% TP fraction in the vicinity of 2 FP/image. A more appropriate test of the detection algorithm on the DDSM database will be done when images will be available in SMF form.

4.4.1.6 Whole Mammograms

The results used in building the previous FROC curves are based on processing cropped samples of mammograms from the Oxford Screening Database. All experiments were performed on a 1.2 GHz Pentium III class workstation with 1 GB RAM. Nevertheless, it was very computationally expensive to test the detection method on whole mammograms, which are sized 3549x4816. This is mainly caused by the implementation of our method in Matlab, which uses extensive memory and slows down the processing time due to the high-level programmeming. By doing some algorithm optimisation, the processing was made possible for the illustration of results on detecting microcalcifications in the full surface of breast.

The breast margin is detected in SMF, thus a threshold above 0 removes the background. Now we can compute the value of k for the inner area of the breast. The detection results are accurate and similar to those achieved on mammogram samples (see Figure 64). The size of the images processed does not influence substantially the number of FP/image in the left side of the FROC curve. On the right side of the FROC curve, where the algorithm aims to achieve a detection rate of 100%, the difference in the number of FP is more substantial. We used a total number of 83 mammograms in SMF format from the Oxford Screening Database. 59 of them contain between 1 and 5 clusters/image, adding the total number of clusters to 85, while 24 mammograms have no sign of abnormality. The clinicians of the Oxford Breast Care Unit of the Churchill Hospital set the ground truth.

The most challenging cluster to detect remains the one shown in Figure 55. The presence of CLS remains the main source of FP, or more precisely their imperfect removal. A few isolated

calcifications were also depicted, but they were not labelled as microcalcification clusters (they were located in groups of less then 3 calcifications, the minimum number required in the detection method). In Figure 65 we present detection results on whole mammograms; we indicate with ellipses the TP microcalcification clusters and with arrows the locations of FP.

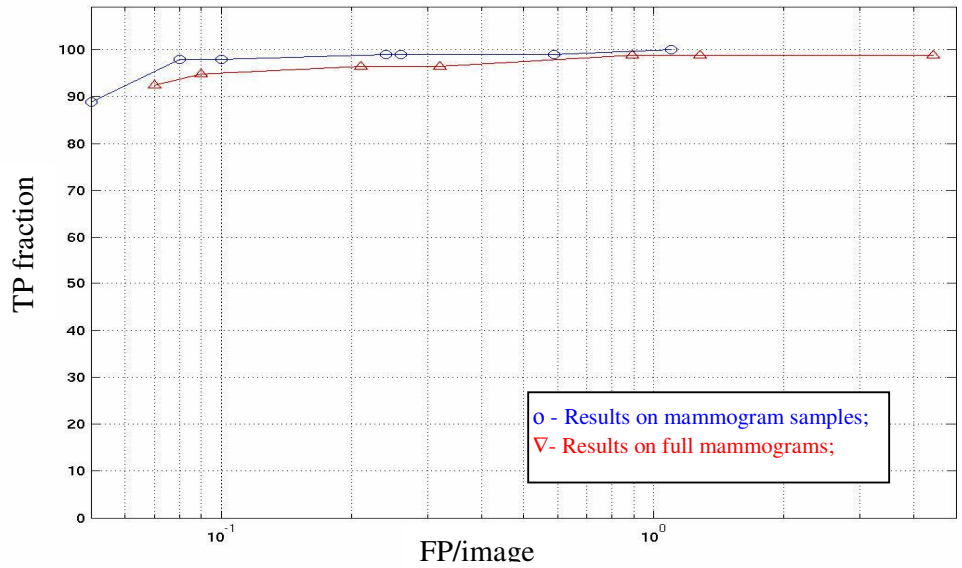

Figure 64: The comparative FROC curve of the detection of microcalcifications when mammogram samples are used versus full mammograms. The behaviour of the algorithm is similar and robust with the image size.

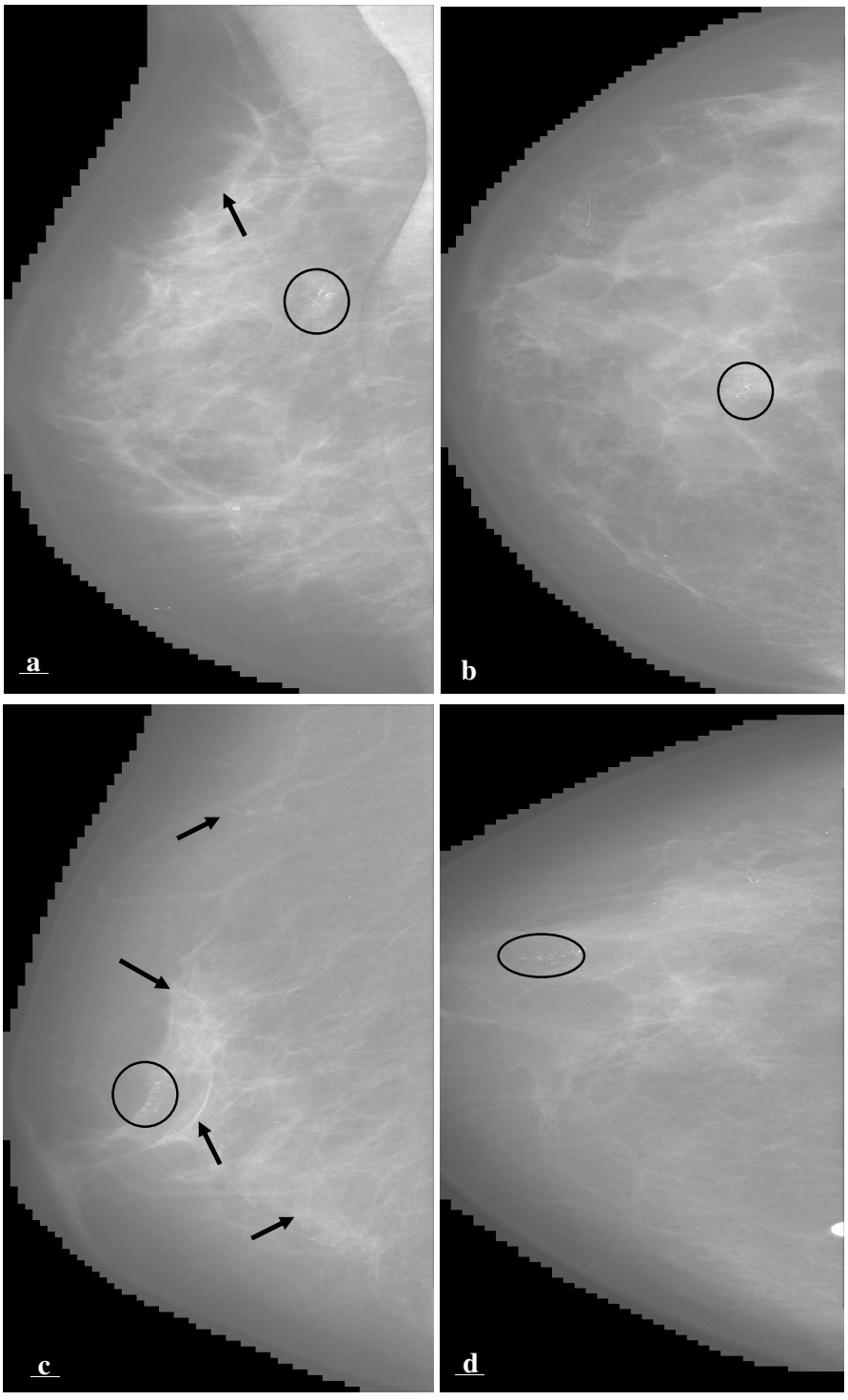

Figure 65: Detection results on whole mammograms; (a) and (c) are the MLO SMF images, while (b) and (d) the corresponding CC images. Ellipses indicate the locations and spread of the detected microcalcification clusters, while arrows indicate the positions of FP.

4.4.2 An Alternative CLS Removal

This alternative method we present here to detect and remove CLS is a refined version of the phase congruency presented earlier in this Chapter (see Section 4.1.2). We have used local energy (LE) and phase congruency (PC) to detect and then remove CLS from mammograms. The results are substantially improved (see Figure 58), but the CLS removal algorithm leaves artefacts in images that can be misinterpreted as microcalcifications. In this section we discuss an alternative method to detect and remove CLS based on multiresolution oriented local energy analysis [154]. We encounter the same major problem, namely the wide range of scales and orientations of CLS. Using multiscale analysis, CLS are detected as a collection of edge-ridge-edge lines with similar orientations at the correct scale. The condition that neighbourhoods must follow the same model removes a substantial number of the CLS candidates highlighted by LE. Through exact interpolation between the edges, no artefacts and undesired smoothing are introduced. The proposed algorithm is detailed below.

4.4.2.1 Theory

The motivations behind detecting and removing CLS have already been discussed in this thesis, but to briefly summarise:

- CLS are thin bright structures corresponding mainly to healthy tissue in the breast;
- They complicate the textured appearance of a mammogram;
- Their scale and brightness resembles that of microcalcifications and CLS crossings correspond to bright blobs;
- CLS related to blood vessels, ducts or ligaments may be confused with tumour spiculations;

Schenk and Brady [154] make the following assumptions in their work on CLS detection: CLS are locally linear; they have well-defined orientation; CLS are high-frequency (small-scale)

structures. Local energy (c.f**.** Appendix A) gives responses to all CLS feature (i.e. the centre and the edges of the CLS) and uses phase to distinguish between these as in Figure 66. An effective computation of orientation can be performed.

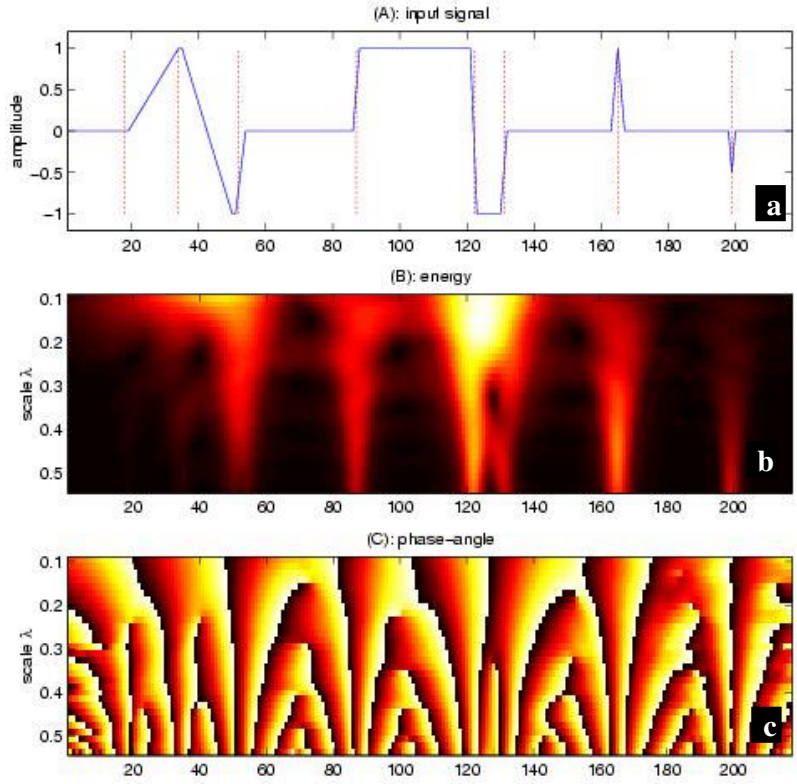

Figure 66: The response of local energy to a variety of input signals: (a) the input signal; (b) the local energy response; (c) the phase-angle response.

The local energy decomposition is done by polar-separable quadrature filters in the Fourier domain, which are implemented as steerable filters. The computation is performed using an even-symmetric filter (71) and a corresponding odd-symmetric filter for the radial part with a negative lobe on the negative frequency axis. For the angular component of the filters (spread at N orientations over a half-circle) the cube of the cosine is used (72) and its absolute value for the odd and respectively even-symmetric filters. Figure 67 shows the steerable quadrature filter pair. Empirically we found good practical results by setting $N = 4$ over three scales.

$$F(\lambda) = \log\left(\frac{1}{\lambda}\cos(x)^2\right) \qquad (71)$$

$$A(\phi_n) = \cos^3(\phi - \phi_n); \qquad \phi_n = \frac{n\pi}{N} \tag{72}$$

The Fourier transform of the image is multiplied by each of the filters and the inverse transform calculated. The filter response is computed for each pixel at each scale by a vector sum weighted by the amplitude of the oriented filter coefficients.

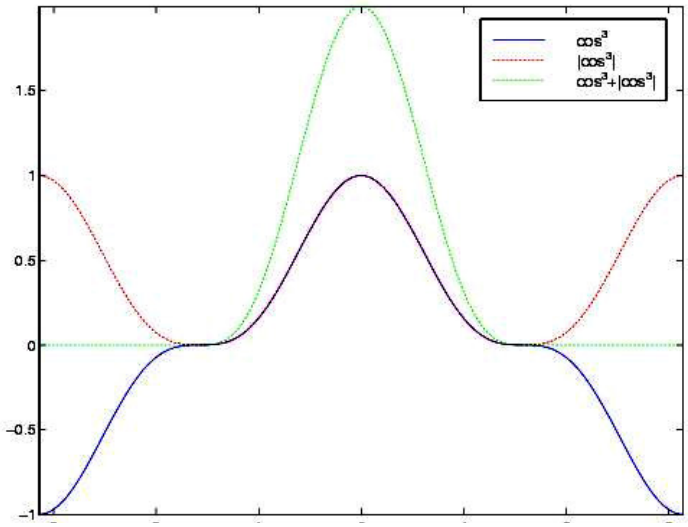

Figure 67: The angular part: a steerable filter.

The method uses phase to find all locations corresponding to positive going lines (ridges) and locations corresponding to positive/negative going edges. A point on a CLS must consist of an edge-ridge-edge triplet of similar orientation and correct scale. Figure 68 shows an example of ridge-edge combinations. The immediate neighbours of the CLS must follow the same scale-dependent rule.

At each pixel of a CLS, an approximate width of the structure is computed by selecting the scale that has the largest magnitude coefficients. The width is used at each pixel to remove the CLS by interpolating between pixels neighbouring each edge. The algorithm uses histograms of immediate small neighbourhoods to randomly sample the points in-between, weighting the values by the distance to either step-edge.

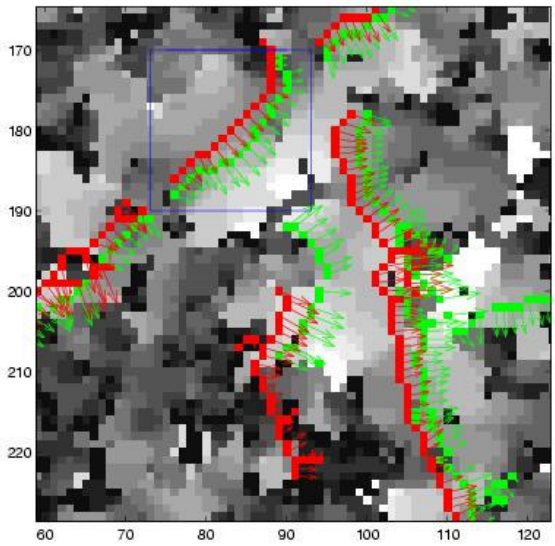

Figure 68: A simplified example of edge-ridge-edge triplet. The background is a scale image; ridges are shown in green, while edges in red. The lengths of the vectors express scale**.**

4.4.2.2 Initial Results

In Figure 69 we can see an example of CLS detection on a sample of real mammogram. The example is design to show the robustness of the detection and removal on an image containing CLS, microcalcifications and a mass. The CLS map over three scales is shown along with a close up exemplifying the edge-ridge-edge triplets detected from the filter response.

Having detected CLS, we removed these lines from the image and applied the microcalcification detection algorithm to both the original mammogram sample and the CLS-free image. The two sets of results are shown in Figure 70. A notable improvement can be seen from the incorporation of this multi-resolution CLS detection stage. The microcalcification clusters are preserved over the CLS removal, since CLS are now manually removed at different scales depending on the filter response. Furthermore, edges are not erroneously detected, as they do not respect the edge-ridge-edge rule, while microcalcifications are not affected, as they do not fit in the model at the right scale. At this initial testing stage, the method to remove CLS seems more performant than the phase congruency-based algorithm presented earlier. Note that the scale selection and CLS detection were done manually

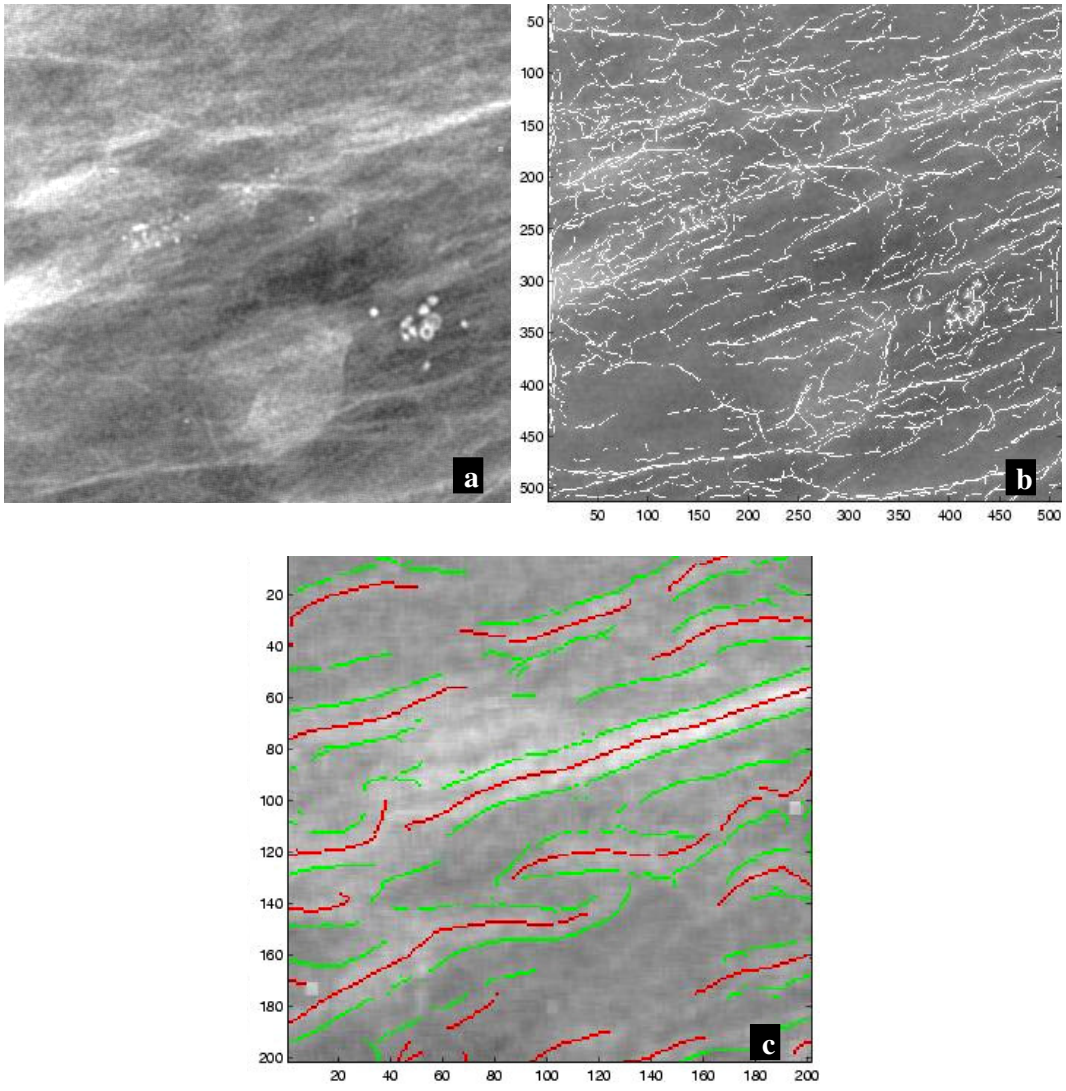

Figure 69: An example of CLS detection: (a) the original mammogram sample containing a mass, two clusters of microcalcifications and CLS; (b) the CLS map over 3 scales; (d) a close-up of the upper right corner of image (a) showing the edge-ridge-edge triplets (edges in green, ridges in red). The CLS are detected using manual thresholding over each scale.

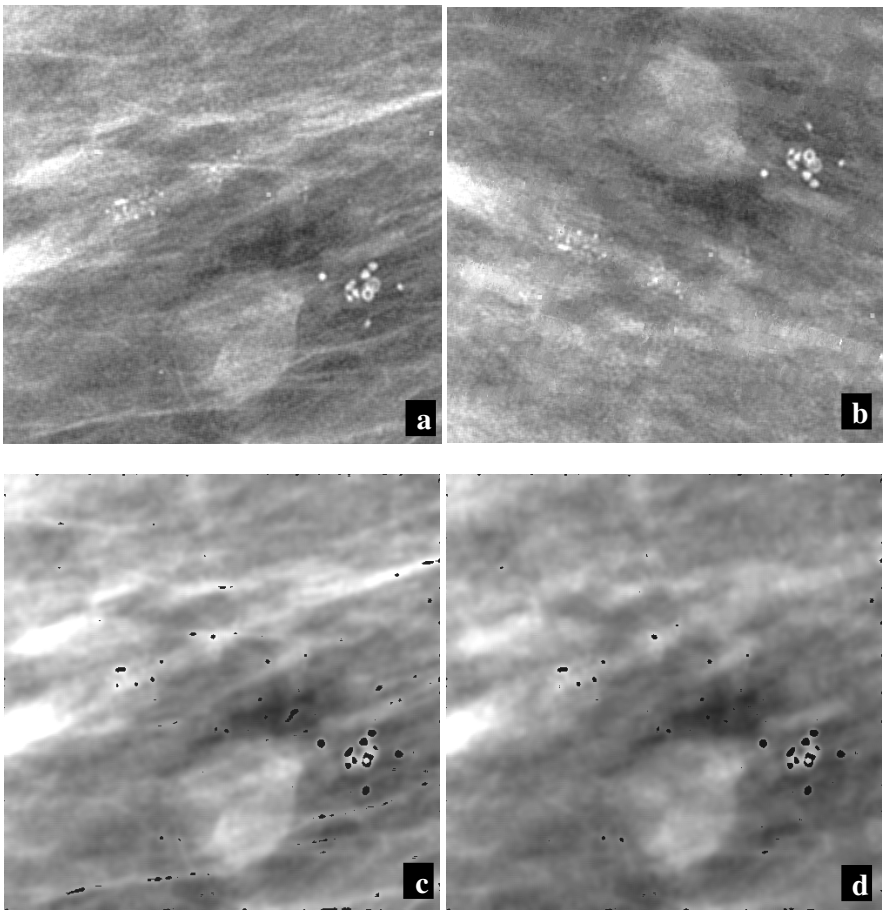

Figure 70: An example of microcalcification detection: (a) the original mammogram sample; (b) the CLS-free mammogram sample using Schenk and Brady's algorithm; (c) the CLS map before CLS removal with a large number of FP; (d) the CLS map after CLS removal with improved results and a significant reduction of the number of FP.

4.4.2.3 Discussion

The new CLS detection method can reliably differentiate between CLS and other high-frequency components in a mammogram, which are congruent over scale. A better and more complete CLS removal can be performed without risking the removal of microcalcifications or excessive interpolation. However, when we performed experiments involving an automated selection of scales the results were different. We marked a CLS at the first scale that gives response to it. Unfortunately, most microcalcifications gave responses to one scale or another when no manual thresholding was used. While the number of FP was significantly lowered, most microcalcifications were lost and the features of the detected clustered seriously altered. Thus, the

CLS detection based on multiresolution oriented local energy analysis must be further developed before imbedding it in an automated detection algorithm for microcalcifications.

4.5 The Detection of Microcalcifications using SMF

4.5.1 Comparative Results

This section compares three algorithms that operate upon the h_{int} representation (or the SMF) to detect microcalcifications. Two of these algorithms have been described previously in this thesis; one is the method presented in the last sections (using image enhancement, CLS removal and foveal segmentation) and referred as the Foveal Approach, the second one is Yam *et al.*'s Physics Based Approach that was described in Chapter 3. The third is a variation of the statistical analysis introduced in Section 4.2. Using ROC analysis, we demonstrate the superiority of the first algorithm. First, however, we describe briefly the third algorithm that we compare here.

The third detection method, which we refer to as the Statistical Approach, differs from the foveal approach only in the final segmentation stage. In common with the foveal approach, the statistical approach applies an adaptive Gaussian derivative filter to the de-noised, glare-removed SMF images, which results in a gradient map and outputs the value of k for the subsequent diffusion stage. Next, the anisotropic diffusion filter is applied to the SMF image using a constant number of iterations t, with a pre-defined value of σ and the pre-computed value of k. With the diffused images ready, we need to ensure that the artefacts emphasised in the gradient maps will be eliminated.

A final segmentation stage uses statistical analysis to classify the content of an image into three main categories:

- background - where the variation of the image gradient is too low to correspond to microcalcifications;
- putative microcalcifications; they are conservative to avoid FN;

- shot noise - where the variation of the image gradient is too high to correspond to anatomical structures.

The filter is based on the same computation as the anisotropic diffusion, but also incorporates some adaptive thresholding suited to the image characteristics and the properties of microcalcifications. This last filtering process outputs a black-and-white map of detection (BWMD), where all pixels different than the black background correspond to calcifications in the breast.

The statistical analysis operates in the following manner. If I is the SMF image we process, the contrast of I is computed by comparing the value of the $mean(I)$ with that of $max(I)/2$. A first threshold is adapted to the image contrast and $I(SetPixels)=mean(I)$, where *SetPixels* are the pixels in image I that have the absolute value of the Gaussian derivative smaller than a constant M. For images with low contrast, we found $M=5$ to give good results, while for images with high contrast M has the value 20. The step is repeated over a few iterations in order to evaluate the steepness of the selected microcalcification candidates at each step. The final version of the image is contrast enhanced and the maximum value of M is used for thresholding. All the pixels that satisfy the thresholding criterion are marked as microcalcifications on the BWDM image.

In summary, the third method uses three filters in sequence:

- an adaptive Gaussian filter, which generates a gradient map and, more important, the value of k;
- an anisotropic diffusion filter, which will enhance certain suspicious regions based on the previous computation of k;
- some more statistical analysis built as an adaptive thresholding filter, which will discriminate between microcalcifications and the rest of the image.

Figure 71 to Figure 75 show the detection results on some mammogram samples containing microcalcification clusters. We present, along with the original contrast-enhanced SMF sample, the detection maps of the Physics-based Approach, Statistical Analysis and Foveal Approach. We used a database of 102 samples of digital SMF images, 78 of them contain 1 to 3 clusters per

image, while 24 are normal mammogram samples. There are a total of 98 clusters of microcalcification. All images were digitised at a resolution of 50μm and have sizes under 1500x1500. Figure 76 shows the comparative FROC curves of the tested detection methods.

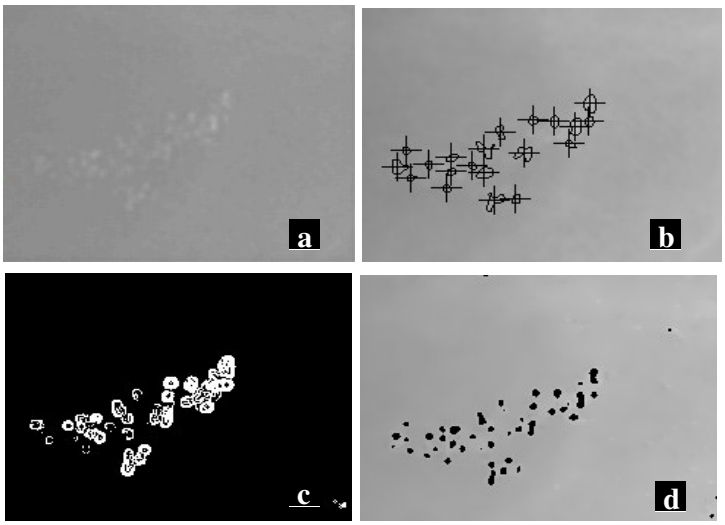

Figure 71: Comparative Results 1 for the Detection of Microcalcifications in SMF; (a) the original SMF image sample; (b) the detection map of the Physics-based Approach; (c) the BWMD of the Statistical Analysis; (c) the detection map of the Foveal Approach.

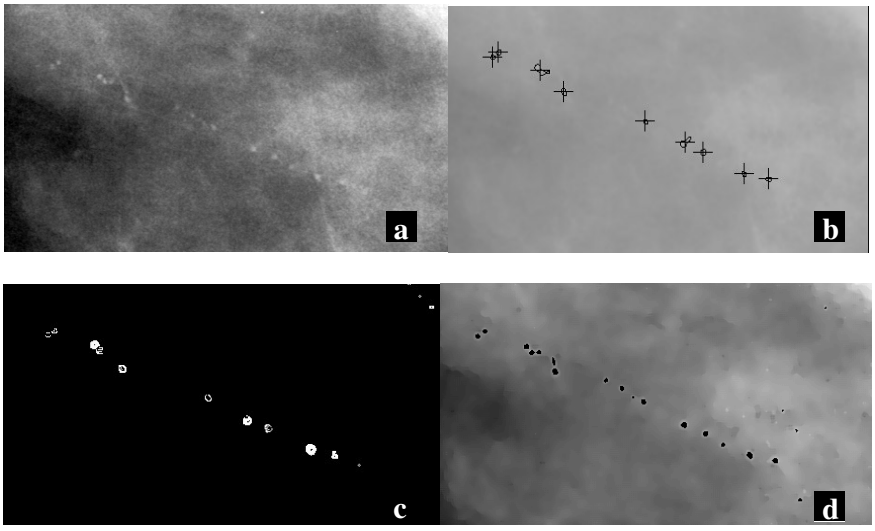

Figure 72: Comparative Results 2 for the Detection of Microcalcifications in SMF; (a) the original SMF image sample; (b) the detection map of the Physics-based Approach; (c) the BWMD of the Statistical Analysis; (c) the detection map of the Foveal Approach.

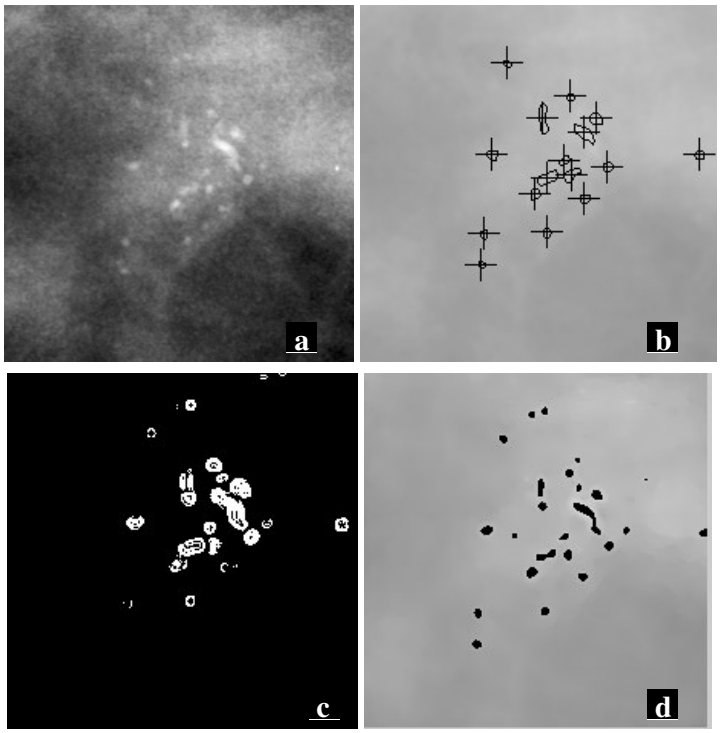

Figure 73: Comparative Results 3 for the Detection of Microcalcifications in SMF; (a) the original SMF image sample; (b) the detection map of the Physics-based Approach; (c) the BWMD of the Statistical Analysis; (c) the detection map of the Foveal Approach.

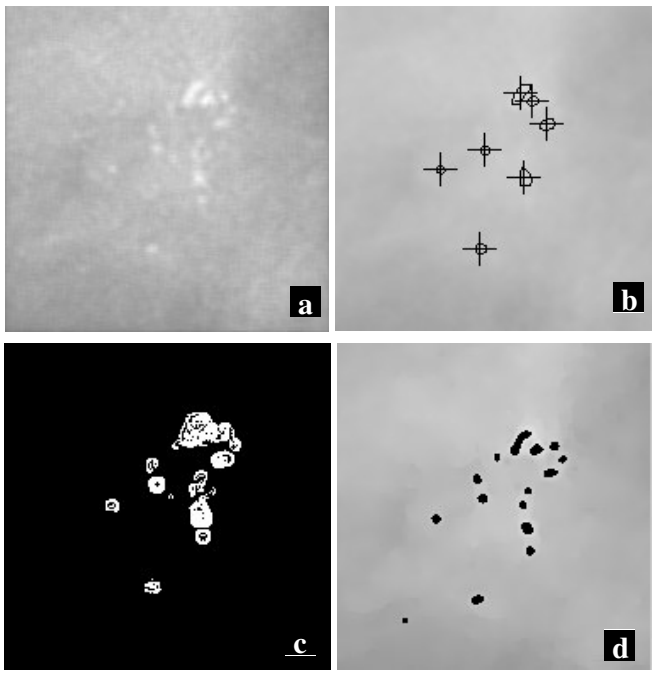

Figure 74: Comparative Results 4 for the Detection of Microcalcifications in SMF; (a) the original SMF image sample; (b) the detection map of the Physics-based Approach; (c) the BWMD of the Statistical Analysis; (c) the detection map of the Foveal Approach.

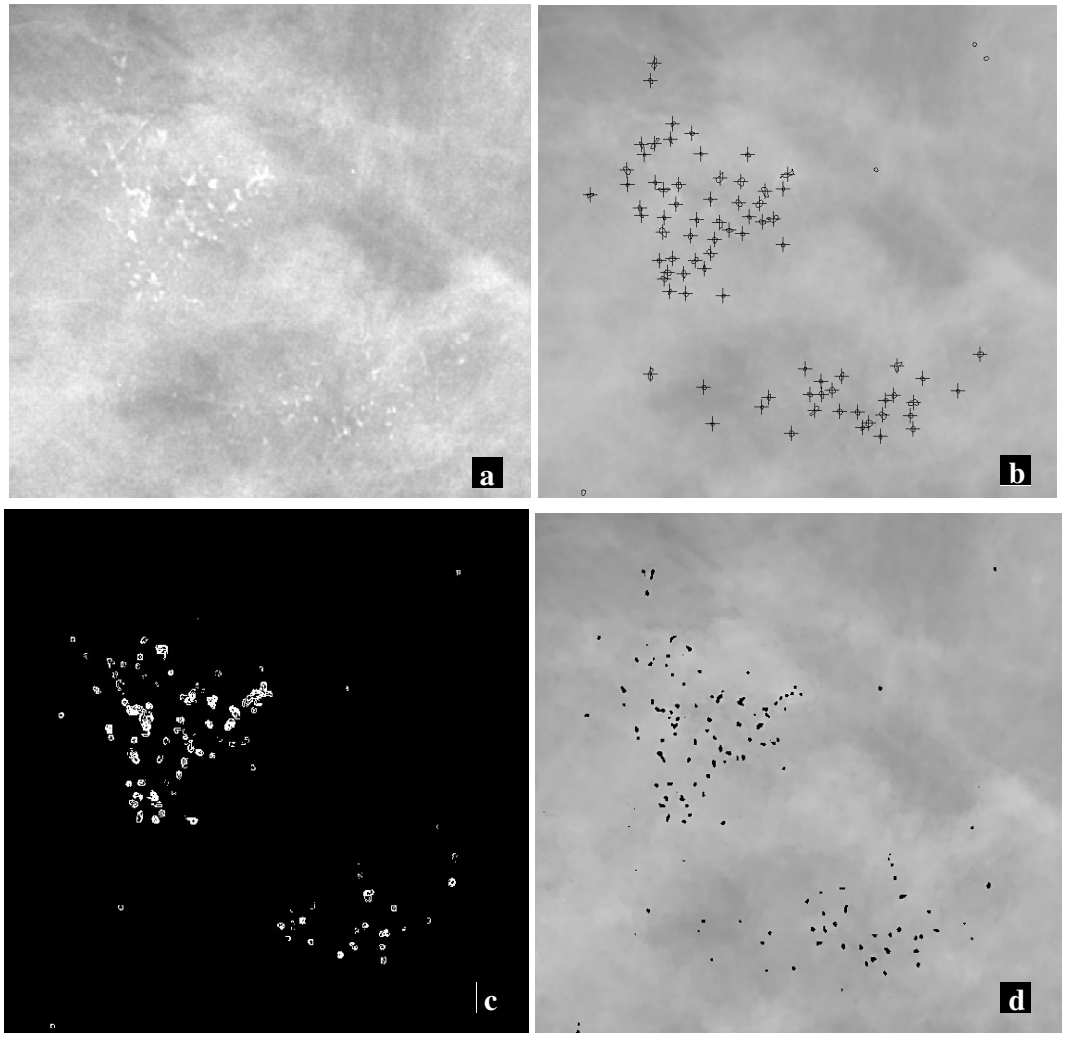

Figure 75: Comparative Results 5 for the Detection of Microcalcifications in SMF; (a) the original SMF image sample; (b) the detection map of the Physics-based Approach; (c) the BWMD of the Statistical Analysis; (c) the detection map of the Foveal Approach**.**

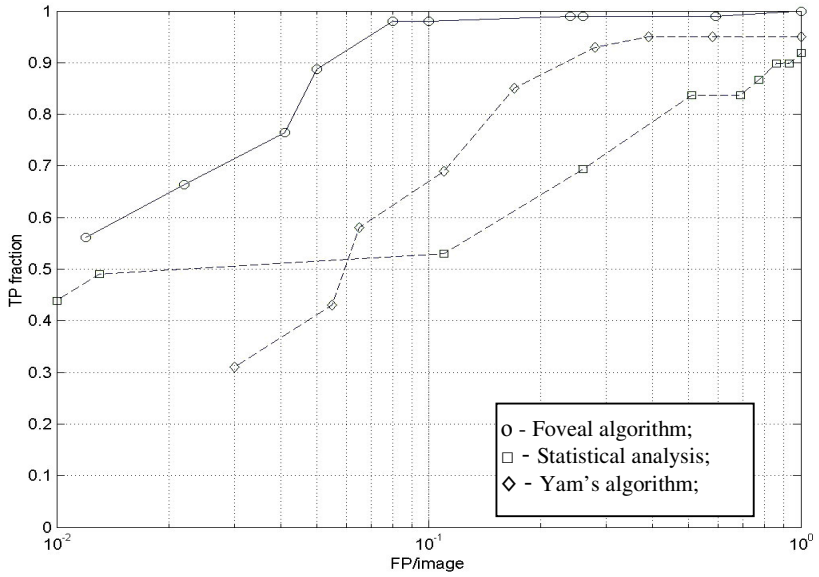

Figure 76: The FROC curves of the three microcalcification-detection methods, where we notice the better performance of the Foveal Approach.

4.5.2 Setting the Parameters

The diffusion process is modelled by three parameters that determine its response to various image situations. Their influence on the smoothing of an input image has been described before in Section 3.2.2, their setting for a specific application, such as image smoothing prior to the detection of microcalcifications is the subject of the following paragraphs.

During the experiments performed and presented in Chapter 3, we aimed to characterise the effect of the choice of specific values for the three diffusion parameters, k, σ and t, on glare-removed SMF images. Since anisotropic diffusion was originally meant to be used as an alternative smoothing technique to the Wiener filter (see Section 2..2.3), though it was subsequently used in combination with it, no such filtering was used on the trial images in Chapter 3 prior to the SMF generation. Hence, the contrast (k) values used in these experiments, which were chosen empirically for the illustration of our first experiments, would be atypical for the validation of our algorithm on glare-removed Wiener-filtered SMF images, as in Chapter 4.

Microcalcifications represent a tiny percentage of a mammogram surface. Typically, they are very small and present in about a quarter of the total number of screening mammograms. Therefore, a percent of about five of the total number of mammogram pixels should be more than sufficient to accommodate the entire population of calcium salts. Furthermore, calcium is very bright in an X-ray image and it would be amongst the brightest/highest pixels of the mammogram. As illustrated in equation (66) we compute k as a value of the gradient (for tall steep microcalcifications) that discriminates between these brightest structures and the background; more precisely, we chose the 4.4% structures with highest contrast (a threshold at mean(g) + 2*std(g)). k becomes a value with well-defined physical meaning (differentiating between high-pointed structures, referred to earlier as towers, on the SMF surface and the rest of the images), which is calculated automatically part of the detection algorithm. Figure 77 illustrates the effect of k.

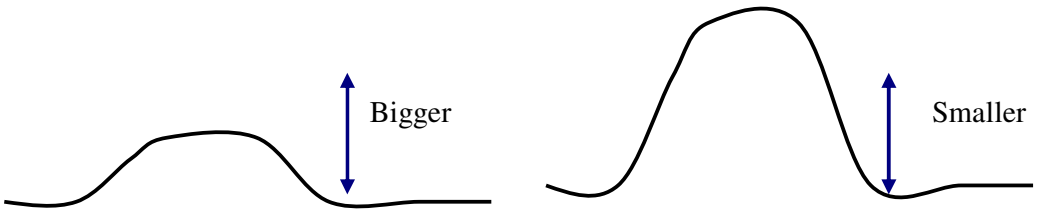

Figure 77: In the left case, the k factor is bigger than the gradient and the diffusivity function $g \rightarrow 1$, which is equivalent to finding an edge and maximising diffusion; in the right case, $g \rightarrow 0$ (for very big gradients) and diffusion is inhibited.

The second parameter to be set is σ, the standard deviation of the Gaussian filter used to smooth the image, which will give the size of the Gaussian kernel that removes noise by convolution with the mammogram. We need to choose a value for σ so that, on the one hand, it removes high-frequency noise (which are very small and spread over a couple of pixels at 50μm/pixel), but, on the other hand, preserves microcalcifications (on average 0.5-1 mm in diameter). To ensure that small calcifications (that is, those whose sizes are 300 microns or more) are preserved in the image, we set σ to 0.6. This will build a Gaussian kernel of 0.35mm ($10\sigma+1$),

which is sufficiently small to clean noise and keep calcium salts. The principle is shown in Figure 78.

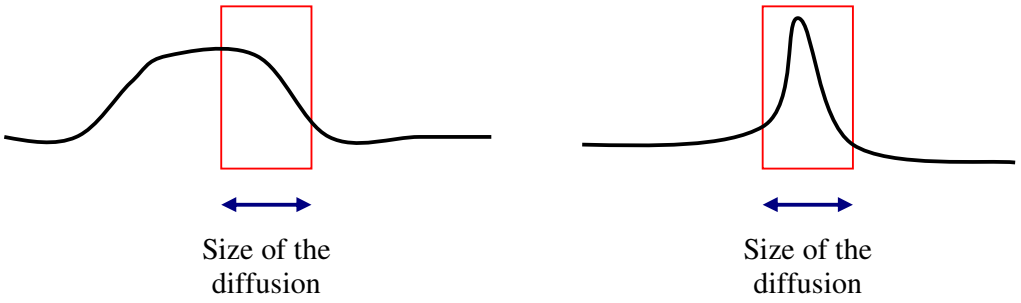

Figure 78: In the left case, the filter width is small compared to the structure, so it essentially detects a step edge; but in the second, it is not obvious that it will .

The experimental results show that *k* has small values for the inner area of the breast, which makes smoothing safe for faint microcalcifications, but that this process is also rather inefficient over the first couple of iterations. Weickert [172] notes that the number of iterations *t* is related to the spatial width of the Gaussian kernel. To blur features of the kernel order (10σ) requires $t = (10\sigma)^2 / 2$. Rounding this value for σ=0.6 , yields *t*=5, which give excellent noise reduction results in the microcalcification preservation framework. We studied experimentally the effect of the variation of *t* and can offer the following comments: 1-3 iterations have too little influence and the output images are still noisy; for *t* greater than or equal to 7, not only is the process is time consuming, but most images are overly smoothed and valuable information is lost.

A reliable application must prove its robustness under different clinical imaging conditions. When parameters are involved, they must be suited for any type of input images. The danger that an algorithm is tuned to a particular data set is a major concern in the validation of clinical applications. Such a discussion is required when evaluating our method for the detection of microcalcifications.

One of the starting points in this method is the employment of a technique of mammographic image normalisation, the SMF. While various hospitals around the world use different X-ray machines to acquire mammograms during screening trial, the SMF finds a common framework in

which mammograms are presented as maps of dense tissue. The major advantage of SMF is the de-parameterisation of mammograms, the normalisation of their appearance. Ideally, the setting of parameters of our algorithm must be done once to make the algorithm work on any normalised image. A justification of the parameter tuning follows.

The first trials for the setting of parameters are done on small mammogram windows with isolated calcifications (c.f. Section 3.2.3). The samples are extracted from the Oxford Screening Database. They are generally of 500x500 pixels at 50μm/pixel, although some of them may be slightly smaller. These experiments are designed to evaluate the removal of noise associated with the differentiation in shape between shot-noise and background versus microcalcifications, as proposed by Yam [178, 179]. In Chapter 4, where the main evaluation of the algorithm is described, we also use mammogram windows (both intensity and SMF) from the Oxford Screening Database. They are samples from the same screening mammographic database, but different windows of different mammograms, since we search microcalcification clusters this time. The first tuning of parameters is therefore done on different images coming from the same screening centre, a different collection of images, but with similar imaging characteristics (as they are acquired and digitised using the same equipment).

The choice of the values for the parameters used in the anisotropic diffusion process has been explained above; but a few more comments are in order. First, k is computed directly from the image and its meaning (depict the most outstanding features in the mammogram) is independent of the data set. σ is strictly related to the size of microcalcifications and the image resolution; the condition imposed here is that databases must be digitised at 50μm/pixel. t is set according to the observed value of k and the proposed value of σ, which are consistent over the Oxford Screening, DDSM and MIAS databases (see Chapter 5). We perform tests with images from several databases to prove the robustness of the algorithm. Moreover, we obtain good results both on images with and without normalisation.

We presented a working example of tuning the parameters of anisotropic diffusion to an application. In a more general framework, anisotropic diffusion is a feature detector, namely an

edge detector. *k,* being closely related to the gradient in the image, can be derived according to the percentage of features that we desire to enhance in an image. σ gives a measure of scale and must be set according to the size of searched features at the image resolution (multiscale analysis may be performed). The literature proposes stopping criteria for *t* as well [23, 171] as functions of σ, which can be well related to noise removing, but may be more difficult to combine with feature enhancement for some applications. With the automatic tuning of parameters that we propose, anisotropic diffusion can finally be used as a robust parameter-free process using little, but essential, a-priori knowledge. This should be a great relief in applications of diffusion, a controversial method for its parametrical dependency.

The other parameters employed by our method are the kernel of inner object (*O*) used to compute μ_O in Section 4.3 and the value of the minimal perceivable contrast c_w. The size of *O* is established according to the size of the microcalcifications for the resolution of the tested images. A kernel of 9x9 pixels has an area of 0.4x0.4mm^2, which is just below the average surface of a microcalcification. It is desirable to have a slightly smaller kernel than the microcalcification diameter to assure the detection of small calcium salts, which are overlooked by larger kernels. Still, the size of *O* must not be extremely small to avoid overlapping *O* and *N* for slightly bigger microcalcifications. The last parameter, c_w, is related to the image contrast (c.f. Section 4.3) and empirically it has values typically between 0.002 and 0.005 for good detection results. We noted that adapting the value of c_w to the image characteristics gives better responses to microcalcifications than a constant c_w. Since *k* is a value of image contrast, we simply had to scale it to the suitable range of values for c_w.

4.5.3 Discussion

Though it is acknowledged that the state of the art of microcalcification detection is probably represented by R2's ImageChecker, unfortunately (though understandably) no details of the R2 detection algorithm are published. The R2 method was originally based on the work published by

Nico Karssemeijer at the University of Nijmegen [80, 81], but it is known that the R2 implementation has been changed substantially over the years (some researchers claim, with no apparent justification, that the R2 implementation of ImageChecker takes the form of a neural network). All other published microcalcification detection algorithms have significant shortcomings, and sensitivities/specificities that fall short of R2's ImageChecker. This appears (to us) mainly because they don't work on normalised images. The key point is that without normalisation, for example by the h_{int}/SMF process described in the thesis, there is inevitably the risk of confounding anatomical information (of interest) and imaging parameter effects (not of interest), whose choice can affect contrast, brightness and level of noise, to name some of the classical limitations.

This is the framework where Yam's work (see Section 2.2.3) is the first to claim results that appear to rival those published by R2, though it must be acknowledge that her results are from a smaller database. Nevertheless, her work is based on SMF, which was the point of departure of the thesis. The advantages of her technique are straightforward and the incentive that we should build on Yam's work followed, but it is important to understand what we considered to be the problems with Yam's algorithm, hence why it needed improvement.

In very few words (more details can be found in Section 2.2.3) Yam's technique works in two steps: (i) detect thin towers in the SMF (towers appear because the SMF generation process is based on the fundamental assumption that the breast (more precisely, the vast majority of projected pixels) contain only fat and "interesting tissue", not calcium. A consequence is that a calcification appears approximately 26 times higher than it should (this is the factor by which the attenuation of calcium exceeds "interesting tissue"); and (ii) then test a 26 fold reduction with footprint in image as a plausible calcification. The major problem arises in step (i) since the SMF is extremely noisy. Yam's solution is to introduce a Wiener filter; but we found that in many cases, which we considered during the first year of our research that this blurred the edges of the microcalcifications, therefore hampering both steps (i) and (ii) above. Faint microcalcifications become "too small" and "less sharp" to be detected, while the remaining noise imposes strong constraints on removing false positives and the algorithm further misses some microcalcifications

(see Figure 76 for comparative results). While clusters of microcalcification are generally still well detected as a whole, some individual calcifications are overlooked and so statistical analysis of a cluster is compromised.

Our suggestion was to develop an alternative way to smooth the image/SMF, namely anisotropic diffusion, a process well known for its quality to smooth while preserving edges. Our initial idea was proposed as in Figure 79.a, as an alternative to Figure 79.b, but in reality, what is done corresponds to Figure 79.c. This is the point where the work done in this thesis intervenes.

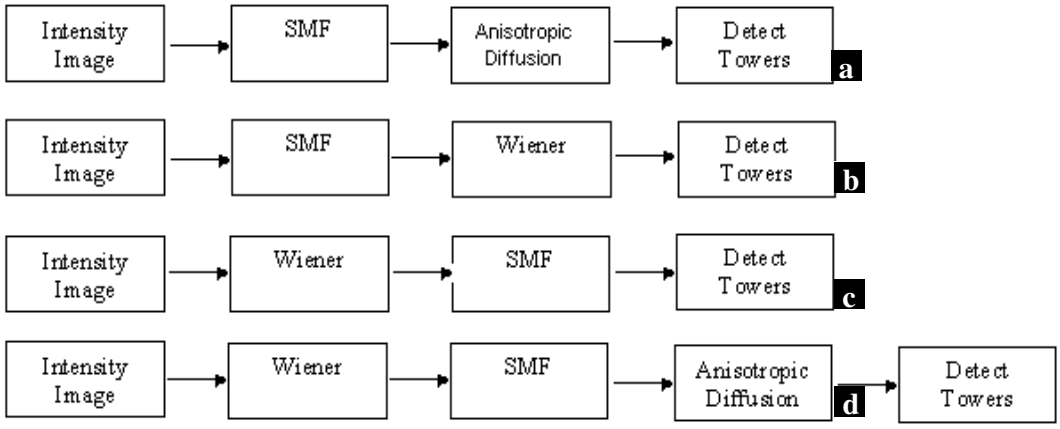

Figure 79: The original idea for the detection of microcalcifications: (a) what we initially proposed; (b) what we thought it was done; (c) what was done in reality; (d) our solution.

The final diagram that we propose is represented in Figure 79.d, adding the anisotropic diffusion filter after the SMF generation and before the detection of towers. Of course, this immediately poses the question: why use two different smoothing filters, namely the Wiener filter and anisotropic diffusion. The noise removal is carried out in two separate steps; the Wiener filter models a noise process (quantum mottle and film granularity), but not glare. Glare, along with scatter and extra-focal radiation and the anode-heel effect, is removed within the SMF generation, which massively reduces SNR by amplifying high frequency noise (see Table 4). Thus, glare removal solves the problem associated with the presence of this type of low frequency noise and sharpens the image, but also creates a new difficulty, the lower SNR. The newly amplified high-frequency noise is a major source of false positives and governs the difference in SNR between columns 2 and 3 in Table 4.

At this point of the SMF generation, most imaging artefacts are dealt with either by the h_{int} model (scatter, glare, anode heel, extra-focal) or the Wiener filter (quantum mottle, film grain). However, as emphasised in Section 2.3, the SMF generation has its imperfections. Yam comments in [178] about the drawbacks of her noise deconvolution arising from the simplification existing in the estimating theory of quantum mottle and the available physics parameters of film-screens. These possible sources of errors leave residual high-frequency noise in mammographic images. Digitiser noise, also of high frequency, and errors of SMF generation add to it. Nevertheless, we can consider the Wiener filter together with the h_{int} generation as one main stage designed to remove imaging specific parameters/errors, basically the image normalisation. The anisotropic diffusion filter aims to smooth the remaining high-frequency noise that interferes with our specific application, the process of detecting microcalcifications.

Table 4: The variation of SNR in generating SMF.

	SMF with Glare no Wiener	**SMF no Glare no Wiener**	**SMF no Glare with Wiener**
SNR	39.86	5.37	29.24

More specifically, would replacing the Wiener filter with anisotropic diffusion have eliminated the need for Wiener and subsequent anisotropic diffusion? Glare would amplify any residual noise after SMF generation, hence would have continued to interfere with the detection of microcalcifications. It follows that smoothing after SMF is needed for any application dealing with very small anatomical features, in particular microcalcifications. On the other hand, not smoothing before computing the SMF would amplify noise to very high levels during the image normalisation process (see Table 4) , which would make it extremely difficult to detect small structures and the subsequent filtering would be inefficient in properly removing noise while preserving microcalcifications. The Wiener filter has the advantage, stressed by Yam, of modelling particular kinds of mammographic noise (see Section 2.2.3).

We implemented the diagram in Figure 79.d for the detection of microcalcifications, as illustrated in Section 3.2 and further in Chapter 4, where a simulation of the detectability properties of the human visual system replaces the detection of towers. Thus, besides the SMF generation and its normalising action, we use two non-linear blurring filters: anisotropic diffusion (see Section 3.1) and Wiener (fundamentally a probabilistic assignment to signal and to noise). Through them, we address two different problems: the Wiener filter models quantum mottle and granularity of film, whereas the anisotropic diffusion filter smoothes the SMF image, but retains the signal (in the form of towers).

The subsequent filters (Wiener, SMF related, and diffusion) model and correct for specific image analysis problems, rather than trying to amalgamate into a single (linear or nonlinear) filter that attempts to do everything. Separating them should make things clearer for the developer of such a filter, even if, for the end user, it is all reduced to a "black-box" that detects microcalcifications. Hence, we have a collection of blurring/low-pass and deblurring/high-pass filters. Is there any danger that they simply counteract/undo each other? As explained above, the Wiener filter and the deconvolutions within the SMF generation address the physics and the condition of the imaging process its controlling parameters. They separately attack different problems on the way to a normalised image. So does the anisotropic diffusion filter for the purpose of detecting salts of calcium, using data estimated parameters. The Wiener filter is a deconvolution tuned for quantum mottle and film grain noise; the glare deblurs and sharpens the image revealing anatomical details (calcium for example), but noise as well; the diffusion filter blurs again, but this time just the high-frequency noise, without losing the anatomical details emphasised in the previous step. The last filter may have to undo the noise amplification, but will preserve the valuable anatomical information that would not have been available without the glare removal. Furthermore, we have a normalised image to work on.

4.6 Conclusion

In this Chapter we presented an algorithm for the detection of microcalcifications in X-ray mammography. The robustness of the algorithm has been demonstrated by the ROC analysis performed over a range of parameters. In each case, the method achieved a 100% TP ratio. Similar results were obtained on intensity images, although for the lower scale of FP/image there is a more marked difference in results.

Our method was tested on mammographic samples for faster processing and simpler validation, and also on whole mammograms. We further compared the performance of our algorithm on data from different institutional databases with good detection results. Adding adaptive contrast segmentation based on characteristics of the human visual system dramatically enhanced the detection of microcalcifications. The parameters are set according to the image attributes and the method is fully automated. In future work, the algorithm could incorporate additional knowledge of X-ray attenuation.

CHAPTER 5

5 Temporal Comparison of Feature Enhanced Mammograms for Mass Detection

What hath night to do with sleep?

John Milton – "Comus"

The development of reliable CAD systems for breast mass detection in digital mammograms remains an important problem that is still only partially solved. In this Chapter, we present a new method for alerting the clinician to "suspicious" dense regions in temporal mammogram sequences that combines feature detection and temporal comparison. We envisage using this during post-screening assessment, when a radiologist recalls a woman for more in-depth analysis after a suspicious mammogram. At this point, the clinician compares the most recent mammogram to previous ones in order to detect significant changes. An important problem in automatic mass detection is the large number of candidate masses. The method presented in this Chapter uses anisotropic filtering (cf. Chapter 3) as a pre-processing step in order to significantly reduce the number of candidate masses, while preserving the important anatomical information about each mass. The method has been tested on the 15 temporal pairs currently available from the Oxford Database, where pathology has been diagnosed in the most recent image. Though we detect 100% of the masses, the number of false positives remains significant, necessitating further work.

.

CHAPTER 6

6 Discussion

Any man who reads too much and uses his own brain
too little falls into lazy habits of thinking.

Albert Einstein

The thesis presented a method for early feature detection of cancer in digital mammography. The detection of microcalcification clusters and breast masses was investigated with both Standard Mammogram Form (SMF) images (c.f. Chapter 2) and original intensity images from multiple institutions. The following section summarises the work and discusses its limitations, followed by some concluding remarks.

6.1 Summary and Discussion

6.1.1 Mammographic Image Filtering

The thesis began with a filter model for SMF images to 'clean' the noisy appearance of h_{int} images and enhance structures of interest. Initially, the filter was designed for the detection of microcalcification (c.f. Chapter 3), but later in Chapter 5 the same filter was used to enhance mammographic masses as part of a temporal detection method.

The need for a pre-processing filter comes from the poor signal-to-noise ratio (SNR) of SMF images and the difficulty this causes in spotting small salts of calcium in a mass of textured ambiguity. Furthermore, it is desirable to have enhanced structures of interest prior to segmentation for a simpler differentiation between microcalcifications and mammographic background.

The use of partial differential equations (PDE) and in particular anisotropic diffusion led to the following observations:

- The parametric format of the proposed filter allowed the user to obtain very reliable results given the right choice of parameters. The appearance of the image was improved, but a non-parametric approach is desirable to make the algorithm robust;
- The filter was stable in time and offers a good alternative to filters previously described in the literature;
- Quantum mottle was smoothed by the filter and errors were minimised, without disrupting microcalcifications;
- Microcalcifications can be depicted according to their physical appearance as thin towers in a smoothed background;
- The main source of false positives (FP) were shot-noise, caused by dust or hair on the film, and curvilinear structures (CLS), long thin bright structures in a mammogram corresponding to blood and lymph vessels, ligaments, ducts or tumour spiculations.

6.1.2 Complex Pre-processing

To eliminate some of the difficulties outlined above, a complex pre-processing step was introduced prior to image segmentation to reduce the number of FP in the detection algorithm. Our aim was to eliminate shot-noise and CLS from mammographic images, as well as to filter mammograms for the purpose of detecting microcalcifications. This adaptive step was designed to improve the

robustness of the algorithm and to obtain consistent results independent of the user's experience and dexterity in setting parameters.

By removing glare in the h_{int} generation process, shot-noise was marked on a binary map that made it easy to remove (c.f. Chapter 4). Information gathered from local energy (LE) and phase congruency (PC) was used to detect and remove CLS from mammograms (c.f. Chapter 4). Using the anisotropic diffusion-based filter described in Chapter 3 and the statistical analysis of the local image characteristics, the parameters of the diffusion process were computed automatically and the pre-processing step became fully automated. A few remarks are necessary here:

- The number of FP was significantly lower after pre-processing;
- CLS removal, being scale dependent, tended to eliminate some microcalcification candidates. To avoid this, we only used a subset of the scales at which CLS were detected. However, as a result, some disruptions appeared in the CLS map, which can leave small bright dots on the processed image. These dots may be interpreted as FP by the segmentation algorithm. A better solution could be provided by an alternative CLS removal algorithm, as proposed in Chapter 4;
- The computation of the diffusion parameters by statistical analysis was robust and consistent over the database. The same computation was used both for intensity and SMF images with similar results, although their image characteristics were different. The value calculated here was further used to automate the segmentation step. Note that the 'natural' contrast of the processed images was not altered. Images with very high contrast would be smoothed more and therefore a prior contrast enhancement of the analysed images (as found in the literature) could lead to different values of the automatically computed parameters. Since the method is adapted to image characteristics, results would still be robust but not optimal, as a different computation of the parameters used to set the minimal perceivable contrast (70) may be required.

6.1.3 Human Vision Based Segmentation

The method for detecting microcalcification clusters was completed with the segmentation of the microcalcification. The aim of this stage is to produce a reliable detection map that indicates the location of clusters by maximising the number of individual calcium salts detected and minimising the impact of FP. A contrast measure based on a model of human vision was introduced in Chapter 4. This new measure is locally adaptive in each processed image and uses the results of the pre-processing step (statistical analysis) to become non-parametric. Combining the pre-processing and the segmentation steps in building a microcalcification detection method, we can conclude the following:

- The method is non-parametric and fully automated, and produced comparably reliable results on both SMF and original intensity images; the technique was also reliable using data from different institutions;
- The variation of parameters showed consistent results with small differences in the detection ratios when parameters were varied around their optimal values;
- The receiver operating characteristic (ROC) curve analysis demonstrated that by adding adaptive contrast segmentation based on human foveal processing the detection of microcalcifications was significantly improved;
- The technique was tested on both mammographic samples for faster processing and simpler validation, and on full mammograms to show robustness; results were similar, but a faster implementation would be necessary for better clinical manipulation of full images;
- The detection rate reached 98% TP fraction at 0.1 FP/image and converged to 100% for each ROC curve when the number of FP/image was 1.1;
- Some measure of the calcium X-ray attenuation combined with image normalisation would be useful in the detection process;

- A cluster classification step is desirable for a complex detection and classification of microcalcification clusters method; possible features to be used by such a detection-classification system include size, shape, distribution, density and orientation.

6.1.4 Temporal Mass Prompting

Another application presented in this thesis was mass detection by temporal comparison of feature enhanced mammogram pairs (c.f. Chapter 5). This represents an expansion of the mammographic image filter originally designed for microcalcifications to breast masses, in combination with image registration and texture analysis. The algorithm enhanced structures of interest, in this case breast masses, and blurred the uninteresting background. The detection of masses came as a natural completion of the microcalcification detection in the early detection of cancers, to assist the clinician in interpreting images and establishing reliable and early diagnosis of pathology.

The algorithm consists of three steps that conclude with mass candidates being prompted in the pair of temporal mammograms: (i) image registration for accurate temporal comparison; (ii) adaptive image filtering for feature enhancement; and mammogram segmentation to define breast dense regions and prompt mass-candidates. Note the assumption that masses appear denser in mammograms than other tissue. From experimental results, the following observations can be drawn:

- The adaptive anisotropic-diffusion filter was robust when used for mass enhancement in digital mammography; some of the diffusion parameters (size and time) were different than for microcalcification enhancement, but the contrast was automatically computed from the statistical analysis of image appearance;
- The algorithm correctly detected all the masses in the tested images; the number of candidate masses dropped significantly after diffusing the images, but the number of FP remained high;

- However, registration facilitated further reduction of FP by temporal comparison of mammograms through the accurate matching between the mass candidates depicted after texture analysis;
- The algorithm would benefit from incorporating fully automated mass matching and FP reduction in the temporal sequence;
- For mass detection, more experiments must be performed on larger databases.

6.1.5 Novel Tumour Features

Using image filtering, similar to pre-processing used to detect microcalcifications, some breast tumour related features were identified. Once the tumour is detected, a number of features can be signalled from its physical and morphological qualities (c.f. Chapter 5). The following characteristics of benign and malignant masses were noted:

- Benign masses, which are more homogenous within their boundaries, diffused differently than malignant masses, which have a more complex internal geometry; diffusion maps can differentiate between types of masses.
- The vector flow of the image Gaussian derivative corresponds respectively to the uniformity versus roughness in benign and malignant masses, through the differing radial or chaotic vector patterns within the masses and along their boundaries.

Note: A mathematical model of these two features would have to be incorporated into a mass characterisation algorithm.

6.2 False Positive's Charateristics

The most obvious room for future improvement in the detection of microcalcifications is the elimination of false positives (FP). The main observed source of FP remains the presence of curvilinear structures (CLS). These have high attenuation and their thin appearance may make

Bibliography

[1] Aghdasi, F.: Application of Neural Network Adaptive Wavelets for Signal Representation and Classification in Digital Mammography. In Doi, K. Giger, M.L. Nishikawa, R.M. Schmidt, R.A. (eds.): Digital Mammography, Elsevier, Amsterdam (1996) 307-310

[2] Alberdi, E. Lee, R. Taylor, P.: Radiologists' Description and Interpretation of Mammographic Calcifications: Knowledge Elicitation for Computerized Decision Support. In Yaffe, M.J. (ed.): Digital Mammography, Medical Physics Publishing, Madison (2000) 135-141

[3] Ancelin, B. Yam, M. Highnam, R.P. Brady, J.M.: Automated Detection of Artefacts on Film-Screen Mammograms Using a Novel Iterative Detection and Correction Scheme. In: Digital Mammography, Lecture Notes in Computer Science, Springer-Verlag, Berlin Heidelberg New York (2002) 174-178

[4] Andersson, I.: Breast Cancer Screening Results. In Karssemeijer, N. Thijssen, M. Hendricks, J. van Erning, L. (eds.): Digital Mammography, Kluwer Academic Publishers, Dordrecht Boston London (1998) 427-433

[5] Andolina, V.F. Lillé, S.L. Willison, K.M.: Mammographic Imaging: A Practical Guide. J.B. Lippincott Company (1992)

[6] Ashdown, I.: Luminance Gradients:Photometric Analysis and Perceptual reproduction. In: Journal of Illuminating Engineering Society, Vol. 25(1) (1996) 69-82.

[7] Beral V., Banks E., Reeves G., Appleby P: Use of HRT and the Subsequent Risk of Cancer. In: Journal Epidemiololy Biostatistics, Vol. 4(3) (1999) 191-210

[8] Betal, D. Roberts, N. Whitehouse, G.H.: Segmentation and Numerical Analysis of Microcalcifications on Mammograms using Mathematical Morphology. In: British Journal of Radiology, Vol. 70 (1997) 903-917

[9] Birdwell, R.L. Ikeda, D.M. O'Shaughnessy, K.F. Sickles, E.A.: Mammographic Characteristics of 115 Missed Cancers Later Detected with Screening Mammography and the Potential Utility of Computer-aided Diagnosis. In: Radiology, Vol. 219 (2001) 192-202

[10] Bishop, C. M.: Neural Networks for Pattern Recognition. Oxford University Press, Oxford (1995)

[11] Blanks, R.G. Wallis, M.G. Moss S.M.: A Comparison of Cancer Detection Rates Achieved by Breast Cancer Screening Programmes by Number of Readers, for One and Two-View Mammography: Results from the UK National Health Breast Screening Programme. In: J Med Screen, Vol. 5 (1998) 195-201

[12] Boedicker, A. Evertsz, C.J.G, Brady, J.M., Hendriks, J.H.C.L. Juergens, H. Karssemeijer, N. Peitgen, H.O.: SCREEN-TRIAL: Softcopy Reading Environment in European Screening Mammography – SCREEN. In: Digital Mammography, Lecture Notes in Computer Science, Springer-Verlag, Berlin Heidelberg New York (2002) 423-427

[13] Brady, J.M. Pan, X.B. Schenk, V.U.B. Terras, M. Molton, N.: Shadow Stereo, Image Filtering and Constraint Propagation. In: Proc. Roy. Soc. (2002) in press

[14] te Brake, G.M. Karssemeijer, N. Hendriks. J.H.C.L.: An Automatic Method to Discriminate Malignant Masses from Normal Tissue in Digital Mammograms. In: Phys. Med. Biol. (2000) 2843-2857

[15] te Brake, G.M.: Computer Aided Detection of Masses in Digital Mammograms, PhD Thesis. The Catholic University of Nijmegen (2000)

[16] te Brake, G.M. Karssemeijer, N.: Single and Multi-Scale Detection of Masses in Digital Mammography. In: IEEE Transactions on Medical Imaging, Vol. 18(7) (1999) 628-639
[17] Brown, M. Eccles, C. Wallis, M.G.: Geographical Distribution of Breast Cancers on the Mammogram: An Interval Cancer Database. In: The British Journal of Radiology, Vol. 74 (2001) 317-322
[18] Burcher, M. Noble, J.A Han, L.: Deformation Correction in Ultrasound Imaging Using Contact Force Information. In: Proc. IEEE Workshop on Mathematical Methods in Biomedical Image Analysis (2001) 63-70
[19] Buscombe, J. Hill, J. Parbhoo, S.: Scintimammography: A Guide to Good Practice. Gibbs Associates Limited (1998)
[20] Byng, J.W., Critten, J.P. Yaffe, M.J.: Thickness-equalization Processing for Mammographic Images. In: Radiology, Vol. 203 (1997) 564-568
[21] Cancer Research Campaign: Breast cancer fact sheet (6.1). Cancer Research Campaign, Oxford (1996)
[22] Caseldine, J. Blamey, R. Roebuck, E.J. Elston, C.: Breast Disease for Radiographers. Wright (1998)
[23] Catté, F. Lions, P.L. Morel, J.M. Coll, T.: Image Selective Smoothing and Edge Detection by Nonlinear Diffusion. In: SIAM Journal on Numerical Analysis, Vol. 29 (1990) 629-639
[24] Chan, H.P. Sahiner, B. Helvie, M.A. Petrick, N. Roubidoux, M.A. Wilson, T.E. Adler, D.D. Paramagul, C. Newman, J.S. Sanjay-Gopal, S.: Improvements of Radiologists' Characterization of Mammographic Masses by Using Computer-aided Diagnosis: A ROC Study. In: Radiology (1999) 817-827
[25] Chan, H.P. Doi, K. Galhorta, S. Vyborny, C.J. MacMahon, H. Jokich, P.M.: Image Features Analysis and Computer-Aided Diagnosis in Digital Radiography: 1.Automated Detection of Microcalcifications in Mammograms. In: Medical Physics, Vol. 14 (1987) 538-548
[26] Couvreur, C.: The EM Algorithm: A Guided Tour. In Proceedings IEEE European Workshop on Computationally Intensive Methods in Control and Signal Processing. Prague (1996) 115-120
[27] Dash, N.: Magnetic Resonance Imaging in the Diagnosis of Breast Diseases. In: American Journal of Roentgenology, Vol.. 146 (1986) 119-125
[28] Davis, R.R. Dance, D.R.: Automatic Detection of Clustered Calcifications in Digital Mammograms. In: Physics in Medicine and Biology, Vol. 35 (1990) 1111-1118
[29] Dean, P.B.: Overview of Breast Cancer Screening. In Doi, K. Giger, M.L. Nishikawa, R.M. Schmidt, R.A. (eds.): Digital Mammography, Elsevier, Amsterdam (1996) 19-26
[30] Dixon, J.M.: ABC of Breast Disease. BMJ Publishing Group, London (1995)
[31] Doyley, M.M. Bamber, J.C. Fuechsel, F. Bush, N.L.: A Freehand Elastographic Imaging Approach for Clinical Breast Imaging: System Development and Performance Evaluation. In: Ultrasound in Med. and Biol., Vol. 27(10) (2001) 1347-1353
[32] Edwards, D.C. Kupinski, M.A. Nagel, R. Nishikawa, R.M. Papaioannou, J.: Using Bayesian Neural Network to Optimally Eliminate False-Positive Microcalcification Detections in a CAD Scheme. In Yaffe, M.J. (ed.): Digital Mammography, Medical Physics Publishing, Madison (2000) 168-173
[33] Van Engeland, S. Karssemeijer, N. Hendriks, J.H.C.L.: Using Information from Two Mammographic Views to Improve Computer-Aided Detection of Mass Lesions. In: Digital Mammography, Lecture Notes in Computer Science, Springer-Verlag, Berlin Heidelberg New York (2002) 377-381
[34] EstEve, J. Kricker, A. Ferlay, J. Parkin, D.M. (eds.): Facts and Figures of Cancers in the European Community. IARCPress, Lyon (1993)
[35] Evans, C.J. Yates, K. Brady, J.M.: Statistical Characterisation of Normal Curvilinear Structures in Mammograms. In: Digital Mammography, Lecture Notes in Computer Science, Springer-Verlag, Berlin Heidelberg New York (2002) 285-291
[36] Evans, C.J.: Detecting and Removing Curvilinear Structures from Mammograms. Internal Report, Department of Engineering Science, University of Oxford (2001)
[37] Evertsz, C.J.G. Bodicker, A. Bohnenkamp, S. Dechow, D. Beck, C. Peitgen, H.O., Berger, L. Weber, U. Jurgens, H. Hendricks, J.H.C.L. Karssemeijer, N. Brady, J.M.: Soft-Copy

Reading Environment for Screening Mammography – SCREEN. In Yaffe, M.J. (ed.): Digital Mammography, Medical Physics Publishing, Madison (2000) 566-572

[38] Fatemi, M. Wold, L.E. Alizad, A. Greenleaf, J.F.: Vibro-Accustic Tissue Mammography. In: IEEE Transactions on Medical Imaging, Vol. 21(1) (2002) 1-8

[39] Felsberg, M. Sommer, G: The Structure Multivector. In: AGACSE 2001, Cambridge, to appear at Birkhäser

[40] Ferlay, J. Bray, F. Pisani, P. Parkin, D.M.: GLOBOCAN 2000: Cancer Incidence, Mortality and Prevalence Worldwide. IARCPress, Lyon (2001)

[41] Freer, T.W. Ulissey, M.J. Screening Mammography with Computer-aided Detection: Prospective Study of 12,860 Patients in a Community Breast Cancer. In: Radiology, Vol. 220 (2001) 781-786

[42] Funovics, M. Schamp, S. Lackner, B. Wunderbaldinger, P. Lechner, G. Wolf, G.: Computer-assisted Diagnosis in Mammography: the R2 ImageChecker System in Detection of Spiculated Lesions. In: *Wien Med Wochenschr*, Vol. 148(14) (1998) 321-324

[43] Le Gal, M. Ollivier, L. Asselain, B. Meunier, M. Laurent, M. Vielh, P. Neuenschwander, S.: Mammographic Features of 455 Invasive Carcinomas. In: Radiology, Vol. 185 (1992) 705-708

[44] Le Gal, M. Durand, J.C. Laurent, M. Pellier, D.: Conduite a Tenir Devant une Mammographie Revelatrice de Microcalcifications Groupees sans Tumeur Palpable. In: La Nouvelle Presse Medicale, Vol. (5) (1973) 1621-1627

[45] Gale, A.G. Cowley, H.C.: Analysis of Breast Cancer Screening Results. In Karssemeijer, N. Thijssen, M. Hendricks, J. van Erning, L. (eds.): Digital Mammography, Kluwer Academic Publishers, Dordrecht Boston London (1998) 19-26

[46] Garra, B.S. Cespedes, E.I. Ophir, J. Spratt, S.R. Zuurbier, R.A. Magnant, C.M. Pennanen, M.F.: Elastography of Breast Lesions: Initial Clinical Results. In: Radiology, Vol. 202(1) (1997) 79-86

[47] Geman, S. Geman, D.:Stochastic Relaxation, Gibbs Distribution and the Bayesian restoration of Images. In: IEEE Transactions on Pattern Analysis and Machine Intelligence, Vol. 6(6) (1984) 721-741

[48] Giger, M.L. Huo, Z. Vyborny, C.J. Lan, L. Nishikawa, R.M. Rosenbourgh, I.: Results of an Observer Study with an Intelligent Mammographic Workstation for CAD. In: Digital Mammography, Lecture Notes in Computer Science, Springer-Verlag, Berlin Heidelberg New York (2002) 297-303

[49] Giger, M.L. Maloney, M. Huo, Z. Vyborny, C.J. Kupinski, M. Venta, L: Computerized Classification of Lesions on Digital Mammography. In Yaffe, M.J. (ed.): Digital Mammography, Medical Physics Publishing, Madison (2000) 189-192

[50] Grady, L Schwartz, E.: Anisotropic Interpolation on Graphs: The Combinatorial Dirichlet Problem. Technical Report CAS/CNS-TR-03-014, Department of Cognitive and Neural Systems, Boston University, Boston, MA (2003). Submitted to IEEE Transactions on Pattern Analysis and Machine Intelligence

[51] Gonzales, R.C. Woods, R.E.: Digital Image Processing. Addison-Wesley Publishing Company (1993)

[52] Groshong, B.R. Kegelmeyer, W.P.: Evaluation of a Hough Transform Method for Circumscribed Lesion detection. In Doi, K. Giger, M.L. Nishikawa, R.M. Schmidt, R.A. (eds.): Digital Mammography, Elsevier, Amsterdam (1996) 361-366

[53] Haagensen, C.C.: Disease of the Breast. W.B. Saunders Company (1986)

[54] ter Haar Romeny, B.M.(ed.): Geometry-Driven Diffusion in Computer Vision. Kluwer Academic Publisher, Dordrecht (1994)

[55] Hadjiiski, L. Sahiner, B. Chan, H.P. Petrick, N: Classification of Malignant and Benign Masses Based on Hybrid ART2LDA Approach. In: IEEE Trans. Med. Imaging, Vol. 18(12) (1999) 1178-1187

[56] Hara, T. Yamada, A. Fujita, H. Iwase, T. Endo, T.: Automated Classification Method of Mammographic Microcalcifications by Using Artificial Neural Network and ACR BI-RADS Criteria for Microcalcification Distribution. In Yaffe, M.J. (ed.): Digital Mammography, Medical Physics Publishing, Madison (2000) 198-204

[57] Haralick, R.M. Shapiro, L.G.: Computer and Robot Vision, Vol. I. Addison-Wesley Publishing Company, Reading MA (1992)
[58] Harris, C.G. Stephens, M.: A Combined Corner and Edge Detector. In: Proceedings of the Fourth Alvey Vision Conference, The University of Sheffield Printing Unit (1988) 147-152
[59] Hayton, P. Brady, J.M. Tarassenko, L. Moore, Niall: Analysis of Dynamic MR Breast Images using a Model of Contrast Enhancement. In: Medical Image Analysis, Vol. 1(3) (1997) 207-224
[60] Hendrinck, R.E. Lewin, J.M. Isaacs, P. Kuni, C.K. D'Orsi, C.J. Moss, L. Karellas, A. Sisney, G.A. Cutter, G.R.: Interim Clinical Evaluation of FFDM in a Screening Cohort: Comparison with Screen-Film Mammography in 4,965 Exams. In Yaffe, M.J. (ed.): Digital Mammography, Medical Physics Publishing, Madison (2000) 468-475
[61] Hendrinck, R.E. Lewin, J.M. D'Orsi, C.J. Kopans, D.M. Conant, E. Cutter, G.R. Sitzler, A.: Non-Inferiority Study of FFDM in an Enriched Diagnostic Cohort: Comparison with Screen-Film Mammography in 625 Women. In Yaffe, M.J. (ed.): Digital Mammography, Medical Physics Publishing, Madison (2000) 475-481
[62] Heucke, L. Knaak, M. Orglmeister, R.: A New Image Segmentation Method Based on Human Brightness Perception and Foveal Adaptation. In: IEEE Signal Processing Letters, Vol. 7, No. 6 (2000) 129-131
[63] Heywang-Koebrunner, S.H. Wolf, A. Pruss, E. *et al*.: MR Imaging of the Breast with Gd-DTPA: Use and Limitations. In: Radiology, Vol. 171 (1989) 95-103
[64] Highnam, R.P. Brady, J.M. Shepstone, B.J.: Computing the Scatter Component of Mammographic Images. In: IEEE Transactions in Medical Imaging, Vol. 13 (1994) 301-313
[65] Highnam, R.P. Brady, J.M.: Mammographic Image Analysis. Kluwer Academic Publishers, Dordrecht Boston London (1999)
[66] Highnam, R.P. Brady, J.M. English, R.: Detecting Film-Screen Artifacts in Mammography using a Model-Based Approach. In: IEEE Transactions in Medical Imaging, Vol. 18 (1999) 1016-1024
[67] Highnam, R.P. Brady, J.M. Shepstone, B.J.: A Quantitative Feature to Aid Diagnosis in Mammography. In Doi, K. Giger, M.L. Nishikawa, R.M. Schmidt, R.A. (eds.): Digital Mammography, Elsevier, Amsterdam (1996) 201-206
[68] Hodge, G.: The Poison on Your Plate. In The Independent on Sunday, LifeEtc, No.649 (14 July 2002), 4-5
[69] Holladay, L.L.: The Fundamentals of Glare and Visibility. In: J.Opt. Soc. Amer, Vol. 12 (1926) 271-320
[70] Hong, B.W.: Segmentation of Mammograms in Topographic Approach. First Year Report. University of Oxford (2002)
[71] Horsch, K. Giger, M.L. Huo, Z. Vyborny, C.J. Venta, L.A.: Computer-Aided Diagnosis of Breast Lesions on Ultrasound. . In Yaffe, M.J. (ed.): Digital Mammography, Medical Physics Publishing, Madison (2000) 233-326
[72] Hume, A. Thamisch, P. Hartswood, M. Procter, R.: On the Evaluation of Microcalcification Detection Algorithms. In Doi, K. Giger, M.L. Nishikawa, R.M. Schmidt, R.A. (eds.): Digital Mammography, Elsevier, Amsterdam (1996) 273-276
[73] Huo, Z. Giger, M.L. Vyborny, C.J. Bick, U. Lu, P. Wolverton, D.E. Schmidt, R.A.: Analysis of Spiculations in the Computerized Classification of Mammographic Masses. In: Med. Phys. Vol. 22(10) (1995) 1569-1579
[74] Jiang, Y. Nishikawa, R.M. Maloney, M.M. Giger, M.L. Venta, L.L.: Computer Classification of Malignant and Benign Microcalcifications in Small-Field Digital Mammograms. In Yaffe, M.J. (ed.): Digital Mammography, Medical Physics Publishing, Madison (2000) 237-242
[75] Kallergi, M.: Digital Mammography: From Theory to Practice. In: Cancer Control Vol. 5(1) (1998) 72-79
[76] Karssemeijer, N.: State of the Art in Computer Aided Detection. In: 6th International Workshop on Digital Mammography, Bremen (2002), Invited Talk
[77] Karssemeijer, N.: Computer Aided Detection and Interpretation in Mammography. In Yaffe, M.J. (ed.): Digital Mammography, Medical Physics Publishing, Madison (2000) 243-252

[78] Karssemeijer, N. te Brake, G.M.: Combining Single View Features and Asymmetry for Detection of Mass Lesions. In Karssemeijer, N. Thijssen, M. Hendricks, J. van Erning, L. (eds.): Digital Mammography, Kluwer Academic Publishers, Dordrecht Boston London (1998) 95-102

[79] Karssemeijer, N. te Brake, G.M.: Detection of Stellate Distortions in Mammograms. In: IEEE Transaction on Medical Imaging, Vol 15(10) (1996) 611-619

[80] Karssemeijer, N.: Adaptive Noise Equalisation and Recognition of Microcalcification Clusters in Mammograms. In: Int. J. of Pattern Recognition and Artificial Intelligence, Vol. 7(6) (1993) 1357-1372

[81] Karssemeijer, N.: Stochastic Model for Automated Detection of Calcifications in Mammograms. In: Image and Vision Computing, Vol. 10 (1992) 369-375

[82] Kedar, R.P. Cosgrove, D. McCready, V.R. Bamber, J.C. Carter, E.R.: Microbubble Contrast Agents for Colour Doppler US: Effect on Breast Masses. In: Radiology, Vol. 198 (1996) 679-686

[83] Kegelmeyer, W.P. Pruneda, J.M. Bourland, P.D. Hillis, A. Riggs, M.W. Nipper, M.L.: Computer-Aided Mammographic Screening for Spiculated Lesions. In: Radiology, Vol. 191 (1994) 331-337

[84] Kichenassamy, S: The Perona-Malik Paradox. In: SIAM Journal of Applied Mathematics, Vol. 57 (1997) 1328-1342

[85] Kim, J.K. Park, H.W.: Statistical Textural Features for Detection of Microcalcifications in Digitized Mammograms. In: IEEE Transactions on Medical Imaging, Vol. (18) (1999) 231-238

[86] Kita, Y. Highnam, R.P. Brady, J.M.: Correspondence between Different View Breast X-Rays Using a Simulation af Breast Deformation. In: Computer Vision and Pattern Recognition (1998) 700-707

[87] Kita, Y. Tohno, E. Highnam, R.P. Brady, J.M.: A CAD System for 3D Locating of Lesions in Mammogram. In Niessen, W. Viergever, M. (eds.): Medical Image Computing and Computer-Assited Intervention 2001, Lecture Notes in Computer Science, Vol. 2208. Springer-Verlag, Berlin Heidelberg New York (2001) 94-102

[88] Kobatake, H. Murakami, M. Takeo, H. Nawano, S: Computerized Detection of Malignant Tumours on digital Mammograms. In: IEEE Transactions on Medical Imaging, Vol. 18(5) (1999) 369-378

[89] Kok-Wiles, S.L. Brady, J.M. Highnam, R.P.: Comparing Mammogram Pairs for the Detection of Lesions. In Karssemeijer, N. Thijssen, M. Hendricks, J. van Erning, L. (eds.): Digital Mammography, Kluwer Academic Publishers, Dordrecht Boston London (1998) 103-110

[90] Kovesi, P.: Image Features from Phase Congruency. In: Videre: Journal of Computer Vision Research, Vol. 1 (1999) 1-26

[91] Kupinski, M.A. Giger, M.L.: Automated Seeded Segmentation on Digital Mammograms. In: IEEE Transactions on Medical Imaging, Vol. 17 (1998) 510-517

[92] Krupinski, E.A. Nodine C.F.: Gaze Duration Predicts the Locations of Missed Lesions in Mammography. In Gale, A.G. Astley, S.M. Dance, D.R. Cairns, A.Y. (eds.): Digital Mammography, Elsevier, Amsterdam (1994) 399-405

[93] Lado, M.J. Tahoces, P.G. Souto, M. Vidal, J.J.: Orthogonal Wavelets and Decision-Making Techniques in Digital Mammography: Computerized Detection of Microcalcifications. In: IEEE Transactions on Medical Imaging, (2003) to be published.

[94] Lai, S.M. Li, X. Bischof, W.F.: On Techniques for Detecting Circumscribed Masses in Mammograms. In: IEEE Transactions on Medical Imaging, Vol. 8 (1989) 377-386

[95] Lee, L. Stickland, V. Wilson, P. Roebuck, E.: Fundamentals of Mammography. W.B. Saunders Company (1995)

[96] Lefebvre, F. Benali, H. Gilles, R. Di Paola, R.: A Simulation of Clustered Breast Microcalcifications. In Medical Physics, Vol. 21(12) (1994) 1865-1874

[97] Li, H. Wang, Y. Liu, K.J.R. Lo, S.C.B. Freedman, M.T.: Computerized Radiographic Mass Detection – Part I: Lesion Site Selection by Morphological Enhancement and Contextual Segmentation. IEEE Transaction on Medical Images 20 (2001) 289-301

[98] Li, H.D. Kallergi, M. Clarke, L.P. Jain, V.K. Clark, R.A.: Markov Random Field for Tumour Detection in Digital Mammography. In: IEEE Transactions on Medical Imaging, Vol. 14 (1995) 565-576
[99] Linguraru, M.G. Brady, J.M. Kadir, T. Yam, M.: A Novel Method to Detect Microcalcifications for Early Signs of Breast Cancer. In: Tenth World Congress on Health and Medical Informatics Medinfo2001. IOS Press, Amsterdam (2001) 946
[100] Linguraru, M.G. Brady, J.M. Yam, M.: Filtering h_{int} Images for the Detection of Microcalcifications. In Niessen, W. Viergever, M. (eds.): Medical Image Computing and Computer-Assited Intervention 2001, Lecture Notes in Computer Science, Vol. 2208. Springer-Verlag, Berlin Heidelberg New York (2001) 629-636
[101] Linguraru, M.G. Brady, J.M.: An Anisotropic Diffusion Approach for Early Detection of Breast Cancer. In: Acta Universitatis Cibiniensis, Vol. XLIII. University of Sibiu (2001) 49-60
[102] Linguraru, M.G. Brady, J.M.: A Non-Parametric Approach to Detecting Microcalcifications. In: Digital Mammography, Lecture Notes in Computer Science, Springer-Verlag, Berlin Heidelberg New York (2002) 339-341
[103] Linguraru, M.G. Brady, J.M. Yam, M.: Detection of Microcalcifications using SMF. In: Digital Mammography, Lecture Notes in Computer Science, Springer-Verlag, Berlin Heidelberg New York (2002) 342-346
[104] Linguraru, M.G. Marias, K. Brady, J.M.: Temporal Mass Detection. In: I Digital Mammography, Lecture Notes in Computer Science, Springer-Verlag, Berlin Heidelberg New York (2002) 347-349
[105] Logan-Young, W. Yanes Hoffman, N.: Breast Cancer: A practical Guide to Diagnosis, Vol. 1- Procedures. Mt. Hope Publishing (1994)
[106] Loscocco, M.F. Thomas, J.A. Chakrabarti, K. Kaczmarek, R.V.: Preference Studies of Workstation Monitor Performance. In Yaffe, M.J. (ed.): Digital Mammography, Medical Physics Publishing, Madison (2000) 612-616
[107] Mallat, S.: A Wavelet Tour of Signal Processing. Academic Press (1999)
[108] Marchese, M.: An Eye on CAD. In Medical Imaging, February (2002) 54-59
[109] Marias, K., M., Brady, J.M. Highnam, R.P., Parbhoo, S., Seifalian, A.M.: Registration of Temporal Mammograms. In Hawkes, D. Hill, D. Gaston, R. (eds.): Medical Image Understanding and Analysis 99. BMVA, London (1999) 97-100
[110] Marias, K.: Registration and Quantitative Comparison of Temporal Mammograms (with Application to HRT Data). Ph.D Thesis, University College London (2001)
[111] Marias, K. Behrenbruch, C.P. Brady, M. Parbhoo, S. Seifalian, A.: Multi-Scale Landmark Selection for Improved Registration of Temporal Mammograms. In Yaffe, M.J. (ed.): Digital Mammography, Medical Physics Publishing, Madison (2000) 580-586
[112] Marias, K.: Texture Analysis for Mammography. MSc Dissertation, Imperial College of Science Technology and Medicine London (1997)
[113] McLeod, G. Parkin, G.J.S. Cowen, A.R.: Automatic Detection of Clustered Microcalcifications in Mammograms. In Doi, K., Giger, M.L. Nishikawa, R.M. Schmidt, R.A. (eds.): Digital Mammography. Elsevier, Amsterdam (1996) 311-316
[114] McLoughlin, K.J. Bones, P.J. Kovesi, P.D.: Detection of Microcalcification Clusters in Digital Mammogram Images. In: Digital Mammography, Lecture Notes in Computer Science, Springer-Verlag, Berlin Heidelberg New York (2002) 353-357
[115] Miller, L. Ramsay, N.: The Detection of Malignant Masses by Non-linear Multiscale Analysis. In Doi, K., Giger, M.L. Nishikawa, R.M. Schmidt, R.A. (eds.): Digital Mammography. Elsevier, Amsterdam (1996) 335-340
[116] The Million Women Study Collaborative Group: The Million Women Study: design and characteristics of the study population. In: Breast Cancer Research, Vol. 1 (1999) 73-80
[117] Montagnat, J. Sermesant, M. Delingette, H. Malandain, G. Ayache, N.: Anisotropic Filtering for Model Based Segmentation of 4D Cylindrical Echocardiographic Images. In: Pattern Recognition Letters (2001)
[118] Moon, P. Spencer, D.E.: The Specification of Foveal Adaptation. In: J. Opt. Soc. Amer., Vol. 33 (1943) 233-248

[119] Morrone, M.C. Owens, R.A.: Feature Detection from Local Energy. In: Pattern Recognition Letters, Vol. 6 (1987) 303-313
[120] Mudigonda, N.R. Rangayyan, R.M. Desautels, J.E.L.: Gradient and Texture Analysis for the Classification of Mammographic Masses. In: IEEE Trans. Med. Imaging, Vol. 19(10) (2000) 1032-1043
[121] Nakahara, H. Namba, K. Fukami, A. Watanabe, R. Mizutani, M. Matsu, T. Nishimura, S. Jinnouchi, S. Nagamachi, S. Ohnishi, T. Futami, S. Flores, I.I.L.G. Nakahara, M. Tamura, S.: Computer-Aided Diagnosis (CAD) for Mammography: Preliminary Results. In: Breast Cancer, Vol. 5(4) (1998) 401-405
[122] Neal, R.M. Hinton, G.E.: A New View of the EM Algorithm that Justifies Incremental and Other Variants In Jordan, M. (ed.): Learning in Graphical Models. Kluwer Academic Publishers, Dordrecht Boston London (1998) 355-368
[123] Ng, S.L. Bischof, W.F.: Automated Detection and Classification of Breast Tumours. In: Comput.Biomed.Res, Vol. 25 (1992) 218-237
[124] Nishikawa, R.M. Giger, M.L. Vyborny, C.J. Schmidt, R.A.: Conputer-Aided Detection of Clustered Microcalcifications: An Improved Method for Grouping Detected Signals. In: Medical Physics, Vol. 10 (1993) 1661-1666
[125] Noble, J.A.: Descriptions of Image Surfaces. DPhil thesis, University of Oxford (1989)
[126] Orel, S.G. Mendonca, M.H. Reynolds, C. Schnall, M.D. Solin, L.J. Sullivan, D.C.: MR Imaging of Ductal Carcinoma in Situ. In: Radiology, Vol. 202(2) (1997) 413-420
[127] D'Orsi, C.J., Basset, L.W. Feig, S.A. Jackson, V.P. Kopans, D.B. Linver, M.N. Sickles, E.A. Stelling, C.B.: BI_RADS: Illustrated Breast Imaging Reporting and Data System. Amrican College of Radiology, Third Edition (1998)
[128] Ozdemir, A. Oznur, I.I. Vural, G. Atasever, T. Karabacak, N.I. Gokcora, N. Isik, S. Unlu, M.: Tl-201 Scintigraphy, Mammography and Ultrasonography in the Evaluation of Palpable and Nonpalpable Breast Lesions: A Correlative Study. In: Eur J Radiol Vol. 24(2) (1997) 145-154
[129] Parker, J. Dance, D.R., Davies, D.H.: Classification of Ductal Carcinoma In-Situ by Image-Analysis of Calcifications from Digital Mammograms. In: British J. of Radiology, Vol. 68 (1990) 241-246
[130] Parr, T.C. Astley, S.M. Taylor, C.J. Boggis, C.R.M.: Model Based Classification of Linear Structures in Digital Mammograms. In Doi, K. Giger, M.L. Nishikawa, R.M. Schmidt, R.A. (eds.): Digital Mammography, Elsevier, Amsterdam (1996) 351-356
[131] Patrick, E.A. Moskowitz, M. Mansukhani, V.T. Gruenstein, E.I.: Expert Learning System Network for Diagnosis of Breast Calcifications. In: Investigative Radiology, Vol. 26 (1991) 534-539
[132] Pearson, H.: Study Refines Breast Cancer Risks. In: Nature News Service, Macmillan Magazines Ltd (2002)
[133] Perona, P. Malik, J.: Scale-space and Edge Detection using Anisotropic Diffusion. In: IEEE Transactions on Pattern Analysis and Machine Intelligence Vol. 12 (1990) 629-639
[134] Petrick, N. Chan, H.P. Sahiner, B. Helvie, M.A. Paquerault, S.: Preclinical Evaluation ofa CAD Algorithm for Early Detection of Breast Cancer. In Yaffe, M.J. (ed.): Digital Mammography, Medical Physics Publishing, Madison (2000) 328-333
[135] Petrick, N. Sahiner, B. Chan, H.P. Helvie, M.A. Paquerault, S. Hadjiiski, L.M.: Breast Cancer Detection: Evaluation of a Mass-Detection Algorithm for Computer-aided Diagnosis. In: Radiology, Vol. 224 (2002) 217-224
[136] Pisano, E.T. Cole, E. Hemminger, B.M. Muller, K. Shumak, R. Yaffe, M. Chakraborty, D. Conant, E. Fajardo, L.L. Feig, S. Jong, R. Kopans, D. Maidment, A. Staiger, M. Williams, M.: Accuracy of Digital Mammography vs. Screen-Film Mammography in a Diagnostic Mammography Population. In Yaffe, M.J. (ed.): Digital Mammography, Medical Physics Publishing, Madison (2000) 504-511
[137] Pohlman, S. Powell, K.A. Obuchowski, N.A. Chilcote, W.A. Grundfest-Broniatowski, S.: Quantitative Classification of Breast Tumours in Digitized Mammograms. In: Med. Phys. Vol. 23 (1996) 1337-1345

[138] Poissonnier, M. Brady, J.M.: 'Noise Equalisation' for Microcalcification Detection? In Yaffe, M.J. (ed.): Digital Mammography, Medical Physics Publishing, Madison (2000) 334-341
[139] Rangayyan, R.M. El-Faramawy, N.M. Desautels, J.E.L. Alim, O.A.: Measures of Acutance and Shape for Classification of Breast Tumours. In: IEEE Trans. Med. Imaging, Vol. 16(6) (1997) 799-810
[140] Rodriguez-Florido, M.A. Krissian, K. Ruiz-Alzola, J. Westin, C.F.: Comparison of Two Restoration Techniques in the Context of 3D Medical Imaging. In Niessen, W. Viergever, M. (eds.): Medical Image Computing and Computer-Assited Intervention 2001, Lecture Notes in Computer Science, Vol. 2208. Springer-Verlag, Berlin Heidelberg New York (2001) 1031-1039
[141] Roehrig, J. Doi, T. Hasegawa, A. Hunt, B. Marshall, J. Romsdahl, H. Schneider, A. Sharbaugh, R. Zhang, W.: Clinical Results with R2 Imagechecker System. In Karssemeijer, N. Thijssen, M. Hendricks, J. van Erning, L. (eds.): Digital Mammography, Kluwer Academic Publishers, Dordrecht Boston London (1998) 395-400
[142] Roelof, T. van Woundenberg, S. Hendriks, J.H.C.L. Boedicker, A. Evertsz, C.J.G. Karssemeijer, N.: Performance Evaluation of a Digital Reading Station for Screening Mammography. In: Digital Mammography, Lecture Notes in Computer Science, Springer-Verlag, Berlin Heidelberg New York (2002) 455-459
[143] Rosen, D. Martin, B. Monheit, M. Wolff, G. Stanton, M.: A Bayesian Neural Network to Detect Microcalcifications in Digitized Mammograms. In Doi, K. Giger, M.L. Nishikawa, R.M. Schmidt, R.A. (eds.): Digital Mammography, Elsevier, Amsterdam (1996) 277-286
[144] Sahiner, B. Hadjiiski, L.M. Chan, H.P. Petrcik, N. Helvie, M.A.: The Use of Joint Two-View Information for Improving Computerized Microcalcification Detection Accuracy. In: Digital Mammography, Lecture Notes in Computer Science, Springer-Verlag, Berlin Heidelberg New York (2002) 358-362
[145] Sahiner, B. Chan, H.P. Petrick, N. Hadjiiski, L.M. Helvie, M.A. Paquerault, S: Active Contour Models for Segmentation and Characterisation of Mammogramphic Masses. In Yaffe, M.J. (ed.): Digital Mammography, Medical Physics Publishing, Madison (2000) 357-362
[146] Sahiner, B. Chan, H.P. Petrick, N. Helvie, M.A.: Computerized Characterisation of Masses on Mammograms: The Rubber Band Straghtening Transform and Texture Analysis. In: Medical Physics, Vol. 25 (1998) 516-526
[147] Sahiner, B. Chan, H.P. Petrick, N. Wei, D. Helvie, M.A. Adler, D.D. Goodsitt, M.M.: Classification of Mass and Normal Breast Tissue: A Convolution Neural Network Classifier with Spatial Domain and Texture Images. In: IEEE Transactions on Medical Images, Vol. 15(10) (1996) 598-610
[148] Samani, A. Bishop, J. Yaffe, M.J. Plewes, D.B.: Biomechanical 3-D Finite Element Modelling of the Human Breast Using MRI Data. In: IEEE Transactions on Medical Imaging, Vol. 20(4) (2001) 271-279
[149] Sanchez-Ortiz, G.I. Rueckert, D. Burger, P.: Knowledge-Based Tensor Anisotropic Diffusion of Cardiac MR Images. In: Medical Image Analysis, Vol. 3(1) (1999) 77-101
[150] Savage, C.J. Gale, A.G. Pawley, E.F. Wilson A.R.M.: To Err is Human; to Compute Divine? In Gale, A.G. Astley, S.M. Dance, D.R. Cairns, A.Y. (eds.): Digital Mammography, Elsevier, Amsterdam (1994) 405-414
[151] Schlief, R.: Ultrasound Contrast Agents. In: Radiology, Vol. 3 (1991) 198-207
[152] Schmidt, R.A. Newstead, G.M. Linver, M.N. O'Shaughnessy, K.: Estimated Expected benefit of CAD in Mammographic Clinical Practice. In: 6th International Workshop on Digital Mammography, Bremen (2002), Invited Talk
[153] Shen, L. Rangayyan, R.M. Desautels, J.E.L: Detection and Classification of Mammographic Calcifications. In: Int. Journal of Pattern Recognition and Artificial Intelligence, Vol. 71 (1993) 1403-1416
[154] Schenk, V.U.B. Brady, J.M.: Finding CLS Using a Multiresolution Oriented Local energy Feature Detection Framework. In: Digital Mammography, Lecture Notes in Computer Science, Springer-Verlag, Berlin Heidelberg New York (2002) 64-68

[155] Smith, S. M. Brady, J. M.: SUSAN - A New Approach to Low-level Image Processing. In: International Journal of Computer Vision, Vol. 23(1) (1997) 45-78
[156] Spiegel, M. R.: Probability and Statistics. McGraw-Hill Book Company, New York (1975)
[157] Stack, J.P. Redmond, O.M. Codd, M.B. Dervan, P.A. Ennis, J.T: Breast Disease: Tissue Characterisation with Gd-DTPA Enhancement Profiles. In: Radiology, Vol. 174 (1990) 491-494.
[158] Stafford, G.: Digital Mammography. http://members.ozemail.com.au/~glensan/digmam2.htm
[159] Swann, C.A. Kopans, D.B. Koerner, F.C. McCarthy, K.A. White, G. Hall, D.A.: The Halo Sign and Malignant Breast Lesions. In: American Journal of Roentgenology, Vol. 149 (1987) 1145-1147
[160] Tanner, C. Schnabel, J.A. Chung, D. Clarkson, M.J. Rueckert, D. Hill, D.L.G. Hawkes, D.J.: Volume and Shape Preservation of Enhancing Lesions when Applying Non-rigid Registration to a Time Series of Contrast Enhancing MR Breast Images. In Proc. MICCAI 2000, Lecture Notes in Computer Science, Springer-Verlag, Berlin Heidelberg New York (2000) 462-471
[161] Taylor, P. Fox, J. Todd-Pokropek, A.: Evaluation of a Decision Aid for the Classification of Microcalcifications. In Karssemeijer, N. Thijssen, M. Hendricks, J. van Erning, L. (eds.): Digital Mammography, Kluwer Academic Publishers, Dordrecht Boston London (1998) 237-244
[162] Taylor, P. Lee, R. Alberdi, E.: Incorporating Explanations into a CAD Tool for the Classification of Calcifications. In: Digital Mammography, Lecture Notes in Computer Science, Springer-Verlag, Berlin Heidelberg New York (2002) 372-376
[163] Thurfjell, E.L. Lindgren, J.A.: Breast Cancer Survival Rates with Mammographic Screening: Similar Favorable Survival Rates for Women Younger and those Older than 50 years. In: Radiology, Vol. 201(2) (1996) 421-426
[154] Valverde, F.L. Munoz, J. Nishikawa, R. Doi, K: Elimination of Calcified False Positives in detection of Microcalcifications in Mammograms Using Hough Transform. In Yaffe, M.J. (ed.): Digital Mammography, Medical Physics Publishing, Madison (2000) 383-389
[165] Veldkamp, W.J.H. Karssemeijer, N. Hendricks, J.H.C.L: Automated Classification of Clustered Microcalcifications into Malignant and Benign Types. In: Medical Physics, Vol. 27 (2000) 2600-2608
[166] Veldkamp, W.J.H. Karssemeijer, N. Hendrick, J.H.C.L.: Fully Automated Classification of Microcalcification Cases Referred from a Nationwide Screening Programme. In Yaffe, M.J. (ed.): Digital Mammography, Medical Physics Publishing, Madison (2000) 390-394
[167] Veldkamp, W.J.H. Karssemeijer, N.: Accurate Segmentation and Contrast Measurement of Microcalcifications in Mammograms: A Phantom Study. In: Medical Physics, Vol. 25(7) (1998) 1102-1110
[168] Viehweg, P. Lampe, D. Buchmann, D. Heywang-Koebrunner, S.H.: In Situ and Minimally Invasive Breast Cancer: Morphologic and Kinetic Features on Contrast-Enhanced MR Imaging. In: MAGMA, Vol. 11(3) (2000) 129-137
[169] Warren Burhenne, L.J. Wood, S.A. D'Orsi, C.J. Feig, S.A. Kopans, D.B. O'Shaugnessy, K.F. Sickles, E.A. Tabar, L. Vyborny, C.J. Castelino, R.A.: The Potential Contribution of Computer Aided Detection to the Sensitivity of Screening Mammography. In: Radiology Vol. 215 (2000) 554-562
[170] Webb, S.(ed.): The Physiscs of Medical Imaging. Institute of Physics Publishing, Bristol Philadelphia (1995)
[171] Weickert, J.: A Review of Nonlinear Diffusion Filtering. In ter Haar Romeny, B. Florack, L. Koenderink, J. Viergever, M. (eds.): Scale-Space Theory in Computer Vision, Lecture Notes in Computer Science. Springer-Verlag, Berlin Heidelberg New York (1997) 3-28.
[172] Weickert, J.: Anisotropic Diffusion in Image Processing. B.G. Teubner, Stuttgart (1998)
[173] Westin, C.F. Maier, S.E. Khidhir, B. Everett, C. Jolesz, F.A. Kikinis, R.: Image Processing for Diffusion Tensor Magnetic Resonance Imaging. In MICCAI (1999) 441-452
[174] Wolfe, J.N.: Breast Patterns as an Index of Risk for Developing Breast Cancer. In: American Journal of Roentgenology, Vol. 126 (1976) 1130-1139

[175] Woods, K. Bowyer, K.: A General View of Detection Algorithms. In Doi, K. Giger, M.L. Nishikawa, R.M. Schmidt, R.A. (eds.): Digital Mammography, Elsevier, Amsterdam (1996) 385-390
[176] Xiao, G.: 3D Free-hand Ultrasound Imaging of the Breast, Ph.D Thesis. Department of Engineering Science, The University of Oxford (2001)
[177] Yaffe, M.: Development of Full Field Digital Mammography. In Karssemeijer, N. Thijssen, M. Hendricks, J. van Erning, L. (eds.): Digital Mammography, Kluwer Academic Publishers, Dordrecht Boston London (1998) 3-10
[178] Yam, M. Brady, J.M. Highnam, R.P. English, R.: Denoising h_{int} Surfaces: a Physics-based Approach. In: Taylor, C. Colchester, A. (eds.): Medical Image Computing and Computer-Assisted Intervention, Springer-Verlag, Berlin Heidelberg New York (1999) 227-234
[179] Yam, M. Brady, J.M. Highnam, R.P. English, R.: Detecting Calcifications in Mammograms using the h_{int} Representation. In: Lemke, H.U. Vannier, M.W. Inamura, K. Farman, A.G. Computer Assisted Radiology and Surgery, Elsevier (1999) 373-377
[180] Yam, M., Brady, J.M. Highnam, R.P. Behrenbruch, C.P. English, R. Kita, Y.: Three-dimensional Reconstruction of Microcalcification Clusters from Two Mammographic Views. In: IEEE Trans Med Imaging, Vol. 20 No. 6 (2001) 479-489
[181] Yates, K. Evans, C. Brady, J.M: Improving teBrake's Mammographic Mass-Detection Algorithm Using Phase Congruency. In: Proc. Digital Image Computing Techniques and Applications (DICTA2002), Melbourne (2002)
[182] Yin, F.F. Giger, M.L. Doi, K. Metz, C.E. Vyborny, C.J.: Computerized Deetection of Masses in Digital Mammograms: Analysis of Bilateral Subtraction Images. In: Medical Physics, Vol. 18 (1991) 955-963
[183] Zhang, Y. Brady, J.M. Smith, S.: Segmentation of Brain MR Images Through a Hidden Markov Random Field Model and the Expectation Maximization Algorithm. In: IEEE Transactions on Medical Imaging, Vol. 20(1) (2001) 45-57
[184] Zwiggelaar, R., Parr, T.C. Schumm, J.E. Hutt, I.W. Taylor, C.J. Astley, S.M. Boggis, C.R.M.: Model-Based Detection of Spiculated Lesions in Mammography. In: Medical Image Analysis, Vol. 3(1) (1999) 39-62
[185] Zwiggelaar, R., Taylor, C.J. Rubin, C.M.E.: Detection of the Central Mass of Spiculated Lesions – Signature Normalisation and Model Data Aspects. In: IPMI'99, Springer (1999) 406-411
[186] Altruis Biomedical Network - http://www.lung-cancers.com/
[187] Altruis Biomedical Network - http://www.breast-cancers.com/
[188] The Center for Orthopaedic Oncology and Musculoskeletal Research - http://www.sarcoma.org
[189] The Breast Clinic - http://www.thebreastclinic.com/
[190] American College of Radiology – Mammography Quality Control Manual (1999)

List of Figures

List of Tables